DISSERTATION

submitted to the
COMBINED FACULTIES FOR THE
NATURAL SCIENCES AND FOR MATHEMATICS
of the
RUPERTO-CAROLA UNIVERSITY
OF HEIDELBERG, GERMANY

for the degree of
DOCTOR OF NATURAL SCIENCES

presented by
Master of Science TATSIANA RYL
born in: Brest, Belarus

Oral-examination: 21.03.2016

MYCN, proliferative heterogeneity and treatment response in neuroblastoma

Referees: Prof. Dr. Thomas Höfer

PD. Dr. Frank Westermann

Acknowledgments

I would like to offer my sincerest gratitude to Prof. Thomas Höfer for giving me the opportunity to do my PhD in his groups. I am grateful to him for his outstanding scientific and strategic support, for giving me excellent guidance but at the same time enough freedom to influence the shape of the project according to my ideas.

Special thanks go to PD Dr. Frank Westermann for allowing me to work in his group with an excellent scientific environment. I thank Dr. Westermann for his great scientific supervision, for explaining me experimental details and in particular for his patience and support throughout all years of my PhD.

My particular thank goes to Dr. Gregor Mönke who assisted me in microscopy analysis, developing new ideas with me and helping me to bring them to fruition. I thank Dr. Chunxuan Shao for the excellent analysis of the Sequencing data. I am also very thankful to Andres Florez for the exciting discussions concerning the project and for his creative ideas.

I would like to express my gratefulness to a number of people, who supported me with advices, their knowledge and skills, their time, ideas, materials and reagents and were kindly helpful whenever asked a question: Dr. Elena Afanasjeva, Dr. Qin Zhang, Nina Claudino, Dr. Erika Kuchen, Diana Haendly, Dr. Hong Ling, Dr. Larissa Savelyeva, Steffen Bannert, Dr. Kai-Oliver Henrich, Dr. Daniel Dreidax, Dr. Sina Gogolin, Alica Torkov, Dr. Lena Brückner, Elisa Maria Hess, Jochen Kreth, Young-Gyu Park, Dr. Congxin Li, Dr. Melanie Rinas, Melania Barile and Dr. Yevhen Vainshtein and Dr. Steffen Schmitt.

My dear friends Nicolas Behl, Elena Afanasjeva, Andres Florez, Olga and Cedric Bodet I thank for being there for me and for the help throughout my time in Heidelberg.

Finally, I thank my parents, my brother Alexander and my husband Frank for their support, patience and love.

Table of contents

Abstract

The amplification of the *MYCN* oncogene, occurring in 20% of neuroblastomas, a tumor of early childhood, is associated with drug-resistant relapse and poor prognosis. High *MYCN* expression has paradoxical effects in most cells: it promotes cell cycle progression and sensitizes to cell death. This work aims to characterize, at population and single-cell level, the mechanisms through which amplified *MYCN* allows tumor regrowth after chemotherapy in neuroblastoma.

In *MYCN*-regulatable neuroblastoma cell line models, MYCN shortens the lengths of cell cycle phases, preferentially in G1, and increases the proportion of cycling cells under exponential growth. Upon DNA-damage induced by the chemotherapeutic agent, doxorubicin (DOX), MYCN delays activation of cell cycle checkpoints and boosts the proportion of transiting cells. During and after chemotherapy MYCN favors cell death and suppresses cellular senescence, shifting p53 downstream effects from cell cycle arrest to apoptosis. However, MYCN also drives clonal regrowth of a small fraction of surviving resister cells after DNA-damage. These resister cells exhibit nearly identical molecular and phenotypic profiles as cells before treatment. Live-cell imaging reveals that resister cells arise exclusively from the G1-phase-arrested subpopulation and rapidly repair DNA-damage-induced double-strand breaks (DSBs). The suppression of DNA repair via ATM inhibition during chemotherapy results in reduction of G1 phase arrest and prevents DNA DSB repair, completely eradicating resister cells.

Taken together, these data show that non-genetic tumor heterogeneity and a key oncogenic lesion, MYCN, synergize to resume cellular proliferation after DNA damage and probably cause chemotherapy resistance. This work indicates that improved first-line therapies could specifically target resister cells and help avoid cellular regrowth.

Zusammenfassung

Die Amplifikation des Onkogens *MYCN* tritt in 20% der Neuroblastome auf und ist mit therapieresistenten Rezidiven sowie einer schlechten Prognose assoziiert. Die Expression von *MYCN* hat paradoxale Effekte in den meisten Zellen: sie fördert die Zellzyklusprogression und sensibilisiert zum Zelltod. Diese Arbeit hat zum Ziel, die Mechanismen, durch welche die *MYCN*-Amplifikation erneutes Tumorwachstum nach einer Chemotherapie ermöglicht, zu charakterisieren. Dies erfolgt sowohl auf Populations- als auch auf Einzelzellebene.

Im Rahmen dieser Arbeit wurde gezeigt, dass in *MYCN*-regulierbaren Neuroblastomzelllinien MYCN die Länge der Zellzyklusphasen verkürzt, vorzugsweise in G1, und den Anteil von zyklierenden Zellen bei exponentiellem Wachstum erhöht. Bei durch das Chemotherapeutikum Doxorubicin (DOX) induzierten DNA-Schäden verzögert MYCN die Aktivierung von Zellzyklus-Checkpoints und erhöht den Anteil der Zellzyklus-durchlaufenden Zellen. Während und nach der Chemotherapie begünstigt MYCN den Zelltod und unterdrückt zelluläre Seneszenz. Dies erfolgt durch Verschieben der p53-nachgeschalteten Effekte von Zellzyklusarrest zu Apoptose. Allerdings treibt MYCN nach der Chemotherapie auch das klonale Wachstum eines kleinen Anteils von überlebenden resistenten Zellen. Diese resistenten Zellen weisen fast identische molekulare und phänotypische Profile auf wie die Zellen vor der Behandlung. Live-Cell-Imaging zeigt, dass resistente Zellen ausschließlich aus der in der G1-Phase-arrestierten Sub-population entstehen. Diese Zellen reparieren zudem schnell die durch DNA-Schäden hervorgerufenen DNA-Doppelstrangbrüche (DSB). Eine Unterdrückung der DNA-Reparatur während der Chemotherapie über eine ATM-Hemmung bewirkt die Reduktion des Arrests in der G1-Phase und verhindert die DNA-DSB Reparatur. Dies führt zur kompletten Ausrottung von resistenten Zellen.

Die Ergebnisse dieser Arbeit zeigen, dass nichtgenetische Tumorheterogenitäten und die onkogene Läsion MYCN, synergieren, um die Wiederaufnahme zellulärer Proliferation im Anschluss an eine Beschädigung der DNA zu starten und somit zu Chemotherapieresistenz führen können. Außerdem wurde gezeigt, dass eine verbesserte Ersttherapie spezifisch auf resistente Zellen zielen könnte, um so erneutes Zellwachstum zu verhindern.

1. Introduction

1.1. Clinical aspects of neuroblastoma

Neuroblastoma is the most common extra cranial solid tumor in children, accounting for 8-10% of childhood cancers in the USA and Europe (Gatta et al., 2014; Maris et al., 2007; Smith et al., 2010). About 37% of the cases are diagnosed as infants, and 90% are younger than 5 years at diagnosis, with a median age at diagnosis of 19 months (London et al., 2005). Neuroblastoma originates from neural crest derived cells, which migrate away from the neural tube early during embryogenesis (Betters et al., 2010). The tumors can affect the whole sympathetic nervous system with a preference to arise in the adrenal medulla (Westermann and Schwab, 2002). The clinical behavior of neuroblastoma is very heterogeneous varying from spontaneous regression to cases of highly aggressive metastatic disease unresponsive to any anti-cancer treatment. The high frequency of spontaneous regression, 10 to 100 fold higher compared to all other tumors, is an unique feature of neuroblastoma (Pritchard and Hickman, 1994).

The age of diagnosis is an important predictive factor for clinical outcome. Infants younger than 1.5 year have a good prognosis for survival, while older patients have adverse prognosis, and in adult and adolescent patients neuroblastoma is ultimately fatal in most cases (Franks et al., 1997; London et al., 2005; Schmidt et al., 2005; Westermann and Schwab, 2002).

The International Neuroblastoma Risk Group Staging System (INRGSS) is used to classify the tumors into stages. This system is based on clinical criteria and image-defined risk factors at the time of diagnosis (Table 1). The INRGSS divides stages into L1, L2, M or MS. In general, patients with low risk disease (L1) have 90% event free survival rates with observation only or minimal therapeutic interventions (Monclair et al., 2009). Patients with intermediate risk disease have event free survival of 78% and usually undergo surgery and chemotherapy. Currently, many groups are focused on using biological markers to help to decrease therapy in specific subpopulations of children (Louis and Shohet, 2015; Park et al., 2013).

Table 1. International neuroblastoma risk group (INRG) staging system (Monclair et al., 2009).

Stage	Definition
L1	Localized tumor not involving vital structures as defined by the list of image-defined risk factors and confined to one body compartment
L2	Locoregional tumor with presence of one or more image-defined risk factors
M	Distant metastatic disease (except stage MS)
MS	Metastatic disease in children younger than 18 months with metastases confined to skin, liver/or bone marrow.

Patients with high-risk disease (M), which account approximately half of all new neuroblastoma cases each year, require treatment with multi-modal therapy using chemotherapy, surgery, radiotherapy high-dose chemotherapy with autologous stem cell rescue and biologic and immunotherapeutic maintenance therapy in order to improve their survival rates (Louis and Shohet, 2015). However, despite these extremely high cytotoxic therapies, children with high-risk neuroblastoma still have survival rates <40% (Kreissman et al., 2013; Kushner et al., 2004; Maris, 2010; Sorkin et al., 2010). Approximately 10% of children have a special form of metastatic disease, characterized as stage MS (metastasis special). This stage is clinically defined by the age of diagnosis (younger than 18 months) and restriction of distant metastases to skin, liver and/or bone marrow (Oberthuer et al., 2009). A high percentage of stage MS patients are expected to undergo spontaneous regression (Maris, 2010), although some children need treatment due to life-threatening initial symptoms or may succumb to disease following rapid tumor growth (Oberthuer et al., 2009).

As a big number of children will still relapse and eventually die from the disease, the aim for investigators is to better understand the origin of the disease and to develop novel treatment strategies for those who are diagnosed with high-risk neuroblastoma.

1.2. Genetic factors in development of neuroblastoma

1.2.1. Genetics of hereditary neuroblastoma

Familiar neuroblastoma concerns only approximately 1% of all cases (Shojaei-Brosseau et al., 2004). Neuroblastoma pedigrees show an autosomal dominant role of inheritance with incomplete penetrance. Constitutional activating anaphase lymphoma kinase (*ALK*) mutations, on chromosome 2p23, have been identified in more than half of all familiar cases (Janoueix-Lerosey et al., 2008; Mosse et al., 2008). ALK is an orphan receptor tyrosine kinase that acts as a major oncogenic driver in different human malignancies, including anaplastic large cell lymphoma and non-small cell lung carcinoma (Bosse and Maris, 2015; Carpenter and Mosse, 2012). In familiar neuroblastoma, constitutive *ALK* activation occurs through kinase domain mutations, and often identical activating mutations also have been found in sporadic neuroblastoma tumors (Bosse and Maris, 2015; Bresler et al., 2014; Carpenter and Mosse, 2012; George et al., 2008; Mosse et al., 2008).

Approximately 10% of familiar neuroblastomas are associated with two neural crest derived congenital anomalies: Hirschsprung's disease, characterized with an aganglionic distal section of bowel, and Ondine's Curse, also called congentialcentral hypoventilation syndrome (CCHS). Majority of children with these diseases have mutations in the paired-like homeobox 2B (*PHOX2B*) gene on chromosome 4p12 that encodes a transcription factor integral to neural crest development, loss of which disrupts terminal differentiation of neuroblastoma cells (Amiel et al., 2003; Mosse et al., 2013).

The cause of the remaining cases of familiar neuroblastoma that do not harbor obvious *ALK* and *PHOX2B* mutations is currently under investigation.

1.2.2. Somatic genetic alterations in neuroblastoma

Approximately 66% of neuroblastoma tumors are hyperdiploid or near-triploid DNA content (Cohn et al., 2009; George et al., 2005; Look et al., 1991). These tumors usually have gains of whole chromosomes and low frequency of chromosomal rearrangements and associated with lower risk of diseases and favorable clinical

outcomes (Maris, 2005; Westermann and Schwab, 2002). In contrast, the majority of aggressive neuroblastoma tumors have either near-diploid or near-tetraploide DNA content (Bosse and Maris, 2015; Janoueix-Lerosey et al., 2009; Schleiermacher et al., 2012). They are characterized by high degree of chromosomal rearrangements, such as amplification, deletions and unbalanced translocations (Cohn et al., 2009; George et al., 2005; Look et al., 1991).

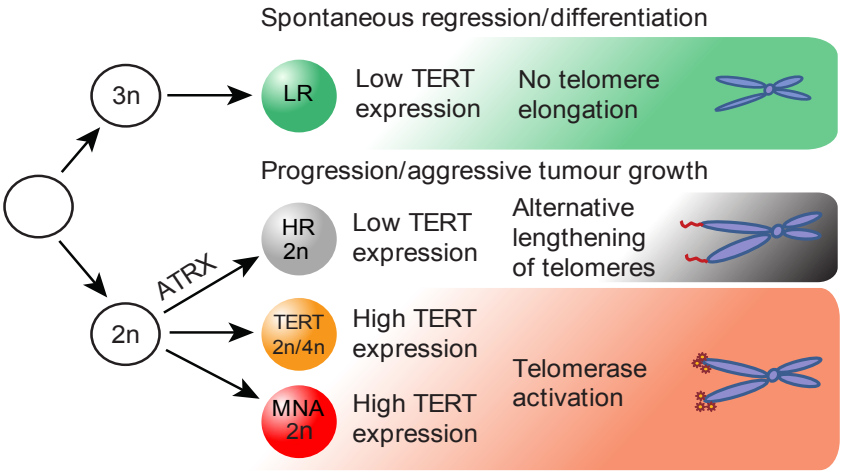

Figure 1. Model for neuroblastoma pathogenesis based on recurrent genomic alterations. Adapted from (Peifer et al., 2015). 3n – near triploid, 2n – near diploid, LR – low risk, HR – high risk, MNA – *MYCN*-amplified.

To date, the most aggressive tumors are defined by three major genomics alterations: *TERT* (telomerase reverse transcriptase) rearrangement, *MYCN* amplification and *ATRX* (a-thalassemia/mental retardation syndrome X-linked) mutations (Brodeur et al., 1984; Peifer et al., 2015). These alterations occur only in high-risk neuroblastomas in a mutually exclusive fashion (Peifer et al., 2015).

Recurrent genomic rearrangements affecting a chromosomal region at 5p15.33 proximal of the TERT gene has been recently discovered by the whole genome sequencing study in approximately one-quarter of high-risk neuroblastomas (Peifer et al., 2015). The 5p15.33 rearrangements juxtapose the *TERT* coding sequence to strong enhancer elements, which results in a massive chromatin remodeling and DNA methylation of the affected regions (Peifer et al., 2015). Not only *TERT* rearrangements but also elevated *TETR* expression were found to be associated with aggressive neuroblastomas (Peifer et al., 2015).

Amplification of the *MYCN* oncogene at chromosome 2p24 is the classic genetic aberration of neuroblastoma consistently associated with poor outcome (Brodeur et

al., 1984; Seeger et al., 1985). MYCN amplification develops in approximately 20% of all primary neuroblastoma tumors and in 50% of high-risk tumors and strongly correlates with aggressive advanced-stage disease and treatment failure (Brodeur et al., 1984; Seeger et al., 1985).

Inactivating *ATRX* mutations have been identified in more than 10% of neuroblastomas enriched in older children (Cheung et al., 2012; Molenaar et al., 2012b; Pugh et al., 2013). Mutations of *ATRX* are associated with increase in telomere lengths and with absence of the *ATRX* protein in the nucleus (Heaphy et al., 2011; Kurihara et al., 2014).

In general, pediatric tumors have a much lower frequency of somatic mutations than most adult cancers (Vogelstein et al., 2013). Recent genomic sequencing efforts discovered only few additional recurrent somatic mutations in neuroblastoma tumors at the time of diagnosis, Table 2. Activating mutations of ALK tyrosine kinase receptor occur in 8-10% of all sporadic neuroblastomas. *ARID1B* and *ARID1A*, chromatin remodeling proteins, are also frequently mutated in neuroblastoma and represent a significant subset of clinically aggressive neuroblastomas (Sausen et al., 2013). Mutations in RAS/MAPK pathway are rare in primary neuroblatoma but recently have been more frequently found in relapsed tumors (Eleveld et al., 2015; Pugh et al., 2013). Chromothripsis has been described to occur in 18% of high-risk neuroblastomas (Molenaar et al., 2012b).

The activity of CyclinD1/CDK4/CDK6/Rb cell cycle regulatory pathway correlates with *MYCN* amplification and provide a biological marker for potentially susceptible patients (Carr-Wilkinson et al., 2010; Gogolin et al., 2013; Molenaar et al., 2003; Rader et al., 2013). The somatic activating mutations in this pathway are rare, however genomic amplifications of *CCND1* and *CDK4* or deletion of *CDKN2A* identified to increase CDK4/6 expression and kinase activity through this drive cell cycle progression (Caren et al., 2008; Krasnoselsky et al., 2005; Molenaar et al., 2012a; Molenaar et al., 2003; Pugh et al., 2013). The frequency of these aberrations may be higher in the relapsed neuroblastomas (Carr-Wilkinson et al., 2010; Eleveld et al., 2015).

Table 2: Potentially actionable genomic alterations in neuroblastoma. Rare indicates <5% prevalence. Modified from and adapted from (Bosse and Maris, 2015).

Clinically Actionable pathway/Gene	Prevalence at diagnosis	Prevalence at relapse	References
Telomerase dysfunction			
TERT rearrangements	21%		(Peifer et al., 2015)
MYCN amplification	16%-38%		(Brodeur et al., 1984; Seeger et al., 1985)
ATRX deletion/mutation	9%-22%	17%	(Cheung et al., 2012; Eleveld et al., 2015; Pugh et al., 2013)
ALK			
Mutation/amplification	8%-10%	26%-43%	(Cheung et al., 2012; Eleveld et al., 2015; Molenaar et al., 2012a; Pugh et al., 2013; Sausen et al., 2013; Schleiermacher et al., 2014; Shukla et al., 2012)
Cell cycle control			
CDK4/6 amplification	4%	-	(Molenaar et al., 2012a)
Cyclin D1 amplification	2%-15%	-	(Molenaar et al., 2003)
CDKN2A deletion	0%-20%	13%-22%	(Carr-Wilkinson et al., 2010; Meijering et al., 2012; Omura-Minamisawa et al., 2001)
DNA damage pathway			
TP53	1%-8%	15%	(Carr-Wilkinson et al., 2010; Omura-Minamisawa et al., 2001; Pugh et al., 2013)
MDM2 amplification	13%	13%	(Carr-Wilkinson et al., 2010)
Chromatin modification			
ARID1A/ARID1B deletion/mutation	11%	Rare	(Eleveld et al., 2015; Sausen et al., 2013)
RAS-MAPK pathways			
NRAS, KRAS, HRAS, NF1, BRAF, PTPN11, FGFR1	Rare	Rare	(Eleveld et al., 2015; Pugh et al., 2013; Shukla et al., 2012)

Allelic losses at chromosome 1p and chromosome 11q also carry prognostic information in neuroblastoma. The deletion at 1p36 and loss of chromosome 11q occur in up to 35% and 33% of primary neuroblastomas respectively. They are markers for poor prognosis and associated with high-risk clinical and genomic

features, such as *MYCN* amplification, older age and metastatic disease (Attiyeh et al., 2005; Caron et al., 1993; Maris et al., 2000; White et al., 2001).

1.3. MYC proteins in normal development

In 1983 Schwab and his colleagues first brought the attention to MYCN as a putative oncogene (Kohl et al., 1983; Schwab et al., 1983). It showed that a subset of human neuroblastoma cells lines harbor multiple copies of a DNA sequence related to the MYCC oncogene and this region was named MYCN.

MYCN belongs to the MYC family of basic-helix-loop-helix-leucine zipper (bHLH-LZ) transcription factors, which are proto-oncogenes (Henriksson and Luscher, 1996). The MYC family also includes MYCC and MYCL. The MYC proteins consist of an amino-terminal transcriptional activation domain and a carboxy-termintal DNA-binding and protein interaction domain. MYCC and MYCN proteins both heterodimerize with MAX at consensus E-box sequences (CANNTG), which is required for direct binding of MYC proteins to DNA (Meyer and Penn, 2008). Whereas MAX is stable and constantly expressed, MYC family members have short half-lives and their expression is highly regulated (Grandori et al., 2000).

The MYC proteins induce a vast number of targets including genes involved in proliferation and cell cycle promotion, metabolism, protein synthesis, mitochondrial biogenesis and function (Dang et al., 2006; Sabo et al., 2014). MYC can also repress gene expression by binding to transcription factors Miz-1 and SP-1 and through this inhibit transcription of their downstream targets (Adhikary and Eilers, 2005). This way MYC can repress many negative cell cycle regulators and genes involved in cell adhesion (Seoane et al., 2002).

Although biochemical properties for MYCC and MYCN are very similar, they are separately regulated. While *MYCC* expression is more generalized, *MYCN* has a restricted expression pattern. MYCC is highly expressed in most rapidly proliferating cells during development and in the adult (Zimmerman et al., 1986). *MYCN* expressed during embryo development in pre-B cells, brain, kidney, lung and heart (Stanton et al., 1992; Zimmerman et al., 1986). After embryonic

development *MYCN* is downregulated and not significantly expressed in adult tissue.

MYCN plays a profound role during embryonic development. MYCN promotes proliferation of granule neuron precursors derived from neuronal progenitor cells of the developing forebrain and hindbrain (Beltran, 2014; Knoepfler et al., 2002). Mutations or constitutive deletions of *MYCN* gene are embryonic lethal whereas conditional inactivation of MYCN in neuronal progenitor cells leads to ataxia, behavior abnormalities and tremors (Charron et al., 1992; Stanton et al., 1992). These developing defects correlate with 2-fold decrease in brain mass that disproportionally affects the cerebellum and the cerebral cortex, both of which show features of disorganization. The analysis of cells revealed that the cell proliferation is compromised through decrease of S phase and mitotic cells, whereas apoptosis is unaffected (Charron et al., 1992; Stanton et al., 1992). Enhanced expression of MYCN in the neural crest enables proliferation of immature neuronal precursor cells and suppresses differentiation (Swartling et al., 2012).

1.4. MYCN oncoprotein in different cancer types

Amplification and/or overexpression of MYCN is not only the feature of neuroblastoma, but also has been found in various other tumor types, cf. Table3. In general the presence of MYCN alteration had been associated with poor prognosis and tumor aggressiveness suggesting a similar driving role in *MYCN*-amplified and/or overexpressing tumors (Beltran, 2014).

Table 3. MYCN amplified tumors. Modified from Beltran et al., 2014.

Tumor type	Frequency of MYCN alteration	Clinical amplification	References
Neuroblastoma	Amplification in 20%	Poor prognosis, selection for aggressive treatment	(Brodeur et al., 1984; Look et al., 1991; Schneiderman et al., 2008; Seeger et al., 1985)
Medulloblastoma	Amplification in 5%	Poor prognosis	(Aldosari et al., 2002; Swartling et al., 2010)

Glioblastoma multiforme	Overexpression in a subset	Histone 3.3 mutations associated with overexpression of *MYCN*	(Bjerke et al., 2013; Hodgson et al., 2009)
Retinoblastoma	Amplification in < 5%	Poor prognosis, early onset, unilateral nonhereditary	(Lee et al., 1984; Rushlow et al., 2013)
Alveolar rhabdomyosarcoma	Amplification in 25% Overexpression in 55%	Poor prognosis, correlates with presence of PAX3-FOXO1 or PAX7-FAXO1 fusion genes	(Tonelli et al., 2012)
Small-cell lung cancer	Amplification in 15%-20%	Poor response to chemotherapy, shorter survival	(Beltran, 2014; Funa et al., 1987; Nau et al., 1986)
Prostate cancer	Amplification in 40% of neuroendocrine prostate cancer, 5% of prostate adenocarcinoma	Clinical aggressiveness	(Beltran et al., 2011; Mizukami et al., 1995; Mosquera et al., 2013)
Breast cancer	Overexpression in a subset	Correlates with poor prognostic features	(Mizukami et al., 1995)

1.5. Cell cycle regulation and MYCN

The cell cycle has four sequential phases: G1, S, G2, M (Figure 2A) .The most important phases are S phase, when DNA replicates, and M phase, when one cell divides into two daughter cells. G1 is the gap after mitosis where the cell has 2n chromosomes. At this time the cell is sensitive to positive and negative factors from the growth signaling network, (Williams and Stoeber, 2012). G2 phase follows the from S phase, cell has already 4n DNA content and prepares for the entry into mitosis (Murray, 1993). G0 is a state during G1 phase when cells have reversibly withdrawn from the cell division cycle in response to high cell density or mitogen deprivation (Zimmerman et al., 1986). Cells can also be irreversibly withdrawn from the cell cycle into terminally differentiated or senescence states (Hall and Watt, 1989; Williams and Stoeber, 2012). Progression through the cell cycle phases is under the control of a family of serine/threonine protein kinases. These kinases are heterodimers consisting of a catalytic subunit, the cyclin dependent kinase (CDK) and their regulatory partners the cyclins (Malumbres and Barbacid, 2006). To date, 21 genes encoding CDKs and 29 genes encoding cyclins are identified in the

human genome (Malumbres and Barbacid, 2005; Malumbres et al., 2009) CDK4/6-cyclin D and CDK2-cyclin E drive G1 progression through the restriction point, which afford the cell to complete the cell cycle. CDK2-cyclin A initiates S phase, and CDK1-cyclin B regulates progression through G2 and entry into mitosis. The activation of G1 phase CDKs leads to the phosphorylation and inactivation of retinoblastoma protein (Rb). The inactivated Rb protein is released from its complex with E2F family of transcription factors and the reaction promotes G1/S transition, Figure 2B (Dyson, 1998; Friend et al., 1986; Nevins, 2001).

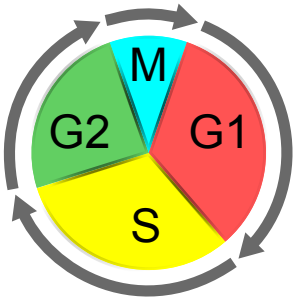

Figure 2. Cell cycle phases in mammalian cell cycle.

Progression and transition through each cell cycle phase are monitored by sensor mechanisms, called checkpoints, which maintain the correct order of events (Hartwell and Weinert, 1989). If the sensor mechanisms detect aberrant of incomplete cell cycle (i.e. DNA damage), checkpoints pathway can carry the signals to effectors that trigger cell cycle arrest until the problem is resolved (Bartek et al., 2004; Musacchio and Salmon, 2007). Effector proteins include the CDK inhibitors (CDKIs), which can reversibly trigger cell cycle arrest. Based on sequence and structure similarity, CDKIs consist of two protein families: the INK4 (inhibitors of CDK4), and the CIP/KIP (CDK Interacting Protein/Kinase inhibitory Protein) families (Pavletich, 1999; Sherr and Roberts, 1999). The INK4 family consists of $p16^{INK4A}$, $p15^{INK4B}$, $p18^{INK4C}$, $p19^{INK4}$, which inhibit CDK4 and CDK6 and arresting the cell cycle in G1-phase (Pavletich, 1999; Sherr and Roberts, 1999). The CIP/KIP family includes three members: $p21^{CIP1}$ (CDK Interacting Protein1, later p21), $P27^{KIP1}$ (Kinase Inhibitory Protein1), and $p57^{KIP2}$ (Kinase Inhibitory Protein 2), which inhibit CDK2 and CDK1 activity and can induce cell cycle arrest at every cell cycle phase (Malumbres et al., 2009).

The best characterized tumorigenic effect of MYC proteins is to promote proliferation and cell cycle progression (Huang and Weiss, 2013). The influence of ectopic *MYCN* expression on the cell cycle was first investigated using TET21N system (Lutz et al., 1996). Similar to *MYCC*, *MYCN* over-expression induces the re-entry of quiescent cells into the cell cycle, shortens the time of cell cycle progression, in particular shortens the G1 phase and decreases cell attachment to the extracellular matrix (Bell et al., 2010; Lutz et al., 1996). Conversely, the reduction of *MYCN* expression by MYCN siRNA was found to cause cell cycle arrest (Bell et al., 2010).

1.6. p53 pathway in neuroblastoma

The p53 tumor suppressor pathway has been described as the “guardian of the genome” (Lane, 1992). Therefore the inactivation of this pathway is the hallmark of cancer and occurs in approximately 50% of all human tumors, which harbor inactivating mutations of the *TP53* gene (Hanahan and Weinberg, 2011). The p53 protein is a transcription factor, which due to its short half-life, is present at very low levels in the cell under normal physiological conditions (Honda et al., 1997). Upon different types of cellular stresses, e.g. DNA damage, p53 protein is rapidly phosphorylated on serine 15 and 20 by the ATM and CHK2 kinases, respectively, which leads to stabilization and activation of the p53 (Banin et al., 1998; Shieh et al., 2000). An important negative regulator of p53 is MDM2. This protein represses p53 mediated transactivation, targets p53 for proteasomal degradation and is transcriptionally activated by p53, thus executing a negative feedback on p53 (Marine et al., 2006; Oliner et al., 1993; Sherr, 1998; Thut et al., 1997). MDM2 is controlled by $p14^{ARF}$, which binds MDM2 directly and prevents the MDM2 mediated p53 degradation, leading to stabilization and activation of p53.

Active p53 induces expression of genes responsible for cell cycle arrest (*CDKN1A*, *14-3-3 sigma*, *GADD45*) or apoptosis induction *PUMA*, *BAX* (Crescenzi et al., 2008). Additionally p53 is known for triggering different types of senescence, including replicative senescence (seen in aging human fibroblasts) and drug-induced senescence. Senescence is a non-reversible, terminal cell cycle exit, characterized by enlarged nuclei, flattened cell morphology presence of β-

Galactosidase activity at suboptimal conditions (by pH 6), and albescence of cell division in metabolically active cells (Noda et al., 1994). Although, the exact molecular pathways underlying the process of senescence remain to be elucidated, several studies have shown that senescence is highly associated with a sustained upregulation of the p21 protein (Mirzayans et al., 2012; Shay, 1999).

Interestingly, p53 is rarely mutated in neuroblastoma. The frequency of p53 mutations in tumors at diagnosis is less than 2% (Tweddle et al., 2003). After tumor relapse or progression p53 still stays active in more than 85% of tumors (Carr-Wilkinson et al., 2010). The defects in the upstream regulators of p53 (MDM2 amplification and $p14^{ARF}$ deletion or methylation) are present in the primary and relapse tumor with the same proportion (Carr-Wilkinson et al., 2010).

1.7. MYCN-induced apoptosis and deregulation of p53 pathway

Most MYCN-amplified neuroblastomas initially respond well to chemotherapy but the tumors frequently relapse. Members of *MYC* family, including *MYCN*, are known to play a dual role in driving proliferation by up and down regulation of cell cycle genes and sensitizing cells to apoptosis. This paradox is observed historically in human *MYCN* amplified neuroblastoma tumors and TH-*MYCN* transgenic mouse neuroblastoma tumors (Altungoz et al., 2007; Goto et al., 2001; Moore et al., 2008; Shimada et al., 1999; Shimada et al., 1995).

TP53 is known to be a direct target gene of MYCC and mediates MYCC induced apoptosis (Reisman et al., 1993; Roy et al., 1994; Zeller et al., 2003). Several studies in neuroblastoma demonstrated that *MYCN* amplified tumors and cell lines express significantly high levels of *p53* mRNA, p53 protein and several p53 target genes in comparison with non-amplified tumors and cell lines (Bell et al., 2006; Chen et al., 2010; Cui et al., 2005; Westermann et al., 2008). It has been shown that MYCN promotes p53 accumulation by interacting directly with the same E-Box motif (CATGTG) as previously found for MYCC (Chen et al., 2010; Reisman et al., 1993). Works from different labs suggest that these functional interactions between MYCN and p53 represent an important and direct mechanism by which MYCN sensitizes cells to apoptosis (Chen et al., 2010). These findings can explain why

human *MYCN* amplified and TH-*MYCN* transgenic mouse neuroblastoma tumors have high levels of apoptosis and *MYCN* amplified and *MYCN* overexpressing neuroblastoma cells undergo higher levels of apoptosis after treatment with chemotherapeutic drugs and with irradiation (Bell et al., 2006; Chesler et al., 2008; Fulda et al., 2000; Paffhausen et al., 2007).

Interestingly, MYCN promotes transcription of p53 negative regulator *MDM2*, through direct transcriptional activation, and through activation of *TP53*, as MDM2 is a target for p53-mediated transcription (Chen et al., 2010; Slack et al., 2005).

Another important way through that MYCN impairs p53 signaling is inhibition of p21 gene expression (Bell et al., 2006). Activation of p21 after DNA damage is required for cell cycle arrest and senescence. *MYCN* amplification is significantly associated with low level of p21 induction and failed G1 arrest after ionizing irradiation in p53 wild type neuroblastoma cell lines (Bell et al., 2006; Tweddle et al., 2001). It has been reported that MYCC suppresses p21 expression by binding to its promoter, through recruitment by MIZ1 and that MYCC expression switches p53 function from a G1 arrest to apoptosis, by increasing the transcription of proapoptotic genes *PUMA* and *BAX* instead of *CDKN1A* (Seoane et al., 2002; Sheen and Dickson, 2002). Additionally MYCN suppresses p21 through direct up-regulation of the oncoprotein SKP2. SKP2 is a component of the ubiquitin ligase complex, which targets p21 for degradation (Wang et al., 2005). Reduction of SKP2 after MYCN knockdown decrease SCF^{SCP2} mediated degradation of p21, which allows p21 to accumulate and induce G1 arrest in *p53* wild type cells (Bell et al., 2007; Bell et al., 2006; Westermann et al., 2007).

Thus, MYCN plays a dual role in p53 pathway. It impairs the G1 arrest through suppression of p21 and sensitizes cells to apoptosis though activation of p53 transcription. Summary of how MYCN influences p53 signaling and G1/S transition is shown in figure 3.

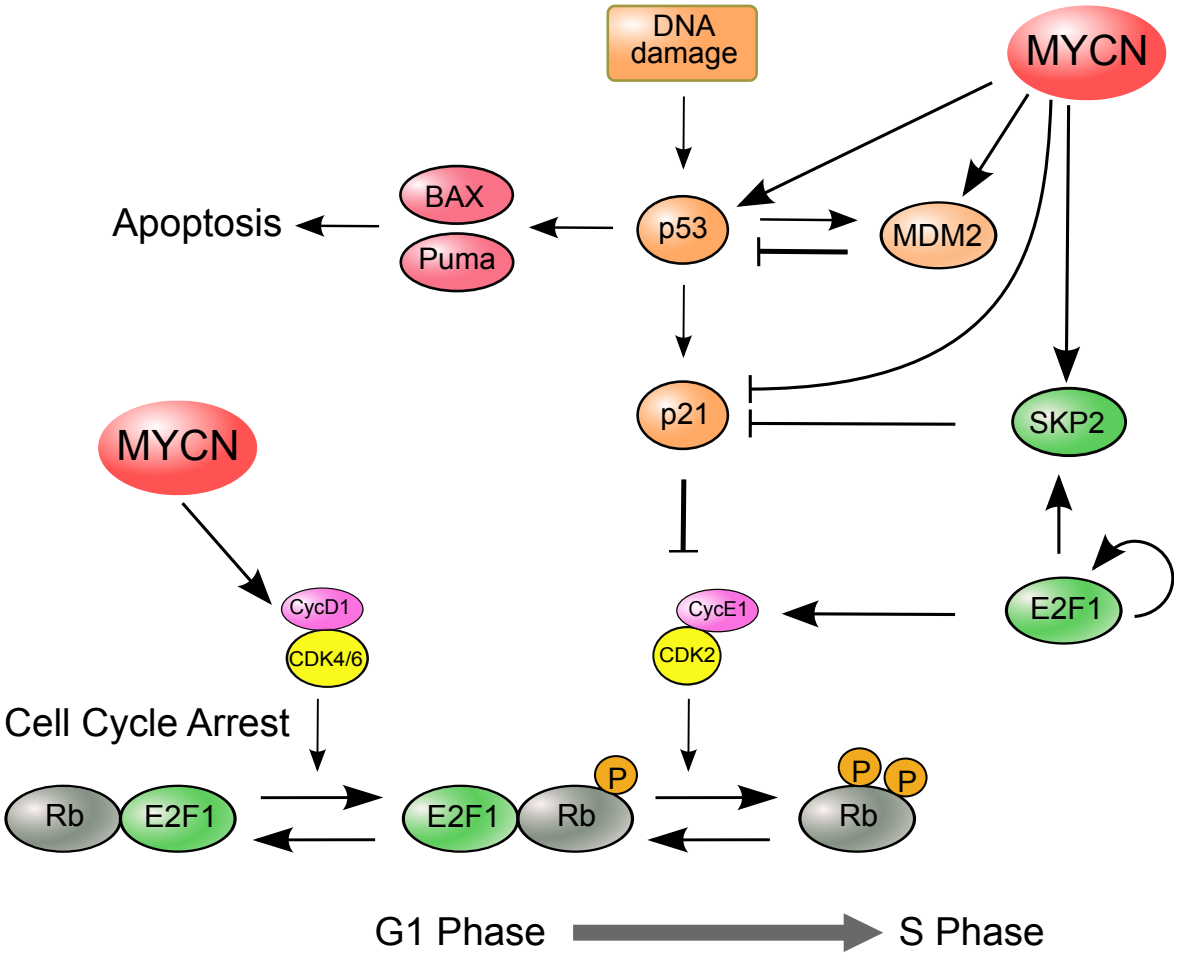

Figure 3. G1 checkpoint. Diagram shows the relationship between MYCN, p53 pathway and E2F1/Rb.

1.8. Treatment of neuroblastoma

The therapeutic approaches for neuroblastomas range from observation only to aggressive multimodal therapy and are based on the event free and overall survival of patients enrolled in clinical trials. Patients with low- or intermediate-risk neuroblastoma have event-free survival outcomes graters than 90% (Hero et al., 2008; Park et al., 2013; Strother et al., 2012). In patients younger than 6 months of age with small, localized lesions, observation alone can be a safe treatment option (Nuchtern et al., 2012). For patients from low-risk group surgery alone is curative in nearly all cases (De Bernardi et al., 2008). Several recent studies demonstrated excellent survival rates for children from the intermediate-risk group with reduced treatment (Baker et al., 2010; De Bernardi et al., 2009; Kohler et al., 2013; Rubie et

al., 2011). Therefore, for the intermediate-risk group the current tendency is to reduce the treatment duration, dose of chemotherapeutic agents and radiation therapy.

Patients with *MYCN*-amplification and/or those, which are older than 18 months of age with metastatic disease, are assumed as high-risk. Modern treatment strategies for these patients include five to six cycles of induction chemotherapy and surgery followed by consolidation therapy with high-dose therapy combined with autologous hematopoietic stem cell rescue and irradiation (Pinto et al., 2015). However, half of the patients who got clinical remission after induction and consolidation therapy will relapse, suggesting the persistence of therapy-resistant minimal residual disease (Pinto et al., 2015). The post-consolidation treatment with immunotherapy and cytokines plus isotretinoin is now a part of the standard-of-care treatment, Figure 4, reviewed in (Pinto et al., 2015).

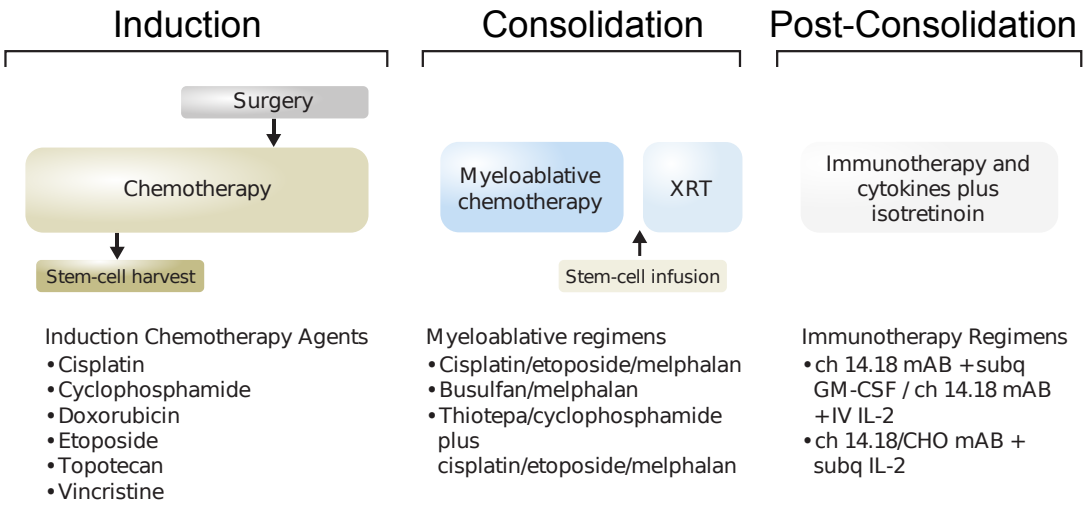

Figure 4: Current standard treatment strategy for high-risk neuroblastoma. Adapted from (Pinto et al., 2015). Therapy includes three treatment blocks: induction (chemotherapy and primary tumor resection); consolidation (high dose chemotherapy with autologous stem-cell rescue and external-beam radiotherapy (XRT)); post-consolidation (anti-ganglioside 2 immunotherapy with cytokines and cis-retinoic acid). Ch – chimeric, CHO – Chinese hamster ovary, GM-CSF – granulocyte macrophage colony-stimulating factor, IL-2 – interleukin-2, IV-intravenous, mAb monoclonal antibody.

In general, treatment of patients with residual disease remains to date a big challenge. Therefore, the advances in targeted therapies and the understanding of the genetics and biology of tumors at the time of original diagnosis are required to design a better first-line therapies that will help to reduce relapses.

1.9. Topoisomerase-II inhibitors

Topoisomerase II (Top2) is a very important anticancer drug target. Chemotherapeutics, such as doxorubicin etoposide are widely used to treat a broad variety of malignancies (Baldwin and Osheroff, 2005; Lieu et al., 2009; Nitiss et al., 2012; Walker and Nitiss, 2002). Top2 is an enzyme, which simultaneously cleaves both DNA strands in order to manage DNA tangles and supercoils (Schoeffler and Berger, 2008; Wang, 1998). Most drugs targeting Top2 generate double strand breaks (DSBs) as a direct consequence of the catalytic activity of the enzyme (Robinson and Osheroff, 1990). Top2 cleaves DNA by forming the covalent complexes between the enzyme and DNA, and drugs that disrupt the catalytic cycle can trap the enzyme and generate DNA damage (Walker and Nitiss, 2002). Agents that inhibit topoisomerase are named topoisomerase poisons to underline the importance of cellular damage induced by these drugs. Top2 poisons not only generate DNA damage but also inhibit Top2 catalytic activity (Nitiss et al., 1992; Nitiss et al., 1993). It has been shown that mammalian cell lines resistant to drugs frequently have reduced Top2 activity (Nitiss and Beck, 1996). Furthermore, it was found that the G2/M cell cycle checkpoint, that delays progression through mitosis, is more activated when Top2 activity is limited (Downes et al., 1994).

It is well known that drugs targeting Top1 kill cells predominantly in S phase, as inhibiting of Top1 generates DSBs only in S phase by collision of replication forks with trapped Top1 covalent complexes (Holm et al., 1989; Zhang et al., 2006). Therefore, the marker for DSBs, yH2AX phosphorylation does not occur in cells treated with drugs targeting Top1 (Huang et al., 2003). In contrast, the killing by Top2 targeting agents occurs in all cell cycle phases and yH2AXA phosphorylation is detected also in non-replicating cells (Huang et al., 2003). However, replication plays a great role in cell death by Top2-targeting agents. Several studies suggested that inhibiting replication reduced cell killing by Top2-targeting agents, and that progression through S phase enhanced cell death by Top2-targeting agents (Holm et al., 1989; Markovits et al., 1987). Currently two related mechanisms explaining the generation of DNA damage during S phase by Top2 poisons are described. First, collisions of a replication fork lead to disruption of a Top2 covalent complex and the generation of DSBs (Howard et al., 1994). A second mechanism suggests

that Top2 complexes block the progression of replication forks, and that the collapse of a blocked fork generates DSBs (Michel et al., 2004).

1.10. Recognition and repair of double strand breaks

Cells defend themselves against cytotoxic DNA damage by activating the DNA damage repair signaling network that is mostly regulated by sensor kinases: ataxia telangiectasia mutated (ATM) and ATM- and Rad3-related (ATR). ATR is activated by single stranded DNA (ssDNA) coated with replication protein A. Whereas ATM is activated by DSBs induced, for example, by Top2 inhibitors or ionizing irradiation. ATM activates a vast number of responses, such as DNA damage repair, cell cycle arrest, gene expression control, chromatin organization, stress control, cell death programs (Paz et al., 2011). ATM phosphorylates the histone 2A (H2A) variant H2AX (known as yH2AX), which forms foci at the sites of double strand breaks (Stiff et al., 2004). yH2AX acts as a docking station for other DNA damage signaling proteins such as p53 binding protein 1 (53BP1) and BRCA1 which rapidly accumulate at DNA break sites (Panier and Boulton, 2014).

The two most important mechanisms for repairing DSBs are homologous recombination (HR) and non-homologous end-joining (NHEJ) which complement each other (Davis et al., 2014; Goodarzi and Jeggo, 2013; Rothkamm et al., 2015). ATM promotes the repair of DNA DSBs by homologous recombination (HR) through recruitment of BRCA1 to DSBs, or it can antagonize BRCA1 and promote non-homologous end-joining (NHEJ) by recruiting p53 binding protein 1 (53BP1) (Kastan and Bartek, 2004). BRCA1 and 53BP1 serve as scaffolds that recruit DSB-effector proteins required for initiation of HR and NHEJ respectively (Escribano-Diaz et al., 2013; Feng et al., 2013).

The pathways of DSB repair are based on whether sequence homology is used to join the DSB ends (Aparicio et al., 2014). Homologous recombination (HR) requires homologous sequences to align DSB ends prior to ligation (Jasin and Rothstein, 2013). The HR is a highly complex process that involves multiple proteins and occurs during the S and G2 phases of the cell cycle when sister chromatids are available as repair templates (Heyer et al., 2010; Shrivastav et al., 2008). Briefly,

HR involves 5' to 3'-end-resection, the loading of replication protein A (RPA) on single-stranded DNA, the replacement of RPA by RAD51 and invasion of the undamaged strand leading to D-loop and heteroduplex formation (Jeggo and Lobrich, 2015). Repair synthesis and branch migration can then occur before the resolution of Holiday junction intermediates (Jeggo and Lobrich, 2015; Sarbajna and West, 2014). Generally, a big number of helper mediator proteins are involved in HR.

Non-homologous end-joining (NHEJ) does not require sequence homology, is active throughout the cell cycle and represents the major pathway for repairing DSBs (Lieber, 2010). NHEJ is initiated by the binding of Ku70/80 heterodimer to blunt or near blunt DNA ends. This leads to recruitment and activation of the DNA-dependent protein kinase catalytic subunit (DNA-PKcs), an ATM-related kinase (Dynan and Yoo, 1998). The DNA-PKcs triggers the signaling cascade that activates and maintains the downstream repair process. NHEJ involves minimal DNA processing and is facilitated by scaffold proteins XRCC4 and XLF that bind to DNA Ligase 4, an enzyme responsible for ligating the breaks (Ma et al., 2002; Mohapatra et al., 2013). NHEJ is usually described as an error-prone method, because NHEJ does not restore sequence information lost in both DNA strands. Nevertheless, introduced DNA errors can be corrected post-rejoining by base excision or mismatch repair (Jeggo and Lobrich, 2015; Symington, 2014; Zelensky et al., 2014).

NHEJ is quicker that HR and can restore the majority of DSB (Iliakis, 2009). The available evidences suggest that in the G2 cell cycle phase, where HR can function, NHEJ anyway acts as the pathway of first choice anyway, consistent with the fact that KU rapidly binds to the DSBs and resection, the initiating step for HR, happens only if NHEJ was not activated (Jeggo and Lobrich, 2015; Shibata et al., 2011).

1.11. FUCCI method for analysis of cell cycle progression in single cells

Traditionally the cell cycle transition was difficult to observe in live samples. While the transition from M to G1 (cell division) can be determined by morphological

changes, the transition from G1 to G2 is very difficult to observe using live cell imaging (Sakaue-Sawano et al., 2008). Traditionally, G1/S has mostly been observed either after staining with nucleotide analogs (BrdU or EdU), which requires sample fixation, or by synchronization of the cell cycle by pharmacological reagents (Sakaue-Sawano et al., 2008).

In 2008, a novel methodology named FUCCI (Fluorescent Ubiquitination-based Cell Cycle Indicator), which allows analysis of cell cycle phases in living cells, was introduced (Sakaue-Sawano et al., 2008). The FUCCI system bases on two components of the DNA replication control system of high eukaryotes, the licensing factor Cdt1 and its inhibitor Geminin (Zielke and Edgar, 2015). In higher eukaryotes, proteolysis and Geminin mediated inhibition of the licensing factor Cdt1 are essential for preventing re-replication (Sakaue-Sawano et al., 2008). Due to the cell cycle-dependent proteolysis Cdt1 and Geminin proteins oscillate in an inverse pattern(Arias and Walter, 2007). Cdt1 peaks in G1 phase just before the onset of DNA replication, and declines rapidly after the initiation of S phase. On the other hand, Geminin levels are high during S and G2 phase, but low during late mitosis and G1 phase (Li et al., 2003; Nishitani et al., 2004). The expression of Cdt1 and Geminin is regulated by the sequential regulation of the F3 ubiquitin ligases APC^{Cdh1} and SCF^{Skp2}, Figure 4A (Nishitani et al., 2000). The APC^{Cdh1} ubiquitin ligase is active in the late M and G1 phases and targets Geminin for degradation, while the SCF^{Skp2} ubiquitin ligase is active only during S and G2 phases and target Cdt1 for degradation (Nishitani et al., 2004). Interestingly, the SCF^{Skp2} complex is a direct substrate of the APC^{Cdh1}complex but also functions as a feedback inhibitor of APC^{Cdh1}(Bashir et al., 2004; Wei et al., 2004).

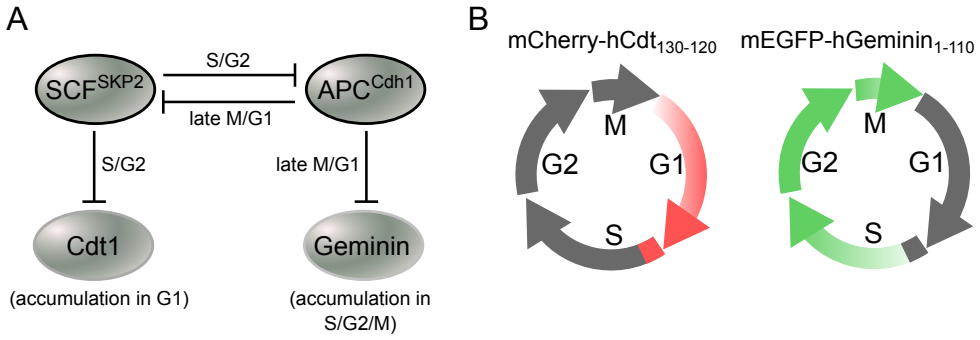

Figure 5. The FUCCI concept. A Cell cycle regulation by SCF^{Skp2} APC^{Cdh1} maintains bistability between G1 and S/G2/M phases. Modified from (Sakaue-Sawano et al., 2008) **B** Right: cells transfected with mCherry-Cdt11-120 marked by red fluorescence in G1 and very early S. Left: Cells transfected with mEGFP-hGeminin11-120 marked by green fluorescence in S/G2/M phases.

The FUCCI system relies on fluorescent proteins fused to degrons derived from Cdt1 and Geminin (Zielke and Edgar, 2015). These fluorescent FUCCI probes are degraded by APC^{Cdh1} and SCF^{Skp2} during different phases of the cell cycle, and thereby allow the visualization of living cells in either G1 or S/G2/M , Figure 4B. Although the original FUCCI system is based on dual probes, it is possible to determine the cell cycle stage with a single FUCCI probe.

Sakaue-Sawano and coworkers first fused the complete human Cdt1 protein to a monomeric version of Kusabira Orange (mKO2), but the ectopic expression of this construct interfered with cell cycle progression (Sakaue-Sawano et al., 2008). Therefore the authors generated different deletion constructs and found that an N-terminal fragment of hCdt1 ($hCdt_{130-120}$) is sufficient for degradation during S and G2 phases. This fragment does not have the Geminin-binding region, but obtains the CY motif (amino acids 68-70), which is critical for mediated proteosomal degradation (Nishitani et al., 2006). Interestingly, the original G1 sensor is only functional when conjugated with mKO2 or mCherry, while the fusions with the AzamiGreen, EGFP or RFP1 were constantly expressed during the whole cell cycle (Sakaue-Sawano et al., 2011; Sakaue-Sawano et al., 2008). For the G2 sensor, Sakaue-Sawano and coworkers also generated a fusion protein consisting of mKO2 and the N-terminal region of hGeminin ($hGem_{1-110}$) that allows robust detection of S/G2/M phase. In contrast to $hCdt_{130-120}$, $hGem_{1-110}$ shows normal cell cycle oscillations in combinations with various fluorescent proteins such as mAG, mCyan, EGFP, Venus, or mCherry (Sakaue-Sawano et al., 2013; Sakaue-Sawano et al., 2011).

To date, a broad range of FUCCI-expressing cell lines and several model systems, including flies, fish, mice and plants are available for a wide range of researches for studies of diverse biological processes. Although only a short time has passed since introduction of the FUCCI method, the fundamental insights into how cells establish quiescence and how G1 phase length impacts the balance between pluripotency and stem cell differentiation are already provided (Zielke and Edgar, 2015).

1.12. Aims of the study

MYCN mediates cells sensitive phenotype that results in the fast initial response to the induction therapy observed in *MYCN*-amplified neuroblastoma patients and cell lines. However, *MYCN* tumors frequently relapse, suggesting that some *MYCN*-amplified cells find the way to escape cell death and are capable to quickly regrow from and metastasis.

This study is aiming to understanding of the mechanisms by which a small fraction of cells (‘resisters’) survive cytotoxic therapy, repair drug-induced DNA damage, and, resume clonal proliferation thereafter. The project addresses the following questions:

1. Which properties help cancer cells to survive therapy?

For this the molecular and phenotypic responses of *MYCN* tunable neuroblastoma cells to the chemotherapy are analyzed on the population and on the single cell level. The influence of cell cycle arrest, DNA damage checkpoint deregulation and DNA damage repair is investigated.

2. Can resister cells be sensitized to chemotherapy and prevented from resuming proliferation after treatment?

With the obtained knowledge about molecular mechanisms involved in chemotherapy resistance novel combinations of chemotherapy and molecularly targeted drugs will be designed to improve the effect of first-line therapy.

2. Materials and Methods

2.1. Materials

Research equipment

Bioanalyzer	Agilent
Cell culture hood HERA	Heraeus
Centrifuges	Eppendorf, Beckman Coulter
Qbit	Qubit
Light Cycler 480	Roche
Microscope Nikon Ti-E	Nikon
Microscope Olympus, CKX41	Olympus
Miltenyi MACSQuant Analyser	Miltenyi
SDS-gel-electrophoresis chamber	BioRAD
Steri-cult CO_2 incubator	Thermo Scientific
Transfer chamber	BioRAD
Tecan Infinite M 200	Tecan
NanoDrop ND-1000 spectrophotometer	NanoDrop
Vortex Genie	NeoLab
Thermo water bads	GFL, Hans Byaer, Julabo

Molecular biology reagents

4x Laemmli Sample Buffer	BioRad
ABSOLUTE qPCR ROX mix	Thermo Scientific
Agencourt AMPure XP beads	Beckton Dickinson
Bovine serum albumin (BSA)	Roche Diagnistics
Cell Titer Blue	Promega
ERCC Spike-in control	Life Technologies
QBit RNA assay	Life TechnologiesMethylene
Methylene Blue	Merck
PBS	Santa Cruz
Ponseau S	Sigma
Prolong	Life Technologis

Running buffer	Bio-Rad
Spike-In	Life technologies
TBS	Santa Cruz
Transfer Buffer	Bio-Rad

Kits for molecular biology

BCA Protein Assay Reagent	Pierce
Click-iT EdU Flow Cytometry Assay Kit	Life Technologies
iDeal ChIP-Seq Kit	Diagenode
Effectene Transfection Ragent	Qiagen
NEBNext ChIP-Seq library Prep Master Mix set Kit	New England Bioscience
ScriptSeq Complete Gold Kit (Human/Mouse/Rat)	Epicenter
Senescence β-Galactosidase Stainig Kit	Cell Signalling
First Strand cDNA Synthesis Kit	Thermo Scientific
RiboGold Kit	Epicenter
RNeasy mini Kit	Qiagen

Chemicals and Reagents

4IPBA	Sigma
4,6-diamidino-2-phenylindol (DAPI)	Sigma
DMSO	AppliChem
EDTA	Sigma
Ethanol	Sigma
Formaldehyde 37%	Sigma
Formaldehyde 4%	BioLegend
FxCycle Violet Stain	Life Technologies
Glycine	AppliChem, Darmstadt
Goat Serum	Sigma
Hydrogen peroxide	Sigma
Isopropanol	Greiner Bio One
luminol	Sigma
Methanol	Greiner Bio One
Nuclease-free water	Ambion
Triton X-100	Sigma

Materials

Menzel-Gläser Polysine Slides	Thermo Scientific
PVDF Membrane, 0.45mm	Schleicher and Schüll
Whattman 3MM Paper	Whatman, Dassel

Table 4 Antibodies for Western Blot

Specificity	Host	Supplier/Catalog number
MYCN	Mouse	Santa Cruz sc-53993
P53	Mouse	Santa Cruz sc-126
P21	Mouse	Cell Signaling
MDM2	Mouse	BD Biosciences 556353
BAX	Rabbit	Cell Signaling 2772S
Actinβ	Mouse	Sigma-Aldrich A-5441
Anti Mouse-HPR	Goat polyclonal	Santa Cruz sc-2031
Anti Rabbit-HPR	Goat polyclonal	Santa Cruz sc-2030
Molecular weight marker for immunoblotting		
BenchMark, pre-stained protein Ladder	10748-010	Invitrogen

Table 5 Antibodies and Isotypes for FACS

Specificity	Host	Supplier/Catalog number
P-p53 (S15) Alexa (R) 488 Conjugate	Mouse	Cell Signaling 9235S
p21 Waf1/Cip1 Alexa (R) 488 Conjugate	Rabbit	Cell Signaling 5487S
p-Rb (S807/811) XP(R) PE Conjugate	Rabbit	Cell Signaling 11917S
pATM (Ser1981) PE Conjugate	Mouse	BioLegend 651203
Skp2	Rabbit	Cell Signaling 2652S
mAb IgG1 Isotype Control Alexa (R) 488 Conjugate	Mouse	Cell Signaling 4878S
mAb IgG XP(R) Isotype Control Alexa (R) 488 Conjugate	Rabbit	Cell Signaling 2975S
mAB IgG1, k Isotype Control PE	Mouse	BioLegend 400112
mAb IgG XP(R) Isotype Control PE Conjugate	Rabbit	Cell Signaling 5742S

Anti-rabbit IgG (H+L), F(ab)2 Fragment Alexa (R) 488 Conjugate	Rabbit	Cell Signaling 4412S

Table 6 Antibodies for Immunofluorescence

Specificity	Host	Supplier/Catalog number
Ki67	Mouse	Cell Signaling 9449S
yH2AX	Rabbit	Cell Signaling 9718S
53BP1	Rabbit	Santa Cruz sc-22760
Anti-Rabbit Alexa Fluor® 405 IgG (H+L)	Goat	Life Technologies A31556
Anti-Rb IgG (H+L) Cy5.5 Conjugated	Goat	Life Technologies L42018
Anti-Rabbit Alexa Fluor® 488 IgG (H+L)	Goat	Life Technologies A11034

Table 7 Antibodies for Chip-Seq

Specificity	Host	Supplier/Catalog number
H3K9me3	Rabbit	Abcam 8898
H3K4me3	Rabbit	Abcam 8580
H3K27me3	Mouse	Abcam 6002

Table 8 Taqman® Real-Time PCR Assays

Gene	Assay ID
MYCN	Hs00232074_m1
C-MYC	Hs00153408_m1
TP53	Hs01034249_m1
CDKN1A	Hs00355782_m1
BAX	Hs00180269_m1
BBC3	Hs00248075_m1
E2F1	Hs00153451_m1
SKP2	Hs01051864_m1
CCNA2	Hs00996788_m1
CCNE1	Hs01026536_m1

CCND1	Hs00765553_m1
GAPDH	Hs02758991_m1
UBC	Hs00824723_m1
HMBS	Hs00609296_m1
SDHA	Hs00188166_m1

All TaqMan assays were obtained from ThermoFisher Scientific

Drugs

Doxorubicin	Tocris
Neocarciostatin	Sigma
RO-3306 (CDK1 inhibitor)	Calbiohem
LEE011 (CDK4 inhibitor)	Selleckchem
KU-60019 (ATM inhibitor)	Tocris
AZD7762 (Chk1&Chk2 inhibitor)	APExBio
LY2603618 (Chk1 inhibitor)	APExBio
VE-821 (ATR inhibitor)	Calbiochem

Antibiotics for cell culture

Blasticidin	Sigma
Penicillin/Streptomycin	PanReac AppliChem
G418	Sigma
Hygromycin B	Sigma
Puromycin	BD Clontech
Zeocin	Invitrogen
Doxycycline	BD Clontech

Media and supplement for cell culture

RPMI 1640 (1mM L-Glutamine, 25mM Hepes)	Gibco, Life Technolofies
RPMI 1640 (with L-Glutamine, without Phenol Red)	PAA, The Cell Culture Company
Fetal Bovine Serum (FCS)	Gibco, Life Technolofies

Plasmids

The pMOWS_puroR_mCherry_hCdt1 and pMOWS_puroR_mEGFP_hGem constructs were kindly provided by Prof. Ursula Klingmüller. The first construct possesses a part of hCdt1 (1-300) and the second a part of hGeminin (1-60). These parts are degraded in a cell cycle dependent manner. Both plasmids have puromycin resistance.

The pRRL-mCherry-53BP1 construct was kindly provided by Prof. Alexander Loewer. This is a lentiviral vector expressing a fragment of human 53BP1 (1228-1922) fused to mCherry under the Ubiquitin C promoter.

Table 9 Tissue culture cell lines used in the study

Cell Line	Description	Reference	Selective antibiotics
SH-EP	*MYCN* – non-amplified neuroblastoma cell line	(Ross et al., 1983)	
TET21N	Derived from SH-EP, transgenic inducible *MYCN*, non amplified neuroblastoma cell line	(Lutz et al., 1996)	90 µg/ml Hygromycin 200 µg/ml G418
IMR5/75_shRNA MYCN	*MYCN* - amplified neuroblastoma cell line, expresses MYCN shRNA under control of tetracycline repressor	(Muth et al., 2010)	5 µg/ml Blasticidin, 45 µg/ml Zeocin
IMR32 _shRNA MYCN	*MYCN* - amplified neuroblastoma cell line, expresses MYCN shRNA under control of tetracycline repressor		5 µg/ml Blasticidin 180 µg/ml Zeocin
SH-SY5Y_MYCN	Derived from *MYCN* non amplified neuroblastoma cell line SH-SY5Y, transgenic inducible *MYCN*		7.5 µg/ml Blasticidin, 1 mg/ml G418

TET21N_hCdt1	Derived from SH-EP, transgenic inducible *MYCN*, with recombinant hCdt1 (30-120)	Generated in the present study	90 µg/ml Hygromycin 200 µg/ml G418 7.5 µg/ml Puromycin
TET21N_Geminin	Derived from SH-EP, transgenic inducible *MYCN*, with recombinant hGeminin (1-60)	Generated in the present study	90 µg/ml Hygromycin 200 µg/ml G418 7.5 µg/ml Puromycin
IMR5/75_hCdt1	*MYCN* - amplified neuroblastoma cell line, expresses MYCN shRNA under control of tetracycline repressor, has recombinant hCdt1	Generated in the present study	5 µg/ml Blasticidin 45 µg/ml Zeocin 2 µg/ml Puromycin
TET21N_hGeminin	Derived from SH-EP, transgenic inducible *MYCN*, with recombinant hGeminin (1-60) and h53BP1	Generated in the present study	90 µg/ml Hygromycin 200 µg/ml G418 7.5 µg/ml Puromycin 2 µg/ml Blasticidin

Software

Adobe Photoshop CS5 12.0.4

Systems Inc.

Inkscape

FIJI

FlowJo 7.6.5

Prism 6

2.2. Methods

2.2.1. Cell culture methods

2.2.1.1 Culturing and cryoconservation of human neuroblastoma cells

All cells were cultivated in RPMI1640 supplemented with 100 U/ml Penicillin/ Streptomycin, and 10% FCS at 37°C, in 5% CO2 atmosphere in a humidified cell culture incubator. The cell culture medium was substituted every 3-4 days, and cells were split at ration 1:5 when they reached subconfluent density. Adherent cells were removed from the substratum by versenization. Visual observation of cell morphology was conducted under the Zeiss Axiovert microscope, equipped with

phase-contrast and bright-field optics. The conservation cells were harvested and resuspended in 4 ml of an ice-cold cryoconservation medium (RPMI with 40% FCS, 10% DMSO). The cellular suspension was dispensed into cryocontainers and incubated at least 24h at -80C prior to deposition into a liquid nitrogen tank for long time storage. For recultivation, frozen cells were quickly thawed and the cryoconservation medium was substituted with a warm fresh growth medium.

2.2.1.2 Transfection of plasmids and selection of transfected cells

In the present study all transfections were carried out using the Effectene Transfection Reagents. This reagent is a non-liposomal lipid formulation allowing high transfection efficiency with minimal cytotoxicity. Plasmids were transfected into cells, which were seeded 18-24h before transfection. Transfection was performed according to manufactural instructions using 1 µg DNA. The transfection medium was replaced by the fresh complete medium 24h post transfection. Selection of stably transfected cells was initiated 24h post transfection by addition of appropriate antibiotics into the growth medium. After selection, transfected cells were sorted into single cells using fluorescence activated cell sorting to generate clonal populations. Individual clones were expanded and analyzed using FACS analysis or time-lapse microscopy.

2.2.1.3. Drug treatment

Doxorubicin (DOX) was used at the concentration of 0.1µg/ml for SHEP, TET21N and SH-SY5Y or at the concentration of 0.05µg/ml for IMR5/75 and IMR32 cells. For the monitoring of the cells after treatment at the indicated time durations the medium with DOX was washed out and replaced with a normal growth medium. The CDK1 inhibitor (RO-3306), CDK4 inhibitor (LEE011), ATM inhibitor (KU-60019), ATR inhibitor (VE-821), Chk1&Chk2 inhibitor (AZD7762) and Chk1 inhibitor (LY2603618) were used with the concentrations 7.5 µM, 4 µm, 10 µM, 5 µM, 300 nM and 3 µM respectively.

2.2.1.4. Colony formation assays

Cells were harvested and $1x10^4$ to $6x10^4$ cells were re-plated into 6 well plates with fresh medium. 14 days after re-seeding cells were fixed with 4% PFA, stained with methylene blue and imaged. The number of colonies was counted using FIJI's particle analyzer.

2.2.1.5 Senescence assay

Cells were fixed with a 1% paraformaldehyde fixative solution, washed twice in 1xPBS and stained with a β-Galactosidase staining kit (Cell Signaling) according the manufacturer's instructions. Brightfield and DAPI images were captured with a color Dr. Gregor Mönke. A color threshold was applied on an ellipsoid stripe surrounding a cell's nucleus. The mean measured intensity of the chosen green color component (30˚ - 120˚ in HSB space) was recorded for every imaged cell.

2.2.1.6 Calculation of growth curves after drug treatment

At the appropriate time points cells were dethatched with versene. 1mL of cell-versene suspension was collected and 100 µL were counted with the MACSQuant Analyser (Milteny) using propidium iodide staining to exclude dead cells.

2.2.2. FACS analysis

2.2.2.1 Cell cycle and Sub G1 analysis

Adherent and non-adherent cells were harvested and centrifuged for 5 min at 800g. The pellets were fixed with ice-cold 70% ethanol and incubated at -20°C overnight. Cells were washed in PBS, stained for 30min with DAPI or with VioBlue (Life Technologies) and analyzed with the Miltenyi MACSQuant Analyzer. Data were analyzed using FlowJo software, and the Dean-Jett-Fox algorithm for cell cycle analysis. Cells with a DNA-content below that of the G1-fraction were considered dead.

2.2.2.2 Antibody staining

10^6 cells were pre-fixed with 4% paraformaldehyde (PFA) for 15 minutes at room temperature (RT), then re-suspended in ice-cold methanol and incubated overnight at -20°C. Cells were then washed in PBS, incubated for 30min in washing buffer (1%BSA, 0,1% TritonX in PBS) and stained with fluorescein-conjugated primary antibodies for 1 h at RT (Table.2). After washing the cells were stained with Violet-Blue dye for cell cycle analysis.

2.2.2.3 EdU incorporation

Cells were incubated with 10 µM EdU for 1h prior to collection. 10^6 cells were fixed, permeabilized and stained with the Click-iT Plus EdU Flow cytometry Assays Kit.

2.2.2.4 FACS-Single cell sorting (Cell cycle outgrowth)

TET21N_hCdt1 cells were harvested and resuspended in ice-cold medium. Cell sorts were performed using FACSariaII (BD). For each conditions ~600 or more single cells were sorted into 96-well plates according to their cell cycle status. 3 weeks after re-seeding, cells were stained with Cell Titer Blue assay, imaged and the number of colonized wells counted. Three biological replicates were performed.

2.2.3. Live-cell microscopy

Cells were grown on 8-well Ibidi µ-slides or Lab-Tek chamber slides in phenolred-free RPMI 1640 medium and imaged every 10-20 min for up to 2 weeks under controlled growth conditions at 37°C, 5% CO2 and 80% humidity (Pecon incubator). The growth media was changed every 2-3 days. Images were acquired with an inverted widefield microscope (Nikon Ti-E) using an EMCCD camera (Andor iXON3 885) and a 20x lens (CFI Plan Apochromat DM 20x, NA 0.75). Phase contrast images were acquired in addition to fluorescence using a light engine lamp (Lumencor) and filters DAPI, GFP (Semrock) and RFP (AHF).

Cells were tracked in FIJI (version 1.48d) (Livak and Schmittgen, 2001) using the plugin MTrackJ (Meijering et al., 2012) for manual tracking. Automatic nuclei segmentation and tracking were done by Dr. Gregor Mönke using ImageJ-based custom written software.

2.2.4. Real-time quantitative PCR

Total RNA was isolated with the RNeasy Mini Kit (Qiagen), following manufacturer's instructions. Nucleic acids were quantified in solution using NanoDrop ND-1000 spectrophotometer by measuring absorbance at 260 nm.

RNA for the gene expression measurement was reverse transcribed using the RevertAid H Minus First Strand cDNA Synthesis Kit (Thermo scientific) according to manufacture instructions. Samples to be used in real-time quantitative PCR were diluted with nuclease-free water to the final concentration of 2 ng/µL (equivalent of total RNA) and stored at -20°C until use.

DNA was quantified in 384-well format using the LightCycler 480 Real-Time PCR System, Table5. For the quantitative gene expression studies, cDNA in the amount of 10 ng of equivalent of total RNA was used per well. 5 µL of cDNA (2 ng/µL) was mixed with 6 µL of enzymatic master mix, yielding 11 µL total sample volume. The mRNA level of each target gene was normalized to the relative average amount of the internal reference genes *GAPDH, UBC, SDHA or HMBS*. The internal reference genes and the target genes were analyzed in parallel for each sample. The relative gene expression was calculated using the comparative cycle crossing point ($\Delta\Delta$Cp) method (Livak and Schmittgen, 2001).

2.2.5. RNA-sequencing

RNA was extracted from $1x10^6$ cells using the RNeasy mini kit (Qiagen) with a separate step for DNAse I digestion (Fermentas). RNA amount was determined using a Qbit (Life Technologies) and quality assessed using a Bioanalyser Total RNA kit, or a small RNA Kit (Agilent). In order to maintain a record of the cell number throughout library preparation, the same amount of ERCC Spike-in control mix-1 (Life technologies) was added to each sample prior to processing (1 µl of a 1:10 dilution of mix-1). RNA from each sample was processed using the RiboGold kit (Epicentre) to remove rRNA. The concentration of the resulting RNA was measured using the Qbin RNA assay. The remaining rRNA-depleted was then used to prepare libraries for sequencing using ScriptSeq Complete Gold Kit low input (Epicenter). The Agencourt AMPure XP beads (BeckmanCoulter) were used to

purify the cDNA. Barcodes for individual samples were added in order to multiplex 6 samples in each sequencing lane. 14 cycles of enrichment PCR were performed prior to size selection with Agencourt Ampure beads (Beckton Dickinson) to select cDNA with a narrow size distribution around 270 base pairs in length. The qualities of libraries were assessed using a DNA1000 chip on a Bioanalyser (Agilent) to ensure the correct size of libraries and the concentration was measured using the Qbit DNA assay. Sequencing was performed on an Illumina platform with HiSeq 2000 Pair-end 100bp sequence type. Bioinformatic analysis of RNA-Seq data was performed by Dr. Chunxuan Shao.

2.2.6. Chromatin Immunoprecipitation and Sequencing (ChIP-Seq)

Chromatin Immunoprecipitation ChIP experiments with TET21N cells were carried out using iDeal ChIP-seq Kit from Diagenode according to the manufacturer's instructions. For fixation 106 TET21N cells were incubated for 10min at room temperature with 1% formaldehyde. Cross-linking was terminated by addition of glycine to a final concentration of 125 mM. Subsequently cells were incubated for 20min at 4°C with a lysis buffer, nuclei were collected by centrifugation for 15min at 20.000xG and 4°C and resuspended in a sonication buffer. The chromatin was fragmented by sonication (Covaris) to an average size of 150bp. 1% of material was saved as "Input". Antibodies, Table4, were added to the sheared chromatin and DiaMag Protein A beads and incubated on a rotating wheel over night at 4°C. Rabbit and mouse normal IgG were used as negative controls. The beads were washed four times with washing buffers. Immune complexes were disrupted by eluting 30min at room temperature with the elution buffer. Eluates were reverse cross-linked by heating at 65°C for 4h and DNA was purified with magnetic beads. Two biological replicates for histone modifications were sequenced using Illumina HiSeq 2000 (50bp single-end) sequencing technology. 12 indexes were used per sequencing lane.

Library preparation for Illumina 10ng of chromatin-immunoprecipitated DNA was end repaired and dA tailed. Subsequently, the adaptor was ligated to the dA-Tailed DNA. DNA was cleaned up using AMpure XP beads after each step. Adaptor ligated DNA was selected in size with AMpure XP beads using different DNA to

beads ratios to an average fragment size of 280bp. As the last step, size-selected and adaptor-ligated DNA was enriched by PCR with different index primers and cleaned up using AMpure XP beads. Purified library DNA was quantified with Qubit 2.0 and fragment size was assessed using Bioanalyzer (Agilent high sensitivity chip). Bioinformatic analysis of RNA-Seq data was performed by Dr. Chunxuan Shao.

2.2.7. Immunofluorescence

Cells were seeded onto sterilized glass slides (Thermo Scientific) placed in the cell culture dishes and cultured as appropriate. Cells were fixed with 4% PFS for 5 min at RT, washed 3x with PBS, permeabilized with 0.5% Triton X-100 in PBS for 5min, washed again and blocked with Goat Serum diluted 1:10 for 30 min. The glass slides were incubated with primary antibodies diluted in a blocking buffer for 1h at RT in a dark humid chamber (Table3). After washing 3x with PBS, glass slips were incubated with diluted fluorescence conjugated secondary antibodies for 1h at RT, Table 3. After 3x washing with PBS, the nuclei were counterstained with DAPI. Images were captured with an EMCCD camera (Andor iXON3 885) using a 60x oil lense.

Quantification of proteins via SDS-PAGE and western blotting

Cells were seeded onto 6-well plates. Directly before protein isolation, ice-cold RIPA buffer was supplemented with 1x Halt Protease Inhibitor Cocktail and 5mM EDTA. Cells were washed with ice-cold PBS, the plate was placed on ice and cells were lysed with 50 µL of complete lysis buffer by scraping with a cell scraper. The lysate was transferred to pre-chilled 1.5mL tubes, agitated for 30 min at 4°C and centrifuged at 4°C, 10000xG for 20 min. The supernatant was transferred to a new 1.5mL tube and stored at -80°C. Before use, lysates were boiled for 10 min at 95°C. **BCA assay** Protein samples were diluted 10x with a RIPA buffer and quantified with a BCA Protein Assays Reagent according to the manufacturer's instructions.

The protein concentration was calculated from a standard curve prepared using serial dilutions of BSA (25-2000 µg/mL).

SDS-PAGE The lysates were separated by sodium dodecyl sulfate-polyacrylamide gel electrophoresis (SDS-PAGE). The 4x Lämmli method of discontinuous electrophoresis was applied (Laemmli, 1970). 50 µg of total protein lysate was mixed with a Protein Loading Buffer, supplemented with 20% β-mercaptoethanol, denatured for 5 min at 95°C and loaded into Any KDTM Criterion TGX Gels (BioRad). The gel was run at 120V, after the run, stacking gel was removed and separating gel was equilibrated for 15 min in the transfer buffer.

Western blot and immunodetection of proteins by ECL The proteins were transferred to a Polyvinylidene Difluoride (PVDF) membrane. The PVDF membrane was activated for 1 min in 100% methanol, followed with equilibration in the transfer buffer for 10 min. The transfer was performed in a fully submerged system from BioRad Transblot for 1 h and at 100V/400 mA. After transfer, the membrane was blocked with 5% BSA in 1x TBS-T buffer for one hour. After blocking, the membrane was washed 3x 5min with 1xTBST and incubated overnight with a primary antibody at 4°C (Table1). The membrane was washed 3 x 5min with 1xTBST, incubated for 1 h with the secondary antibody conjugated to horseradish peroxidase (Table1) and washed 3x 5 min with 1x TBST.

Detection was performed using non-commercial ECL solution. 6.6µL of H_20_2 were added directly before use to the 20 mL of ECL solution. The blots were incubated for 1 min with the ECL solution and luminescence was detected with the CCD camera.

3. Results

3.1. MYCN determines growth phenotype

3.1.1. Model systems to examine MYCN effects on cell cycle

The effect of MYCN on cell cycle progression and response to chemotherapy was studied in two *MYCN*-regulatable neuroblastoma cell lines: SHEP TET21N (later TET21N) and IMR5/7. TET21N is a non-*MYCN* amplified, p53 wild-type cell line, which harbors a tet-off system with transgenic inducible *MYCN* expression (Lutz et al., 1996). In this system *MYCN* can be switched off by the presence of doxycycline in the media, Figure 6A. IMR5/75 are *MYCN*-amplified cells, containing around 75 copies of the *MYCN* oncogene and harboring tet-inducible shRNA against *MYCN*, (Muth et al., 2010). In these cells, by adding doxycycline to the media MYCN protein expression can be reduced to approximately 35%, Figure 6B. These two cell lines provide two complementary means of controlling the MYCN level, with tunable inducible overexpression of integrated *MYCN* transgene in TET21N cells and tunable knockdown in *MYCN*-amplified IMR5/75 cells.

Cell cycle analysis of exponentially growing cells revealed that switching MYCN expression to high or low levels influences the proportion of cells in different cell cycle phases. Thus, under MYCN-high conditions cells have a higher fraction of cycling cells (S and G2/M) and a lower fraction of cells in G1 when compared to MYCN-low conditions, Figure 6C,D. Live-cell imaging of TET21N cells revealed that MYCN accelerates cellular proliferation, Figure 6E. The calculated average doubling times were 13.8 hours for MYCN-high cells versus 18.2 hours for MYCN-low cells.

The main advantage of using TET21N cells is that they can be used for live-cell imaging and analysis on the single cell level. TET21N cells belong to the substrate adherent type of neuroblastoma cells and are characterized by a flat oval nucleus with abundant cytoplasm. These features allow easy and precise segmentation and tracking of cells. In contrast, IMR5/75 cells belong to the neuronal type and are characterized by a round nucleus, high nuclear to cytoplasm ratio and a low substrate adherence, which makes them extremely difficult to analyze on the single

cell level. Therefore, in the present study the TET21N cell line was predominantly used to examine the effects of MYCN in the single cells.

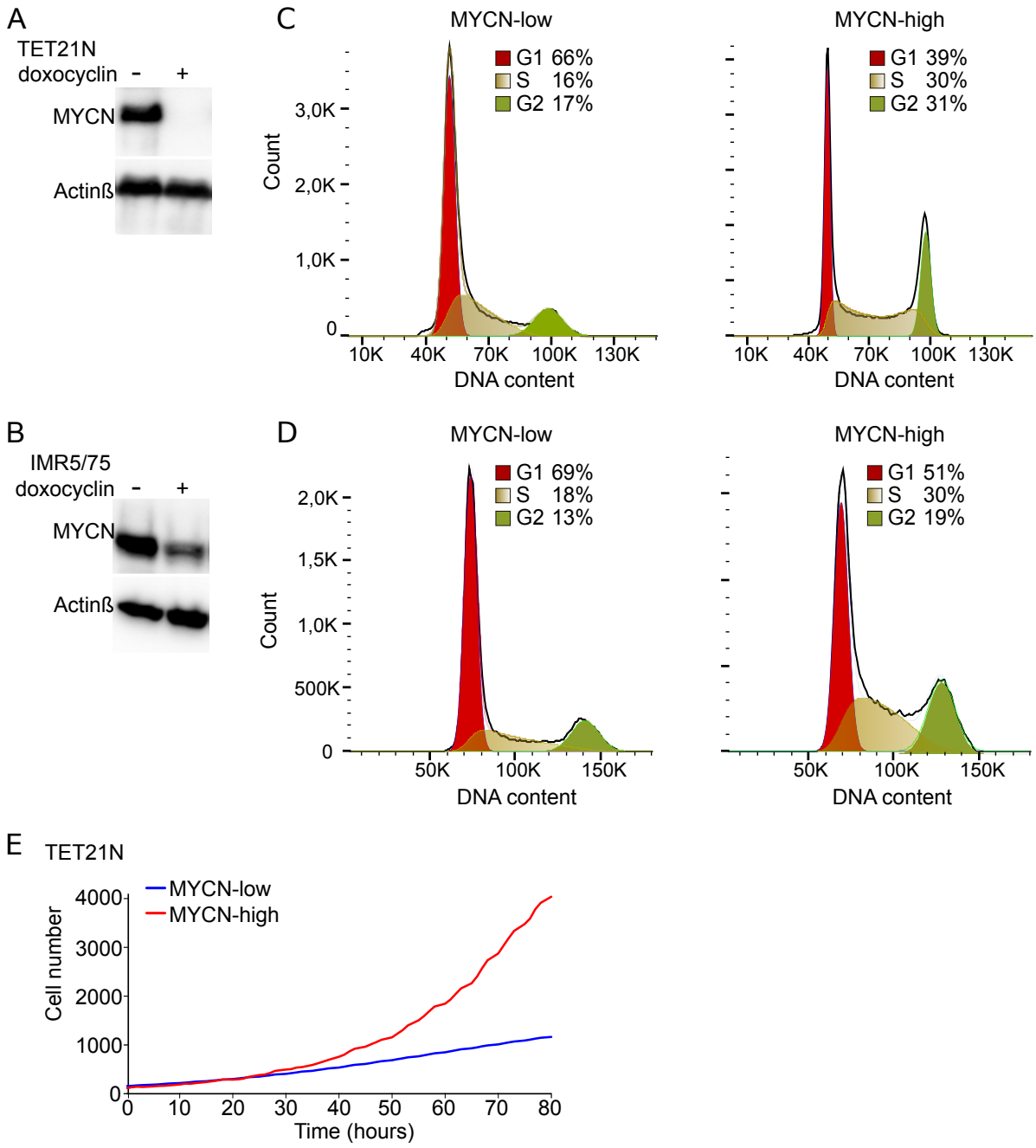

Figure 6. MYCN influences cell cycle and cell growth in *MYCN*-amplified and *MYCN*-overexpressing cell lines A. Western blot analysis of MYCN protein expression in TET21N cells measured 48h after incubation in medium with or without of doxycycline. **B** Cell cycle in TET21N cells under MYCN-high and MYCN-low conditions measured by FACS. **C** Western blot analysis of MYCN protein expression in IMR5/75 cells measured 48h after incubation in medium with or without of doxycycline. **D** Cell cycle in IMR5/75 cells under MYCN-high and MYCN-low conditions measured by FACS. **E** MYCN-dependent growth curves in TET21N cells. Cells were imaged for 80h and the absolute cell numbers were calculated using FIJI software.

3.1.2. MYCN shortens lengths of cell cycle phases

To better understand the effect of MYCN on cell cycle progression and to monitor cell cycle phases in individual living cells the FUCCI system was used. EGFP-Geminin construct was transfected into TET21N cells. EGFP-Geminin slowly accumulates in cells after division, reaches maximum levels as cell enter mitosis, and then rapidly degrades during cytokinesis, Figure 7A,C. The mCherry_Cdt1 construct was transfected into TET21N and into IMR5/75 cells. Cdt1 is highly expressed in G1 phase, but after G1/S transition Cdt1 level rapidly drops and in G2 phase cells remain mostly Cdt1 negative, Figure 7B,C.

To observe cell cycle progression directly in individual cells, live cell imaging of TET21N cells with FUCCI sensors was performed. The dynamics of Cdt1 and Geminin expression allow do determine the lengths of cell cycle phases in single cells even if cells transfected with only one of the FUCCI sensors, Figure 7C. Analysis of single cells with Cdt1 FUCCI marker showed fast G1/S progression of MYCN-high cells, with lower Cdt1 accumulation, versus long residence in G0/1 in MYCN-low cells with higher Cdt1 accumulation. Geminin FUCCI marker also revealed that MYCN-high cells transit from G1 into G2 earlier as compared to MYCN-low cells and have lower accumulation of Geminin during G2 phase, Figure 6D.

Imaging and analyzing of cells with FUCCI sensors identified that high MYCN levels decrease the total length of cell cycle, Figure 7E. This MYCN effect exerted mainly in G1, with MYCN-high cells showing faster and more synchronous G1/S transitions. However, also the S/G2/M duration was shorter in MYCN-high cells.

These findings indicate that MYCN accelerates the cell cycle entry by shortening the lengths of both cell cycle phases, whereas the G1 phase appears to be more affected by MYCN.

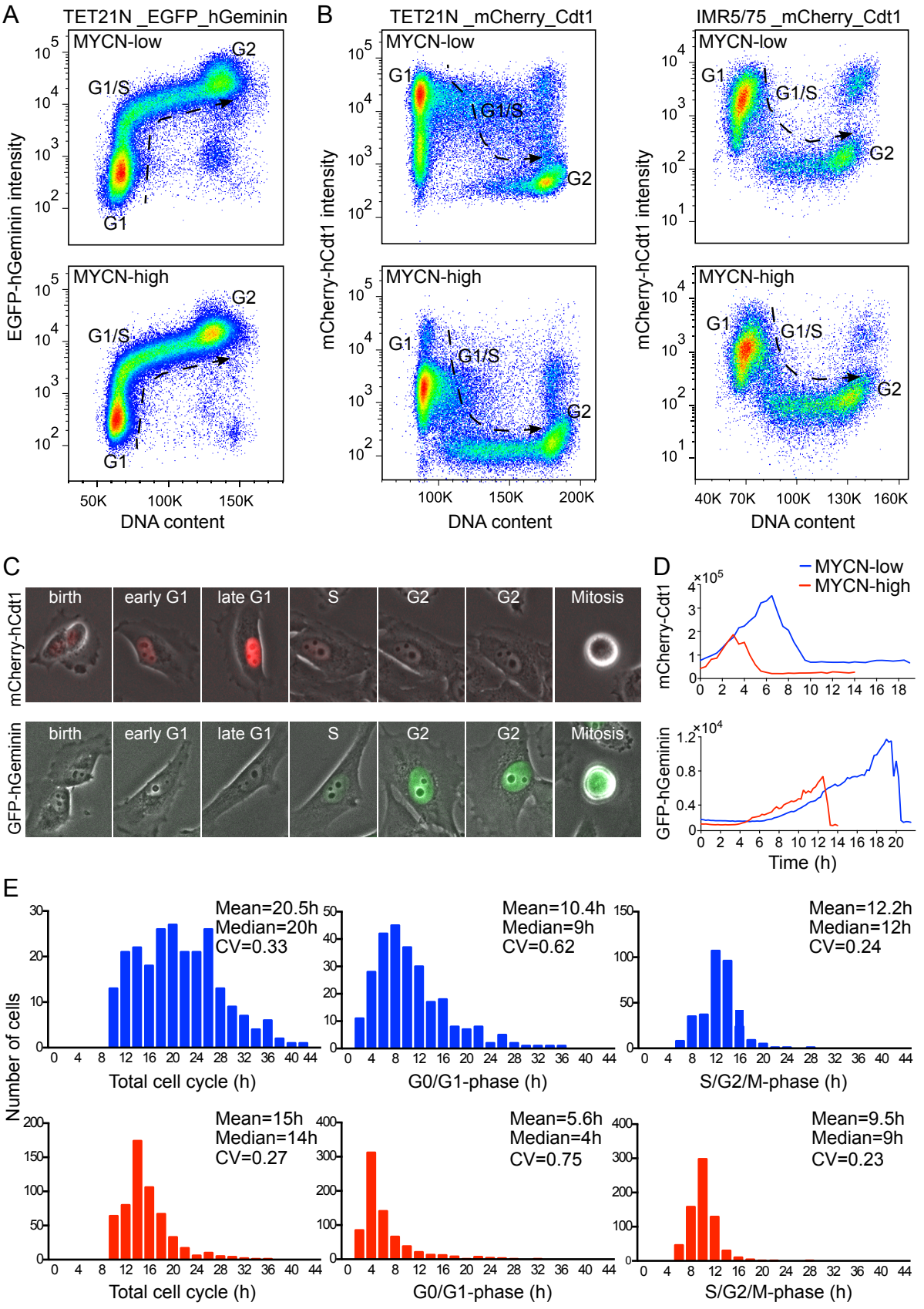

Figure 7. MYCN shortens G1 cell cycle phase. A FACS analysis of Geminin expression throughout the cell cycle in TET21N cell stably transfected with GFP-Geminin construct. **B** FACS analysis of Cdt1 expression throughout the cell cycle in TET21N and IMR5/75 cells stably transfected with mCherry-Cdt1 construct. **C** Single-cell resolved cell cycle dynamics for TET21N

cells with mCherry-Cdt1 (red) and for TET21N cells with GFP-Geminin (green) captured by time-lapse microscopy. **D** Quantification of fluorescence intensity of G1 or G2 FUCCI markers in TET21N single cells. For mCherry-Cdt1 a rapid reduction in Cdt1 intensity indicates S-phase entry. For GFP-Geminin cells an increase in Geminin intensity indicates S-phase entry. **E** Distribution of total cell cycle lengths and duration of cell cycle phases of MYCN-low (blue) and MYCN-high (red) populations in TET21 cells.

3.2. MYCN sensitizes cells to chemotherapy-induced death and drives cellular regrowth after chemotherapy

3.2.1. TET21N cells have active cell cycle checkpoints after DNA damage

After showing that MYCN accelerates the cell cycle in untreated cells, it was analysed how MYCN affects the cells cycle arrest and checkpoints activation during DNA damage. For this, TET21N cells were treated with the DNA-damage inducing chemotherapeutic drug, doxorubicin (DOX), which is commonly used to treat neuroblastoma.

Cell cycle progression of DOX treated cells was analysed by FACS and the proportion of proliferating (S phase) cells was visualised by EdU staining. Analysis of cell cycle showed that G1/S checkpoint was activated after 9 hours of treatment in MYCN-low cells and after 12 hours of treatment in MYCN-high cells. Which was indicated by the abolishing of cells in the S phase, Figure 8A. This resulted in an extended arrest of MYCN-low and MYCN-high cells in both G1 and G2 cell cycle phases.

To investigate the cell cycle transitions on the single cell level the live-cell imaging of TET21N_Cdt1 cells during DOX treatment was performed. Tracking of single cells showed that both G1/S and G2/M checkpoints were affected by MYCN, Figure 8B,C. First, MYCN-high cells were shown to transit from G1 to S and from G2 to M approximately 2 to 3 hours longer when compared to MYCN-low cells, which suggests the delayed activation of the cell cycle checkpoints in the presence of MYCN. Second, MYCN increased the proportion of cells making checkpoint transitions after DNA damage. Thus, 78% of G1 MYCN-high and 53% of G1 MYCN-low cells proceeded into S phase. The G2/M transition was observed in 32% and 54% of G2 cells with low and high MYCN respectively, Figure 8C.

Taken together, both MYCN-low and MYCN-high cells arrest in G1 and G2 phases after DOX treatment. Strikingly, the cell cycle arrest occurs only several hours after induction of DNA damage and cells still have time to move from one cell cycle phase to the next. MYCN delays the activation of the cell cycle checkpoints and increases the proportion of transiting cells.

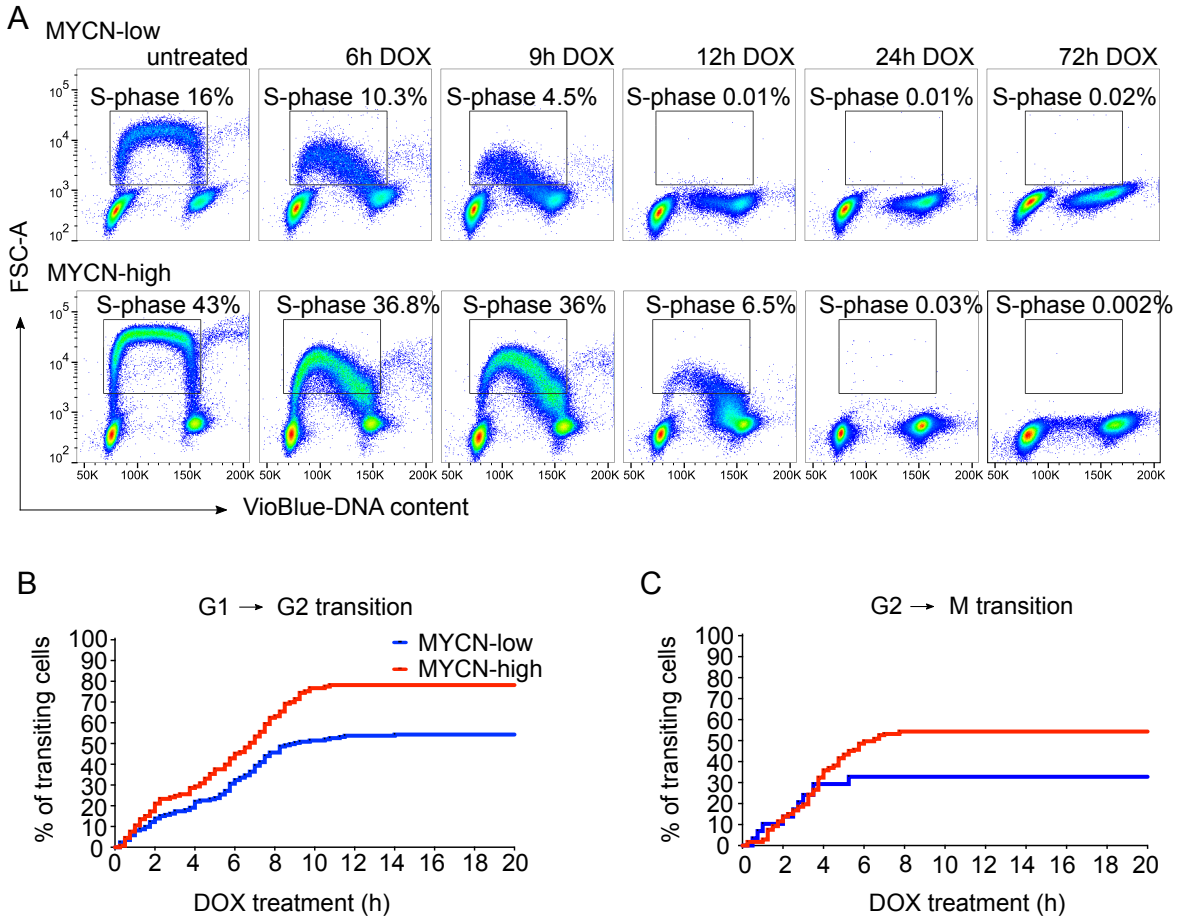

Figure 8. TET21N cells have active cell cycle checkpoints after DNA damage. A Cell cycle progression of cells treated with DOX for 24h at different time points measured by FACS. DNA synthesis (S-phase) determined by EdU incorporation versus DNA content. n=3; a representative experiment is shown. **B** Transitions of cells through G1/S, and **C** through G2/M cell cycle checkpoints at the first 20 hours during DOX treatment. TET21N_Cdt1 cells were imaged every 15 minutes. Cell cycle transitions were determined according to changes in Cdt1 intensity. Cells were tracked in FIJI using the plugin MTrackJ for manual tracking.

3.2.2. MYCN sensitizes cells to chemotherapy-induced death and rescues cells from cell cycle arrest.

After finding that DNA damage induces cell cycle arrest in both MYCN-low and MYCN-high cells it was examined how MYCN influences cellular behaviors after treatment. For this, 72h after DOX treatment the drug was washed-out and cells were subsequently incubated in drug-free media and analyzed at different time points, Figure 9A.

The analysis of extended live-cell imaging showed that during treatment cells underwent cell cycle arrest and the fraction of cells died, as indicated by decrease in relative cell numbers, Figure 9B. MYCN-high cells were more sensitive to cell death during and after treatment. Interestingly, after prolonged incubation in drug-free media, MYCN-high cells showed the capacity to regrow, whereas MYCN-low cells stayed arrested and the cell numbers were slowly decreasing. The FACS analysis of dead cells, shown by Sub-G1 fraction, also revealed that MYCN-high cells were more sensitive to death when compared to MYCN-low cells. However, when MYCN-high cells regrew after chemotherapy the cell death rates decreased and were compared to those of untreated cells, Figure 9C. The MYCN-low cells, however, continued to slowly increase the proportion of dead cells.

Visualizing the proliferating cells using EdU staining showed that after drug removal MYCN-low cells were not able to escape the cell cycle arrest obtained during treatment, Figure 9D. In contrast, a proportion of treatment-arrested MYCN-high cells were able to resume the cell cycle within less than three days after DOX washout. The proportion of proliferating cells was increasing with the longer incubation of cells in drug-free medium.

Additionally, the expression of Ki67 protein, which is known to be present only in proliferating cells, was investigated. Untreated MYCN-low and MYCN-high cells were positive for Ki67 immunostaining, however during treatment the Ki67 expression disappeared suggesting that cells were not proliferating, Figure 10. After treatment, as already expected, MYCN-low cells remained Ki67-negative as expected, whereas regrown MYCN-high cells reestablished Ki67 expression.

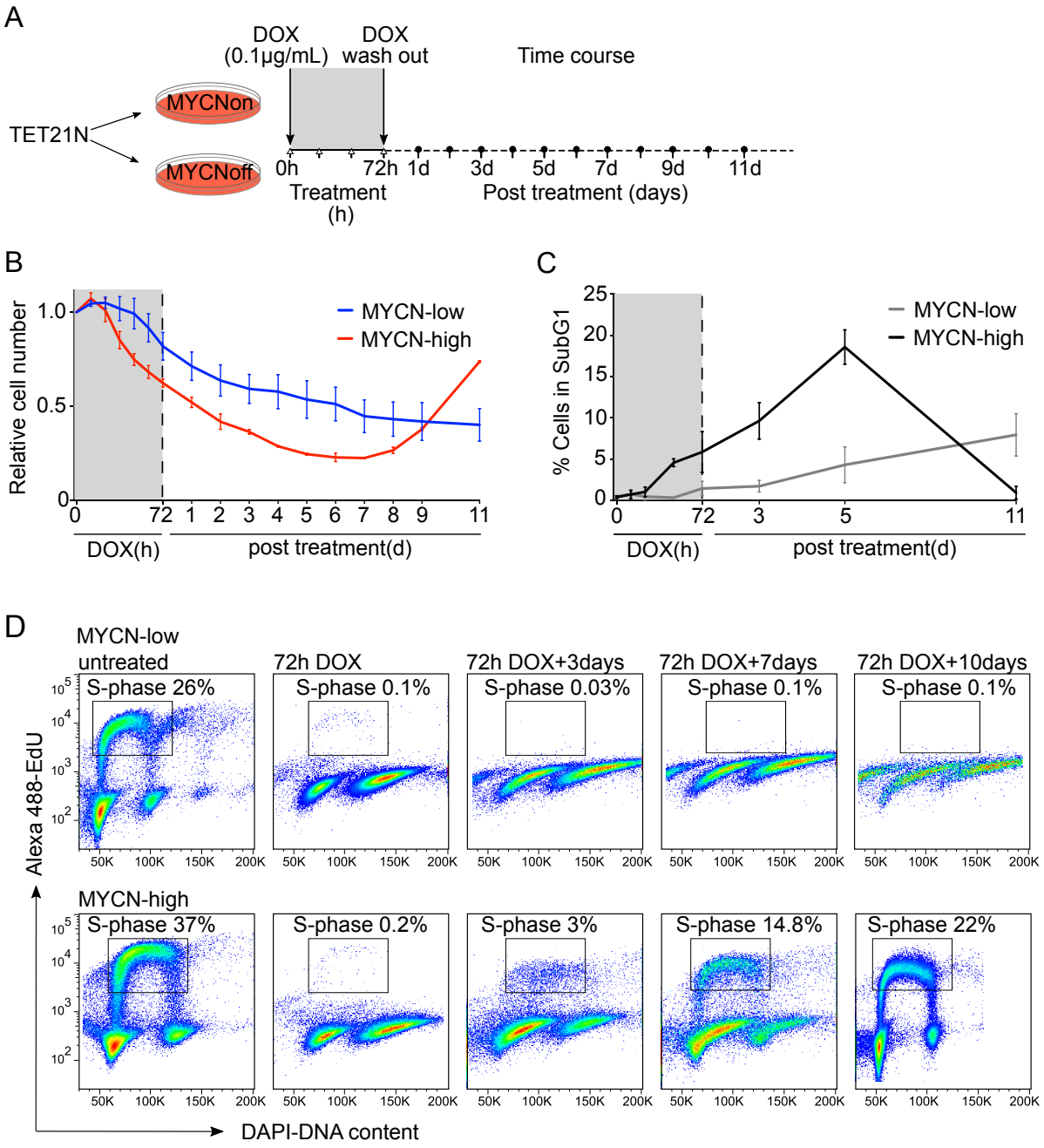

Figure 9. MYCN sensitizes cells to chemotherapy-induced death and drives cellular regrowth after chemotherapy. A Experimental approach: cells were pre-incubated with +/- doxycycline to obtain MYCN-low and MYCN-high status and treated with 0.1µg/ml DOX for 72h. After treatment DOX was washed out and cells were subsequently incubated in drug-free medium for indicated time points. **B** Relative cells numbers of population dynamics captured by live-cell imaging. MYCN-low and MYCN-high populations treaded with DOX for 72h and subsequently incubated in drug-free medium. Cells were imaged every 20 min. Grey area indicates time of DOX treatment. Mean ±SD, n=2. **C** Cell death measured by gating Sub-G1 fraction from DNA content using FACS. Grey area indicates time of DOX treatment. Mean ±SEM, n=3 **D** Cell cycle progression of cells treated with DOX for 72h and subsequently incubated in drugs-free medium for 10 days. DNA synthesis (S-phase) determined by EdU incorporation versus DNA content. n=3; a representative experiment is shown.

Taken together, MYCN sensitizes cells to death during and after chemotherapy. Nevertheless, the remaining cells are able to escape drug-induced cells cycle arrest and re-establish cell proliferation. Cells with low MYCN level stay arrested after chemotherapy.

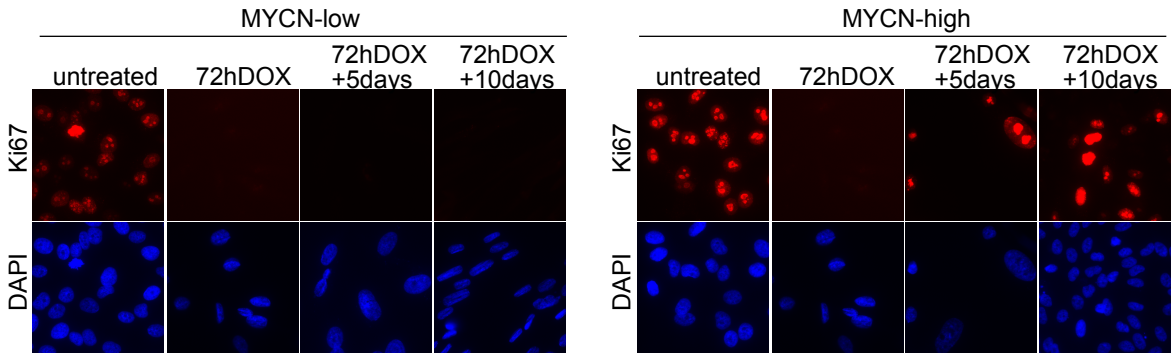

Figure 10. MYCN-high cells restore expression of proliferation marker Ki67 after DOX treatment. Cells were collected at indicated time points and immunostained with the Ki67 antibody following by fluorescent antibody. DAPI used as a nuclear marker. n=3; representative experiment is shown.

3.2.3. MYCN rescues cells from chemotherapy induced cellular senescence

Next, the phenotypical responses of cells during and after treatment were investigated. Live-cell imaging showed that during DOX treatment, when both MYCN-low and MYCN-high cells were arrested, the Cdt1 was overexpressed in G1 and G2 cells cycle phases, Figure 11. After treatment the majority of MYCN-low cells stayed arrested. The arrested MYCN-low cells obtained certain morphological features, such as flattened shape and enlarged nuclei, which are the characteristics of senescent cells, Figure 11A. Indeed, staining of MYCN-low cells for the senescence marker, senescence associated β-Galactosidase (SA-β-Gal), revealed positive SA-β-Gal activity, Figure 12A. Interestingly, the proportion of cells positive for the SA-β-Gal marker increased continuously and 14 days post treatment more than 90% of cells were stained positive for senescence, and overexpressed Cdt1, Figure 12C, 11A.

MYCN-high cells displayed greater phenotypic variability after DOX washout, Figure 11B. A fraction of cells died after treatment without entering the cell cycle. A subpopulation of the MYCN-high cells was able to resume the cell cycle within less

than three days after treatment wash out and entered mitosis. Most of these cells failed to correctly carry out the cytokinesis, which resulted in undivided cells with two nuclei or cells with fragmented nuclei. The multinuclear cells died soon after mitosis. A minority of cells could divide successfully into two normally looking daughter cells, which progressed in the cell cycle and gave birth to new cells. These properly dividing cells after treatment were named ‘resister’ cells.

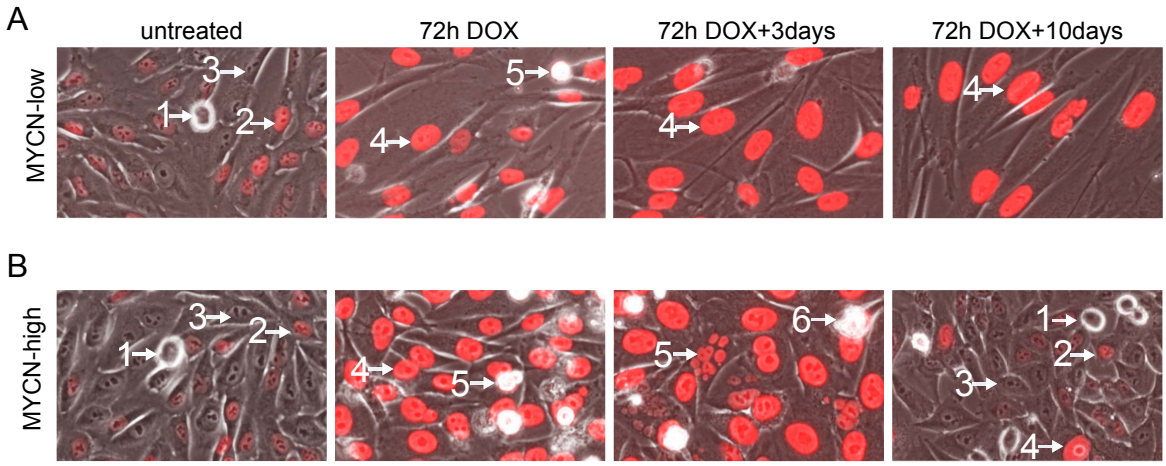

Figure 11. Different cell fates after treatment visualized by live-cell imaging. Live cell imaging of TET21N-Cdt1 treated with DOX for 72h and subsequently incubated in drug-free medium. During treatment cells arrest and accumulate mCherry-hCdt in all cell cycle phases. Examples of cells in 1-mitosis; 2-G1 phase; 3-G2 phase; 4-arrested cell; 5-dead cell after treatment; 6-multinuclear cell after failed cell division.

Early after treatment, the majority of MYCN-high cells were positive for SA-β-Gal activity. Nevertheless, over the time the senescent population became diluted by the regrowing resisters, which looked phenotypically similar to the untreated cells. The resister cells had the same shape and nuclear size as cells before treatment, were negative for SA-β-Gal, and the Cdt1 was expressed only in G1 phase, Figure 11B, 12B-D.

Taken together, MYCN is required to escape chemotherapy-induce senescence through cell cycle re-entry. In a majority of cases, the cell cycle re-entry sensitized cells to death after mitosis, but in very few cases MYCN-driven cells were able to proliferate successful after treatment.

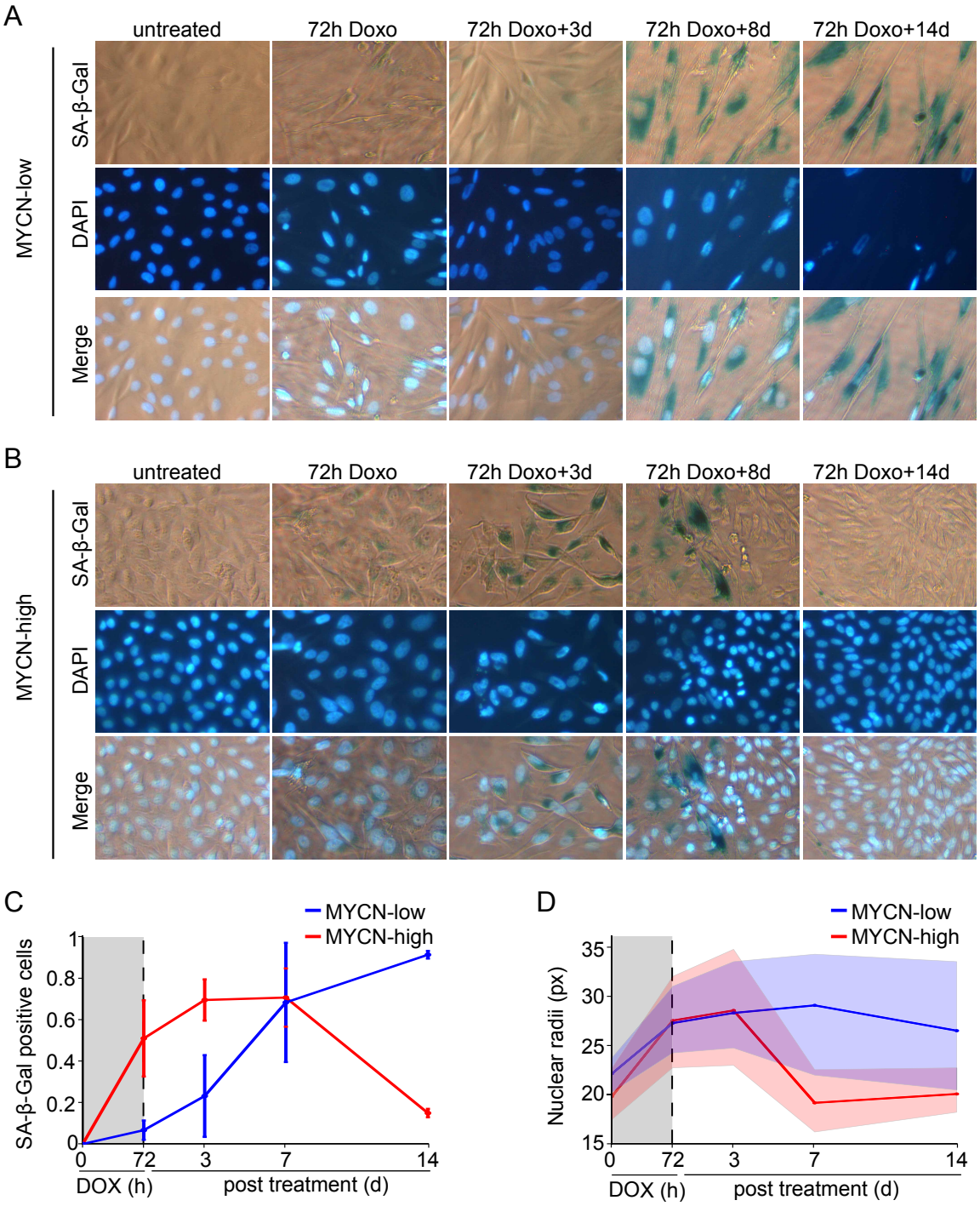

Figure 12. MYCN rescues cells from chemotherapy induced cellular senescence. A, B Senescence associated β-Galactosidase (SA-β-Gal) staining of MYCN-low (B) and MYCN-high cells at different time-points after DOX treatment. DAPI used as a nuclear marker. n=3; representative experiment is shown. **C** Quantification of SA-β-Gal positive cells. Analysis was performed by FIJI software, Mean ± SD, n=2. **D** Changes of average population nuclear radii sizes in TET21N_Geminin_53BP1 cells after DOX treatment. Sells were segmented according to nuclear expression of 53BP1 and nuclear radii were analyzed by FIJI. Grey area indicates time of DOX treatment. Shadow areas represent population deviations.

3.2.4. MYCN-driven regrowth is clonal and not heritable

To better characterize the resister cells their properties of regrowth were analyzed. It was observed that after DOX treatment MYCN-low cells looked untighten and homologously distributed in the cell culture dishes, whereas regrown MYCN-high cells were concentrating in dense colonies, Figure 13A. The analysis of clonogenicity showed that MYCN-low cells were not able to build sufficient colonies after treatment, Figure 13B. In contrast, MYCN-high cell showed clonal regrowth and the colonies were growing over time.

Next, it was tested whether the MYCN-driven cellular regrowth can also be observed in MYCN-amplified cell lines. Two cell lines IMR5/75 and IMR32 with shRNA against MYCN were used and the regrowth after three different DOX concentrations was tested. In general, MYCN-amplified cell lines are more sensitive to DOX chemotherapy, therefore after treatment with 0.1 µg/mL DOX almost all cells were died and only a few colonies in MYCN-high IMR5/75 cells were observed, Figure 13C. After treatment with 0.05 µg/mL DOX the IMR5/75 and IMR32 cells showed clonal regrowth at MYCN-high conditions and no regrowth was observed at MYCN-low conditions, Figure 13C,D. The reduction of DOX concentration to the very low level, 0.025 µg/mL, resulted in regrowth of both MYCN-low and MYCN-high cells but the colonies with MYCN were growing much faster as compared to cells without MYCN.

To investigate whether the therapy selected for genetically distinct subpopulations that are immune to DOX, resister cells were characterized more closely. The growth rates of the resister and untreated cells were found to be similar, Figure 14A. Exposing the resister cells to a second treatment with DOX resulted again in clonal regrowth with a comparable number of colonies as after the first treatment, Figure 14B. Thus, resister cells showed the same probability to regrow as the untreated population.

Thus, for all tested cell lines the regrowth was MYCN-dependent and clonal, suggesting that only a small fraction of cells resisted therapy. Importantly, resister cells did not have a higher probability to survive subsequent treatment pulses indicating that non-genetic heterogeneity rather than selection of genetic subpopulations was responsible for resistance.

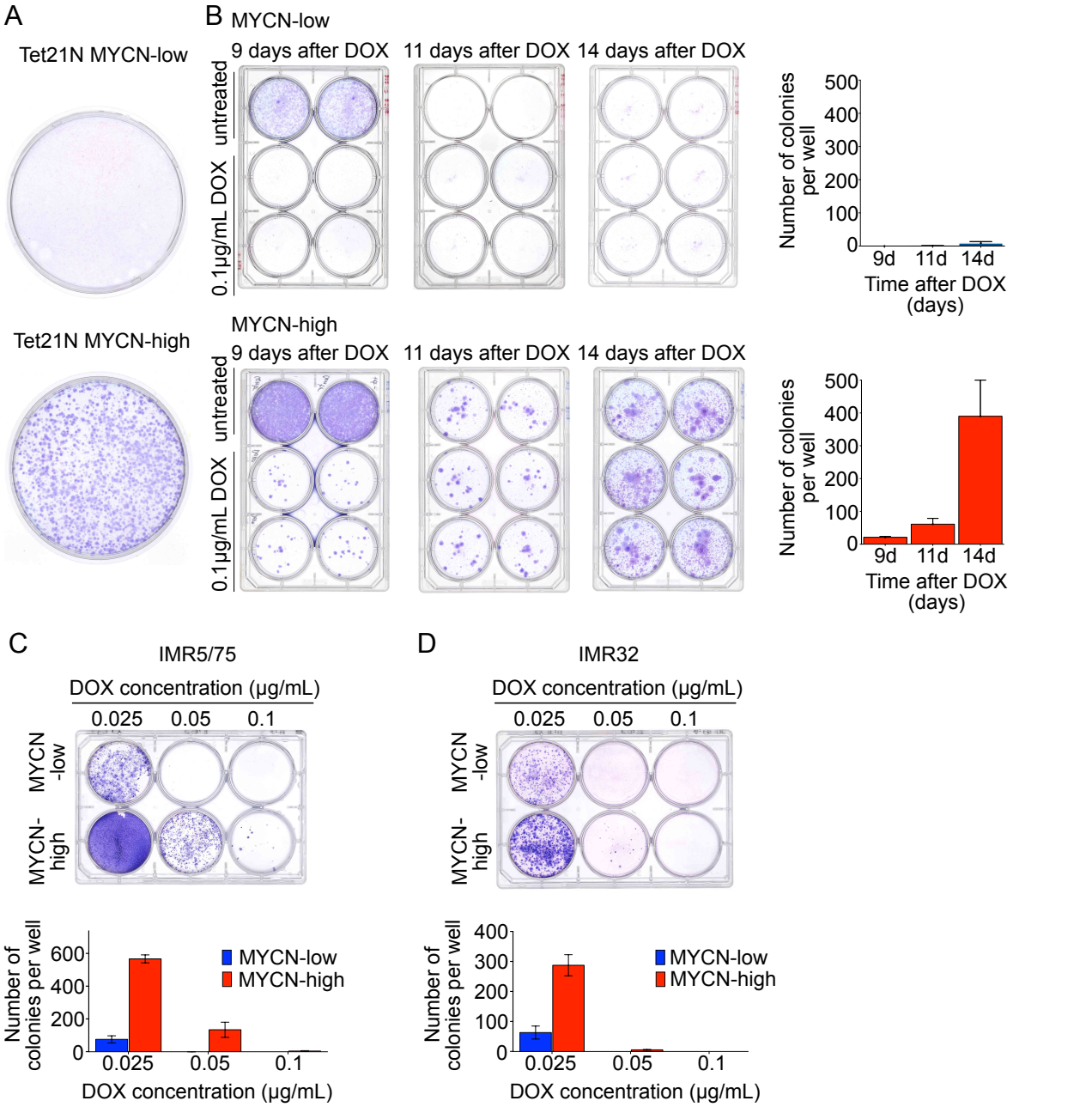

Figure 13. Clonal regrowth of MYCN-high cells. A 10^6 TET21N MYCN-low or MYCN-high cells were seeded in 10cm^2 dishes and treated with 0.1µg/ml DOX for 72h. 9 days after treatment cells were fixed with 4% PFA, stained with methylene blue and imaged. **B** MYCN-low and MYCN-high cells were treated with 0.1µg/ml DOX for 72h, after treatment 10000 cells were reseed into 6-well plates. After indicated period of time colonies were fixed with 4% PFA, stained with methylene blue and imaged. The number of colonies was counted using FIJI's particle analyzer. IMR5/75 (**C**) and IMR32 (**D**) cells were treated with three different DOX concentrations for 24 hours. Staining and quantification of colonies was performed 14 days after reseeding with the same protocol as in **B**. Mean ±SEM, n=3

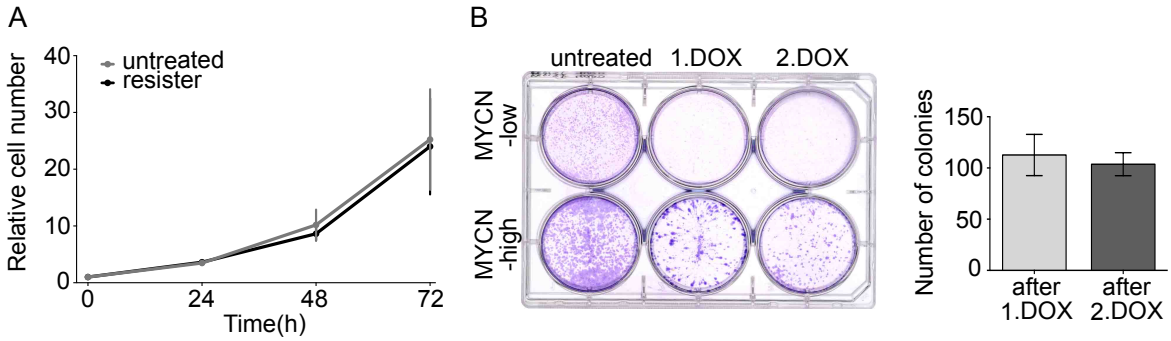

Figure 14. Regrowth of MYCN-high cells is not heritable. A Growth kinetics of untreated and resister cells. Resister cells, which survived first treatment with DOX, were incubated for one week in the cell culture. The growth rate of resister cells was compared with the growth rate of untreated cells by counting the number of cells with MACSQuant analyzer, Mean ±SEM, n=3. **B** Cells were treated with DOX for 24h and 10000 cells were reseeded into 6-well plates. Untreated = without DOX treatment, 1.DOX= first time treatment with DOX, 2.DOX= resister cells which regrown after first DOX treatment were treated second time with DOX. 9 days after treatment cells were fixed with 4% PFA, stained with methylene blue and imaged. The number of colonies was counted using FIJI's particle analyzer. Mean ±SEM, n=3.

3.3. Molecular response to DNA damage

3.3.1. Doxorubicin treatment activates p53 signaling and suppresses cell cycle genes

To explore the role of MYCN on the molecular responses of cells during chemotherapy, proteins and mRNA involved into DNA damage, cell death and cell cycle signaling were analyzed. The DNA damage response pathway was activated during DOX treatment as indicated by the increase of p53 protein and its targets, Figure 15A. In line with a higher cell death rate observed in MYCN-high cells, p53 mRNA and protein were more strongly expressed in untreated and DOX treated MYCN-high compared to MYCN-low cells. The p53 protein levels increased as early as 3 hours after treatment, achieved maximum 9 hours after treatment and started to decline after 18 hours. The p53 mRNA expression was not affected by DOX and stayed constant during the treatment period, suggesting that after DNA damage p53 is regulated on the translational level. The p53 endogenous targets MDM2 and p21 increased significantly 6 hours after treatment. MDM2 protein was

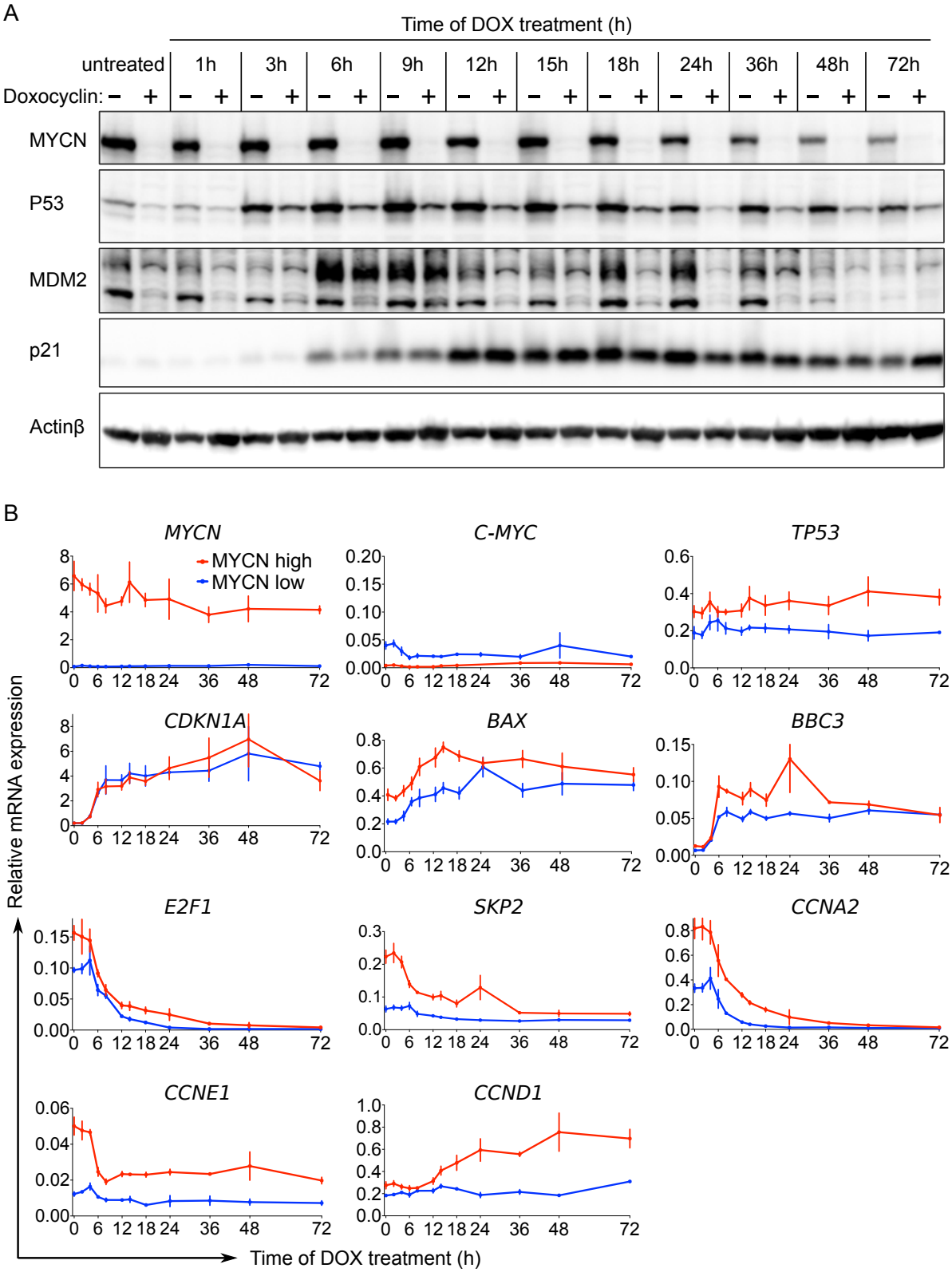

Figure 15. Doxorubicin treatment activates p53 signaling and suppresses cell cycle genes. A Expression of proteins involved in p53 pathway. TET21N Cells were harvested at indicated time points after DOX treatment and lysates were analyzed by western blot. n=3. Representative experiment is shown. **B** Expression of genes involved in p53 and Rb/E2F1 pathways. Cells were harvested at indicated time points after DOX treatment. RNA was extracted, reversely transcribed and expression of genes was quantified via qRT-PCR. Mean ±SEM, n=3

more highly expressed in MYCN-high cells, whereas p21 protein and mRNA expression was comparable in MYCN-low and MYCN-high cells. Further p53 targets, *BAX* and *PUMA*, involved in apoptotic signaling, were more highly activated in MYCN-high cells, Figure 15B. Genes involved in cell cycle regulation e.g. *E2F1*, *SKP2*, *CCNA2*, *CCNE1* were more highly expressed in untreated MYCN-high cells compared to untreated MYCN-low cells. During treatment the expression of the cell cycle genes was strongly reduced for both MYCN conditions, which is consistent with observed cell cycle arrest and activation of p21 during DOX treatment. The expression of *CCND1* continuously increased in MYCN-high cells continuously during treatment.

Thus, during DNA damage TET21N cells activate p53 signaling and downregulate genes responsible for proliferation. MYCN enhances p53 expression, which leads to higher expression of p53 targets genes. However, despite elevated p53 activation in MYCN-high cells, the levels of the cell cycle suppressor p21 were similar to those of MYCN-low cells, suggesting that MYCN suppresses p21 expression.

3.3.2. MYCN-high resister cells overcome transient p53-p21 activation

Phenotypically resister cells displayed the same behavior as untreated cells and appeared to reestablish the untreated population. Therefore, it was analyzed whether resister cells share the same molecular expression patterns as untreated cells. To this end, the activation status of p53 signaling after DOX washout was investigated. The activity of p53 signaling was monitored by its phosphorylation on serine 15 (Ser15) and expression of p21 protein, Figure 15. It was confirmed that p53 signaling was activated during treatment, but after DOX removal MYCN-high and MYCN-low cells displayed different molecular responses. In the senescent MYCN-low cells, p53 phosphorylation and p21 expression remained elevated even after drug removal. In contrast, in MYCN-high cells the continuous decrease of p53 phosphorylation and p21 expression was observed, and 14 days after treatment the expression of these proteins was as low as in the untreated cells.

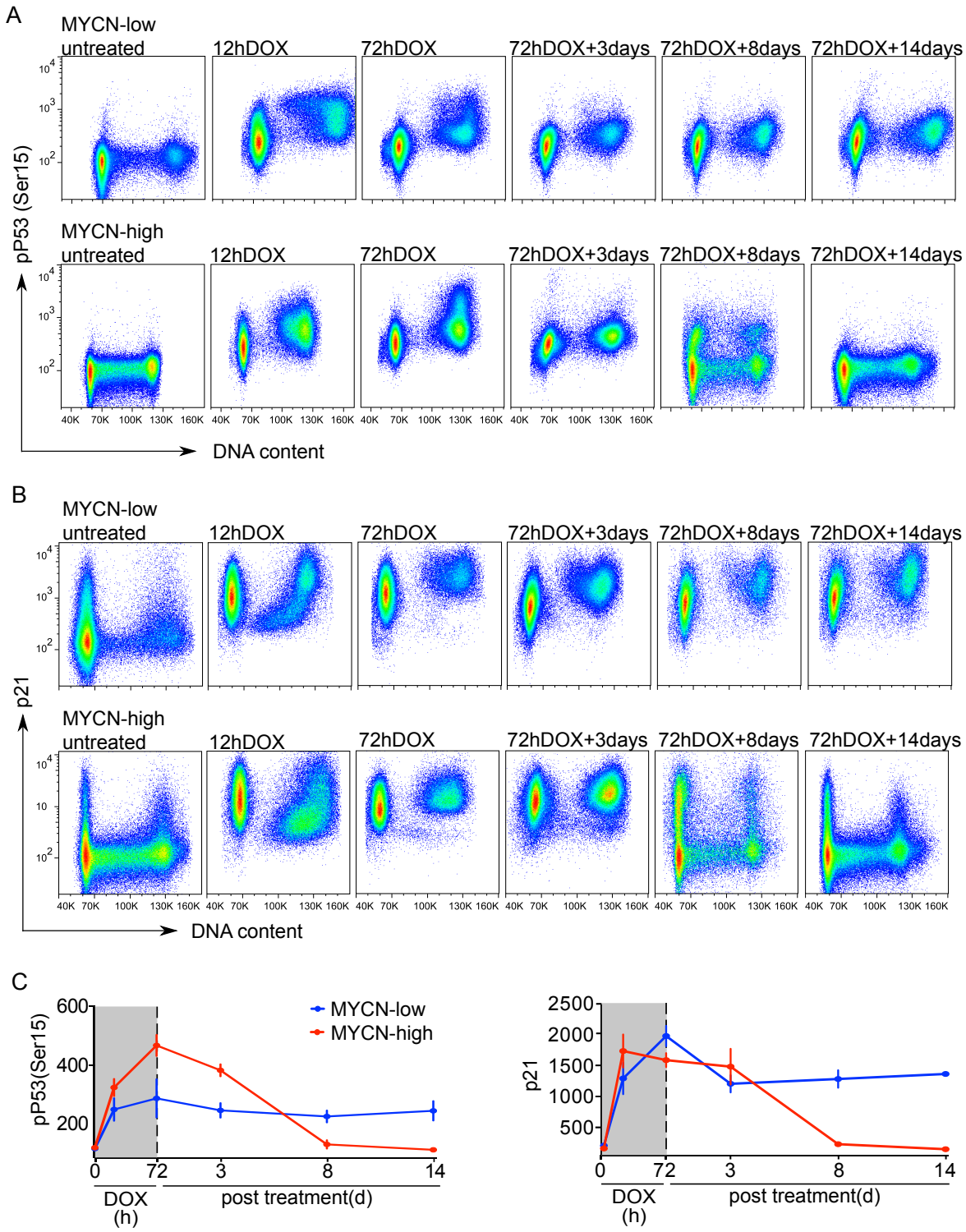

Figure 16. Resister cells recover pre-treatment pP53 (Ser15) and p21 expression. A Expression of p53 protein phosphorylated at Ser15 **B** Expression of p21 protein during and after DOX treatment. Cells were collected at indicated time points, fixed, and stained with conjugated antibodies. The protein intensity versus DNA content was measured by FACS and analyzed by FlowJo. n=3; a representative experiment is shown . **C** Medium intensities of p53 phosphorylated at Ser15 and p21 levels measured in **A**. Mean ±SEM, n=3.

While it is possible that all MYCN-high cells reduced their p53 signaling, it is more likely that this reduction was a result of the observed changes in the composition of the population over time (see Figure 11, 12). Early after treatment the culture was dominated by senescent cells, which were diluted by regrown resister cells that took over the population.

3.3.3. MYCN causes full recovery of transcriptome after therapy

To analyze the cellular responses on the global level, the RNA-Seq of cells before, during and treatment was performed. The analysis of global transcriptome revealed similar dynamics as were observed for the DNA damage response, Figure 17A. MYCN-low cells during and after treatment clustered together, separately from untreated cells, suggesting that senescent cells maintained the treatment-induced expression profile even after drug removal. The transcriptome of MYCN-high cells changed during treatment but returned to the untreated cells over time-course after treatment. Again, this could be explained by continuous domination of resister cell in the population.

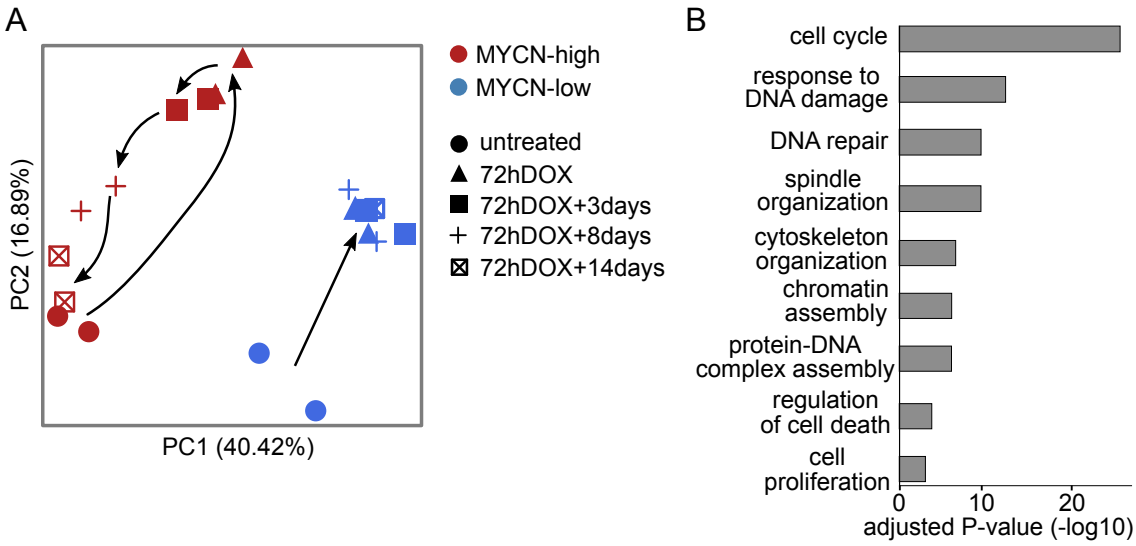

Figure 17. MYCN causes full recovery of transcriptome after DNA damage. A Principal component analysis of whole-genome RNA-Seq data of TET21N cells treated with DOX. Arrows highlight the changes in expression during and after treatment. Cells were harvested, RNA was isolated and libraries for RNA-Seq were prepared and sequenced on Illumina platform. Two biological replicates are shown. **B** Gene ontology enrichment terms ($p<0.05$) of genes showing significant differences in the likelihood-ratio test in response to doxorubicin treatment between MYCN-low and MYCN-high TET21N cells.

Furthermore, 2831 genes showing significant difference between MYCN-high and MYCN-low cells in over the time course were identified via likelihood ratio test. Gene ontology analysis revealed that the identified genes were most highly enriched in the cell cycle, DNA damage response and DNA damage repair pathways, Figure 17B.

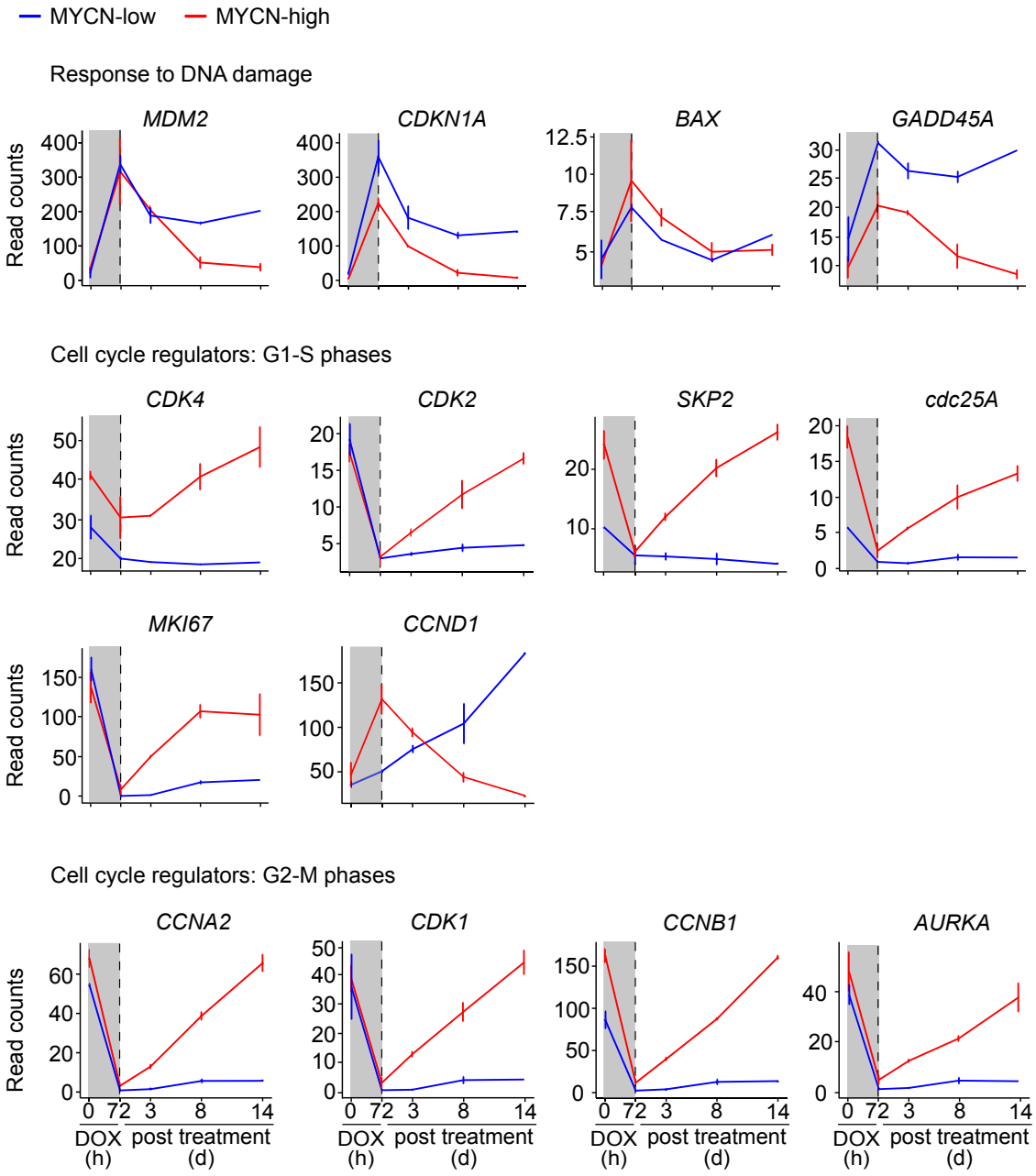

Figure 18. DNA damage and cell cycle pathways are differently activated in resister and senescent cells. RNA-Seq expression of selected genes which show different response to DOX treatment between MYCN-low and MYCN-high populations. Mean ±SEM, n=2.

Examples of selected genes demonstrate that DNA damage response was completely inactivated in MYCN-high cells after regrowth and stay active in senescent cells, Figure18. As expected, *MDM2* expression stays elevated in senescent cells, indicating active p53 signaling. *CDN1A* and *GADD45A*, both p53 target genes and markers for cells cycle arrest, stay highly expressed in MYCN-low senescent cells. Expression of *BAX* in MYCN-low cells was reduced after treatment, suggesting that senescent cells are not sensitive to apoptosis. Cell cycle genes demonstrated that the cell cycle machinery shuts down during treatment and completely recovers after treatment only in MYCN-high cells. This was true for genes involved in G1/S and G2/M transitions. Interestingly, the expression of *CCND1* was highly upregulated in MYCN-low senescent cells, in line with previous reports on senescence (Atadja et al., 1995; Fukami et al., 1995; Lucibello et al., 1993). Whereas in MYCN-high cells the *CCND1* level was first upregulated but when the resister cells dominated the population *CCND1* expression decreased to the level of untreated cells.

3.3.4. MYCN causes full recovery of epigenome after therapy

In addition to genetic changes, the treatment-induced dynamics of epigenetic histone modifications were investigated using ChIP-Seq. The analysis of histone modifications, known to mark active promoters (H3K4me3), Polycomb repressive complex 2-related gene silencing (H3K27me3), and DNA methylation (H3K9me3) was performed. It was found that the read density in these three epigenetic markers decreased during DOX treatment in both MYCN-low and MYCN-high cells, Figure19A. After treatment MYCN-low senescent cells kept low read density for H3K4me3 and numbers of reads for H3K27me3 and H3K9me3 decreased even stronger over time. In MYCN-high cells the read density of all modified histones was recovered to the same or even higher levels. Among these three epigenetic modifications, H3K4me3 demonstrated a recovered read density as early as three days after DOX washout, which may suggest its key role in cell regrowth.

Interestingly, it was found that the expression of histone-specific methyltransferases and demethylases correlated with epigenetic patterns and was in agreement with the reports about cellular senescence, Figure 19B. The loss of methyltransferase

DPY30 and overexpression of demethylase KDM5B, which are both H3K4me3 specific, was observed in MYCN-low cells. H3K37me3 specific modifier, EZH2, was downregulated in MYCN-low senescent cells. KDM6B, a H3K27me3 specific demethylase, was upregulated in MYCN-low cells. The key methyltransferase for

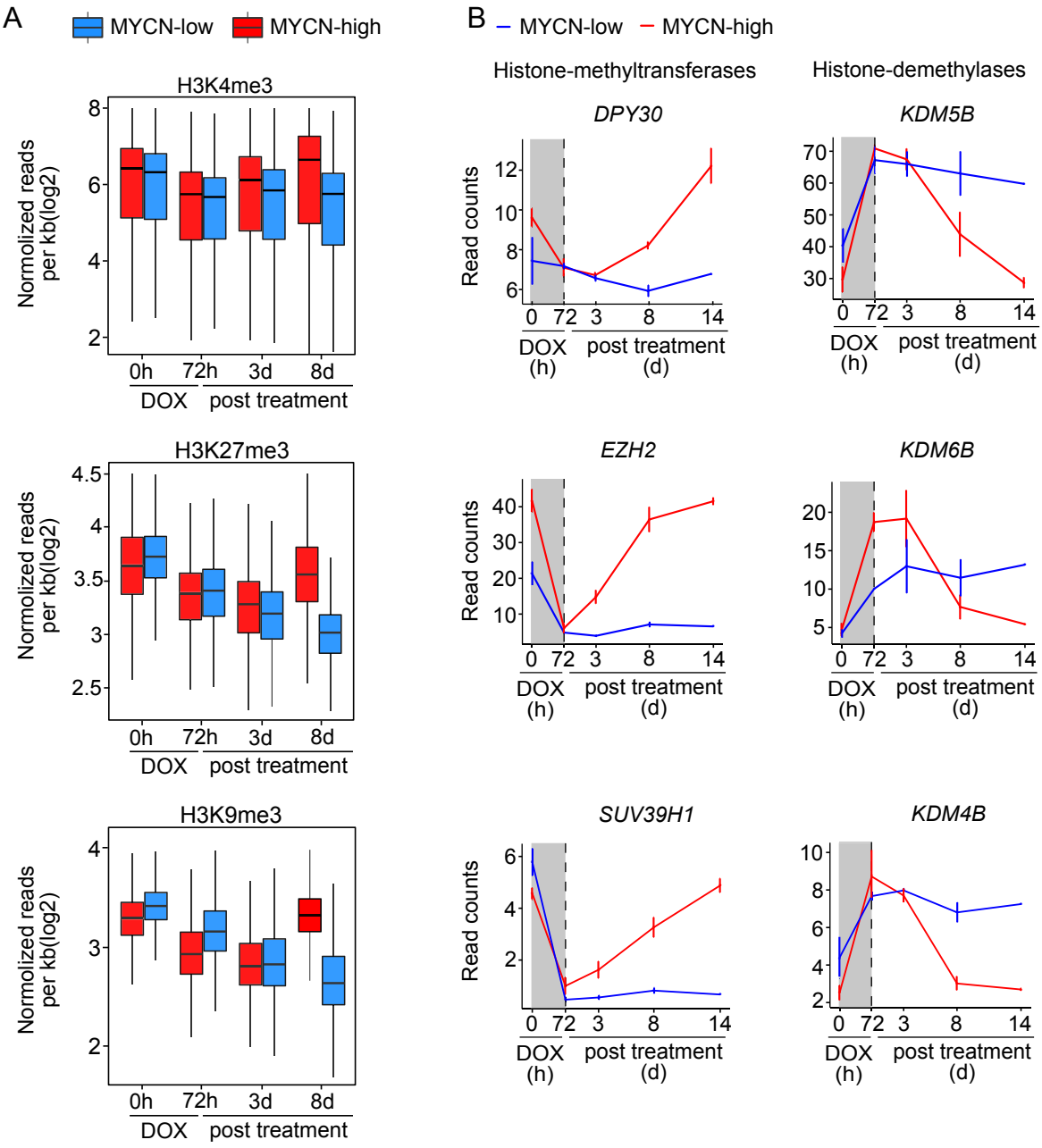

Figure 19. MYCN causes recovery of epigenetic histone marks after therapy. A Treatment induced changes in Chip-Seq occupancy of H3K4me3, H3K27me3 and H3K9me3. Cells were treated with DOX for 72h, harvested at indicate time points, fixed and chromatin-immunoprecipitated with antibodies. DNA libraries were prepared and sequenced on the Illumina platform. Mean ±SEM, n=2. **B** RNA-Seq expression of regulators of histone modifications, Mean ±SEM, n=2.

H3K9me3, SUV39H1 was suppressed in senescent cells but upregulated in the resister cells, which correlate with the recovery of H3K9me3 signals. In contrast, KDM4B, the demethylase for H3K9me3, was elevated in senescent cells and repressed in resister cells.

To summarize, for every molecular profile the studied MYCN-high resister cells re-established the pre-treatment profile, including gene expression, protein, expression and epigenetic histone markers. Whereas the MYCN-low cells exhibited altered molecular profiles after treatment, which may contribute to induction and/or maintenance of the senescence phenotype.

3.3.5. Regrowth after chemotherapy is MYCN and p21 dependent

Upon untreated conditions, MYCN shortens the lengths of cell cycle phases and increases the proportion of cycling cells due to the activation of genes involved into the cell cycle progression and suppression of cell cycle inhibitor p21. It was hypothesized whether MYCN promotes escape from therapy-induced long-term arrest via the same mechanisms as cell cycle transition under normal growth conditions. Therefore it was tested whether regrowth after chemotherapy can be explained by MYCN mediated suppression of p21.

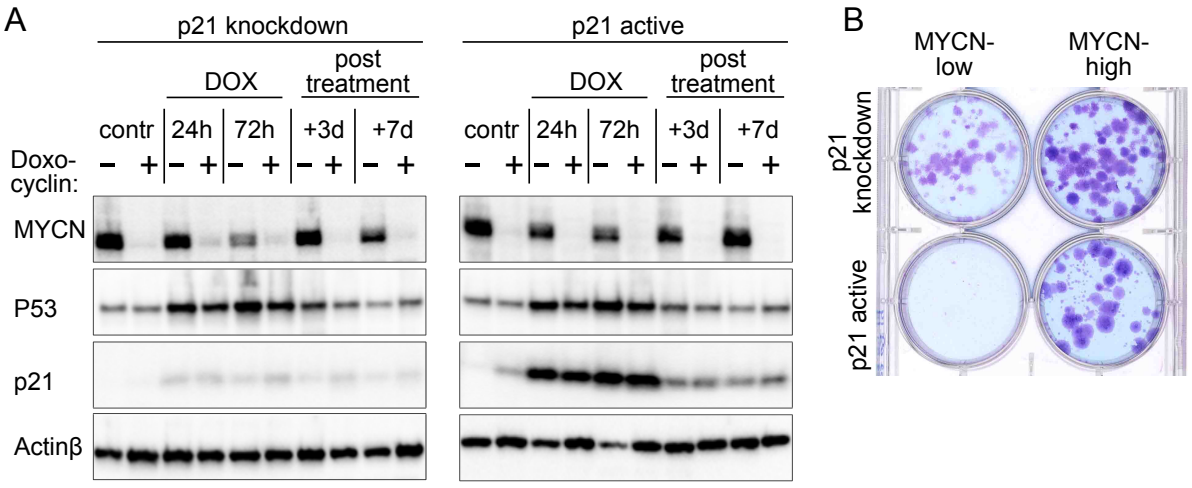

Figure 20. p21 knockdown induces clonal regrowth after DOX treatment in TET21N MYCN-low cells. A Expression of MYCN, p53 and p21 proteins during and after DOX treatment in TET21N cells with stable expression of p21 shRNA (p21 knockdown) and cells with scrambled shRNA (p21 functional). **B** p21 shRNA cells show clonogenic regrowth in both MYCN-low and MYCN-high conditions. Cells were treated with 0.1µg/ml DOX for 72h, after treatment 10000 cells were reseed into 6-well plates. After 14 days colonies were fixed, stained with methylene blue and imaged.

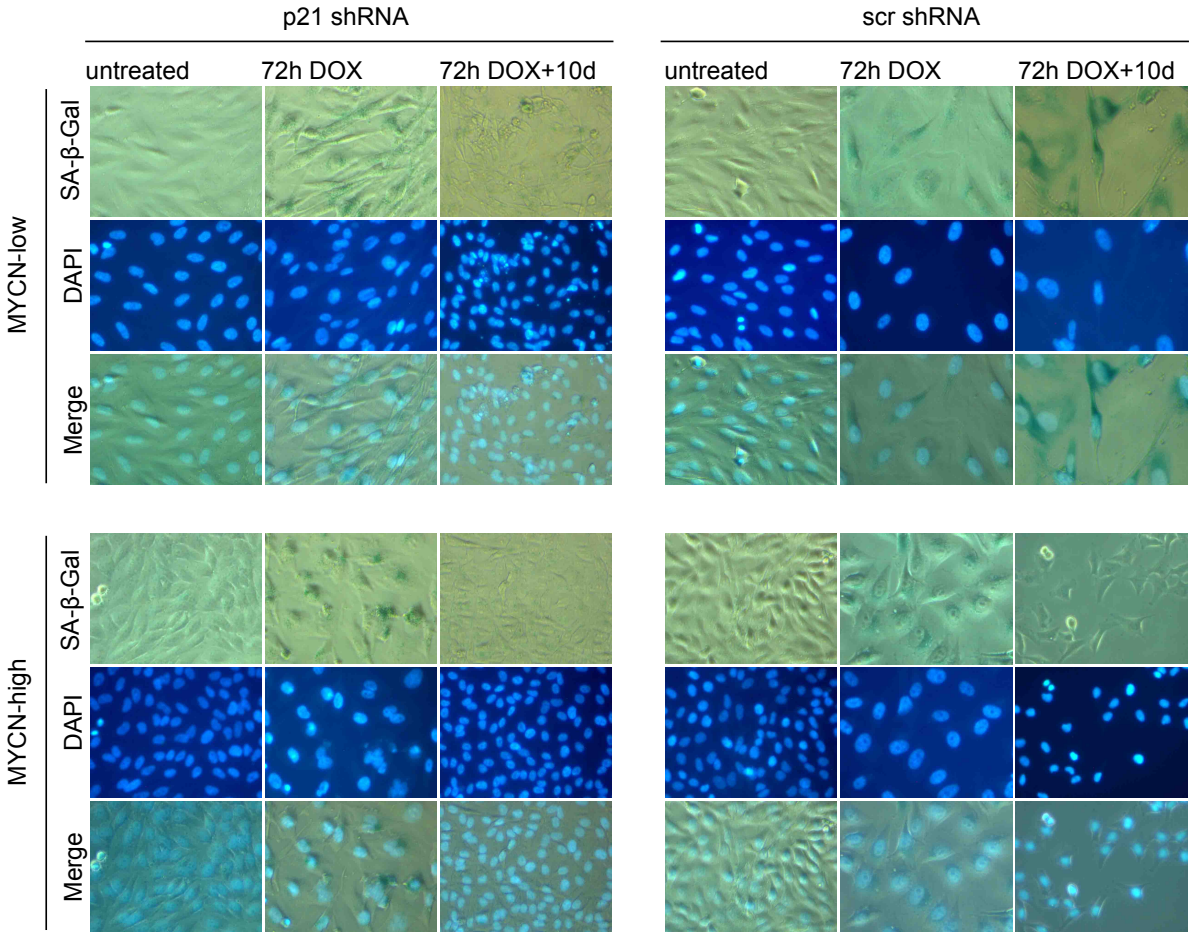

Figure 21. p21 knockdown helps to escape chemotherapy-induced senescence. Senescence associated β-Galactosidase (SA-β-Gal) staining of TET21N p21 shRNA and scr shRNA cells. Cells were treated with DOX for 72h and subsequently incubated in drugs-free medium for 3 days. DAPI used as a nuclear marker. n=3; a representative experiment is shown.

To test this hypothesis the TET21N cells stably expressing shRNA against p21 were used. In these cells p53 signaling is activated by DOX treatment, as indicated by the increase of p53 level, but p21 protein expression stays low, Figure 20A. The colony formation assay revealed that MYCN-low cells with reduced p21 expression were able to build colonies and regrow after DOX treatment, while cells with functional p21 were not able to regrow, Figure 20B. Additionally, it was observed that MYCN-high cells lacking p21 built a higher number of colonies than cells with functional p21.

Furthermore, it was found that p21 expression is crucial for induction and maintenance of drug-induced senescence after DOX treatment. 10 days after treatment MYCN-low cells with scr shRNA had, as expected, a flattened cell shape, enlarged nuclei and stained positive for SA-β-Gal, Figure 21. While the MYCN- low

cells with p21 shRNA, similar to MYCN-high cells, had the same shape and nuclear size as cells before treatment and were negative for SA-β-Gal.

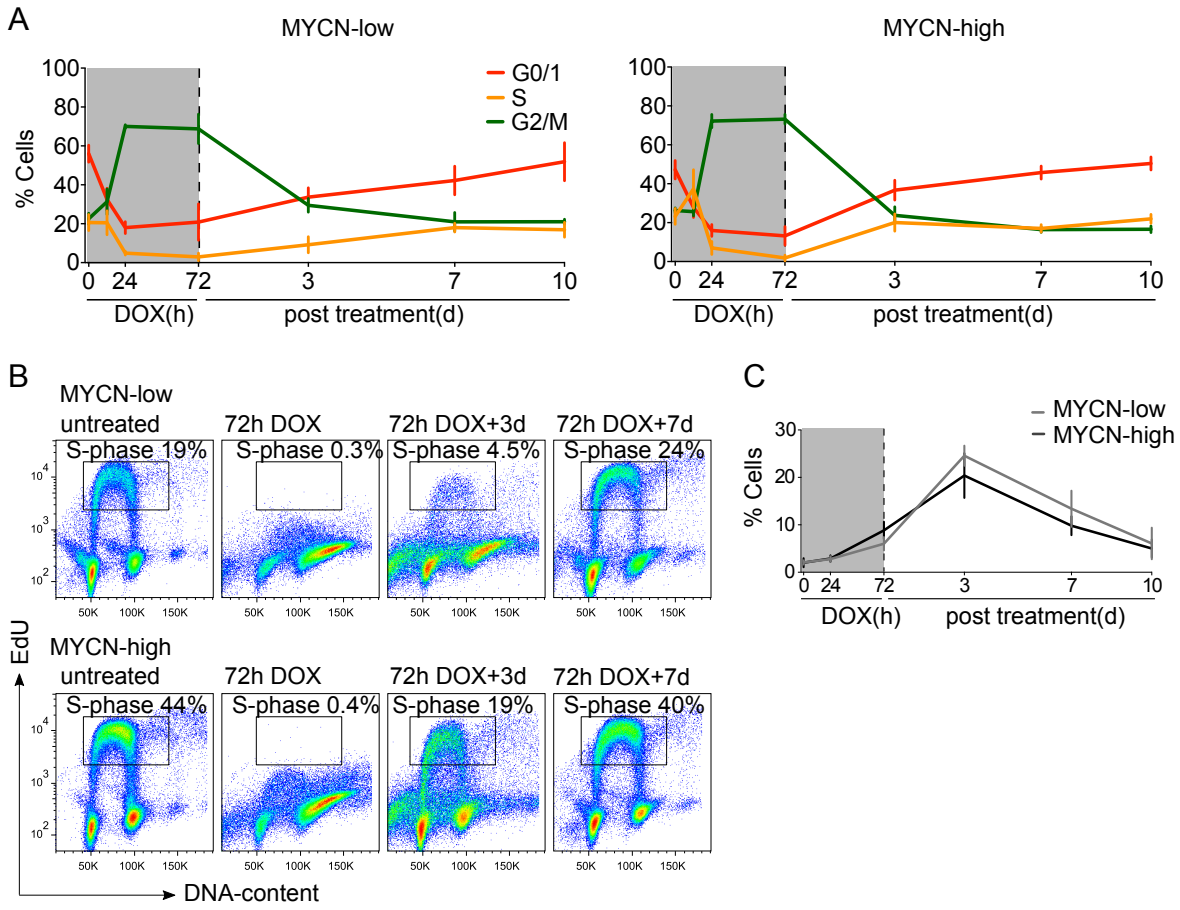

Figure 22. p21 knockdown suppresses G1 arrest and increases cell death during and after treatment. A Time course of cell cycle distributions in TET21N p21 shRNA cells during and after DOX treatment measured by FACS and analyzed by FlowJo. Mean ±SD; n=3. **B** Cell cycle progression of TET21N cells treated with DOX for 72h and subsequently incubated in drugs-free medium for 3 days. DNA synthesis (S-phase) determined by EdU incorporation versus DNA content. n=2; a representative experiment is shown. **C** Cell death in TET21N p21shRNA cells measured by gating Sub-G1 fraction from DNA content using FACS. Mean ±SEM, n=3. Grey area indicates time of DOX treatment.

Next, it was analyzed how p21 knockdown influences cell cycle arrest during and after DOX treatment. Distribution of cell cycle phases measured by FACS revealed that G1/S transition was affected in both MYCN-low and MYCN-high cells. 24h after treatment cells reduced the fraction of G1 and S cells and arrested predominantly in G2 phase, Figure 22A. However, already 3 days after treatment proportions of cells in G1 and S phases increased, while those in G2 phase decreased, suggesting that cells escaped cell cycle arrest and started cycling again. The reduction of cells in G1 phase during treatment suggests that p21 is required for the activation of G1 arrest whereas G2 arrest can be maintained without p21 activation. Additionally the

proportion of proliferating cells was visualized using EdU incorporation. Again, 72h after DOX treatment cells were mostly arrested in G2 phase, however, already three days after DOX washout 4.5% of MYCN-low and 21% of MYCN-high cells entered S-phase. Notably, 3 days after DOX washout a higher fraction of p21 knockdown MYCN-high cells entered S-phase when compared to cells with active p21 (compare Figures 9D and 22B).

Interestingly, MYCN-low and MYCN-high cells showed similar dynamics in cell death, Figure 22C. The proportion of dead cells increased during treatment and continued to increase up to 3 days after treatment. When normally dividing resister cells started to dominate the population the fraction of dead cells decreased. The results demonstrate that lowering the p21 level sensitizes cells to apoptosis.

Thus, it was shown hat regrowth after chemotherapy depends on p21 expression.

3.3.6. Switching the MYCN conditional expression after treatment influences cellular regrowth

To confirm that the regulation of p21 is mediated via MYCN, the conditional MYCN expression in TET21N was taken in advantage. For this, MYCN-low and MYCN-high cells were treated with DOX for 72 hours and at the treatment washout the conditional MYCN expression was switched by adding or removing doxycycline. Cells were analyzed 16 days after switching MYCN status.

Cells, which expressed low MYCN levels during treatment and high levels after treatment showed a regrowth potential similar to those of cells with continuously high MYCN expression, Figure 23A compare to Figure 9D. In contrast, cells, which expressed high MYCN levels during treatment and low MYCN levels after treatment reduced potential to proliferate. Staining for senescence confirmed the results obtained by cell cycle analysis, Figure 23B. It was found that the majority of cells that were MYCN-low during and MYCN-high after treatment were able to escape senescence. Whereas MYCN-high cells during and low after treatment had a high proportion of senescent cells.

The p21 protein expression level was consistent with observed cellular phenotypes. Cells, which were MYCN-low during and MYCN-high after treatment had reduced

p21 expression and p21 protein levels were similar to resister cells with continuously high MYCN expression, Figure 23C, D, compared to Figure 16B. While cells, which were MYCN-high during and MYCN-low after treatment showed elevated p21 expression with p21 levels comparable to MYCN-low senescent cells.

Taken together, MYCN strongly enhances the regrowth probability of cells after chemotherapy primarily by repressing p21 expression after treatment washout.

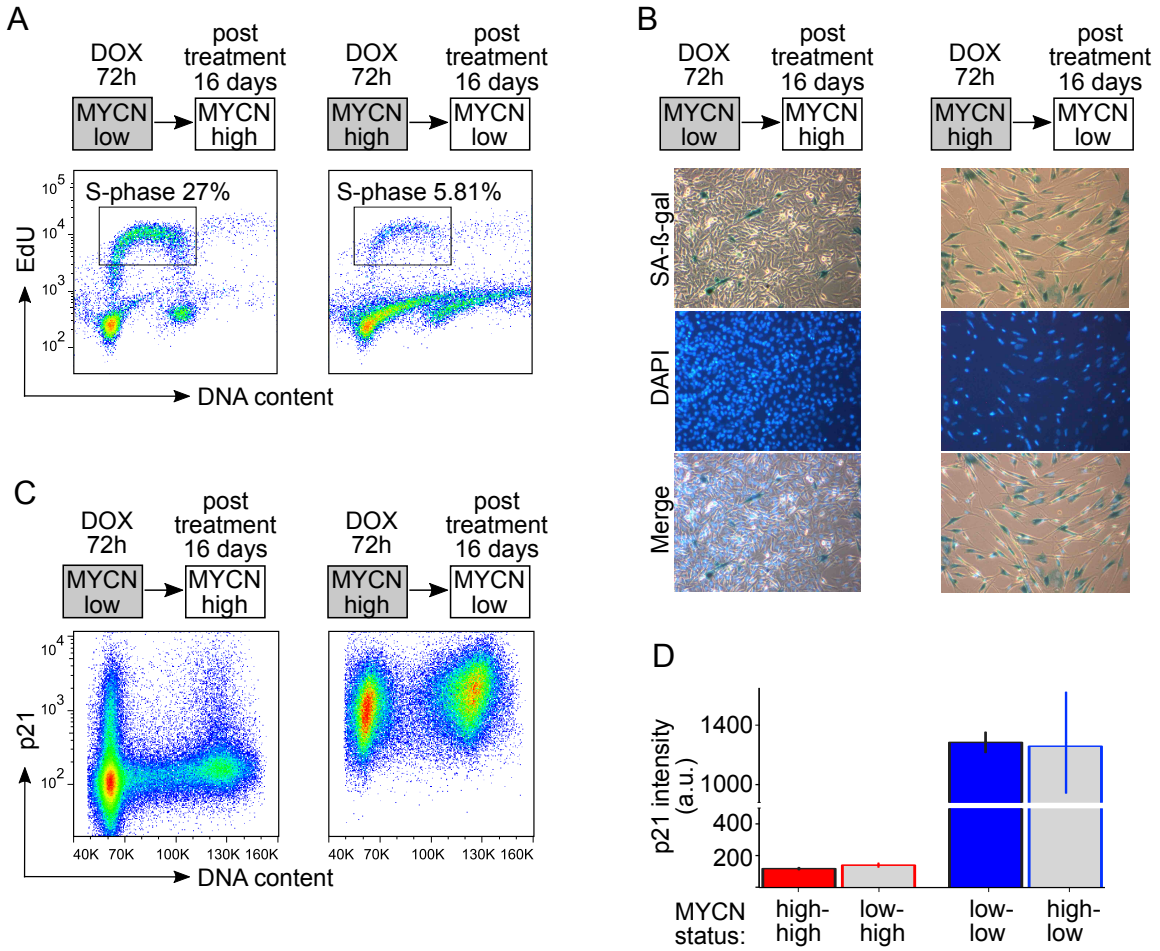

Figure 23. Switching the MYCN conditional expression in TET21N cells after treatment influences cellular regrowth. MYCN-low and MYCN-high cells were treated for 72h with DOX. During DOX washout MYCN expression was switched by removing doxycycline from the media or by adding doxycycline to the media. 16 days after DOX treatment cells were analyzed. **A** Cells were stained by EdU; DNA synthesis was measured by FACS. **B** Cells were stained with SA-β-Gal assay and imaged (10x objective is used). **C** Cells were collected, fixed and stained with p21 fluorescein-conjugated antibody. The p21 protein intensity was measured by FACS and analyzed by FlowJo. **D** Median intensities of p21 protein measured in C, n=2 to 3; representative experiments are shown.

3.4. Resister cells arise from G1-arrested subpopulation with an efficient DNA-damage repair response

3.4.1. High Cdt1 expression in G2 phase correlates with low Skp2 levels.

Live cell imaging performed on TET21N_Cdt1 cells revealed that in normally cycling cells hCdt expressed only during G1 cell cycle phase, whereas cells arrested during DNA damage exhibited strong Cdt1 expression also in G2 phase, Figure 11. Another FUCCI marker, Geminin, was also deregulated after cell cycle arrest. Normally, Geminin is expressed only in S, G2 and M cell cycle phases; however after DOX treatment all cells lost Geminin expression. To explain and to understand this unspecific expression change of FUCCI markers the levels of Skp2 protein, which is the regulator of Cdt1 and Geminin, were analyzed.

The Cdt1 FUCCI construct contains a CY motif (aa 68-70), which is recognized by Skp2 and targeted for proteasomal-mediated degradation in the S and G2 cell cycle phases. In fact, staining for Skp2 protein in normally cycling cells revealed that Skp2 and Cdt1 expression were mutually exclusive, Figure 24A. Skp2 was low expressed in G1 cell cycle phase, accumulated in S phase and highly expressed in G2 phase, while high Cdt1 expression was observed in G1 cells.

The results obtained with qPCR and RNA-Seq indicated that *Skp2* expression was highly reduced during DOX treatment, probably due to the loss of its activator *E2F1*. Therefore, it was tested whether the loss of Skp2 expression can lead to Cdt1 accumulation. For this, the cell cycle restricted expression of Skp2 and Cdt1 in G1 and G2/S cell cycle phases were analyzed over the time course during and after treatment. The expression of the Skp2 protein and Cdt1 reporter were measured by FACS, and quantification of expression levels are shown in Figure 24B. MYCN-low and MYCN-high G1 phase cells maintained low Skp2 expression level over all analyzed time points. Cdt1 expression in G1 cells increased slightly during DOX treatment and decreased to the untreated levels in regrowing MYCN-high cells, whereas in senescent MYCN-low cells Cdt1 stayed elevated. In MYCN-low G2 cells, Skp2 decreased and Cdt1 strongly increased already 24h after treatment. Low Skp2 and high Cdt1 levels in G2 phase remained persistent in MYCN-low senescent cells. In contrast, MYCN-high G2 phase cells first reduced Skp2 and increased Cdt1 but after regrowth the levels of Skp2 and Cdt1 were returned to

those of untreated cells. The Skp2 and Cdt1 dynamics in MYCN-high cells can be explained by the domination of normally dividing resister cells in the population over time.

Low Skp2 expression in arrested cells can also explain loss of the Geminin, as Skp2 indirectly regulates Geminin through suppression of APC, a negative regulator of Geminin.

Taken together, the Cdt1 and Geminin expression are very strictly controlled by cell cycle proteins. During DNA damage expression of the majority of cell cycle regulating molecules is altered, which results in cell cycle arrest and altered expression of FUCCI markers.

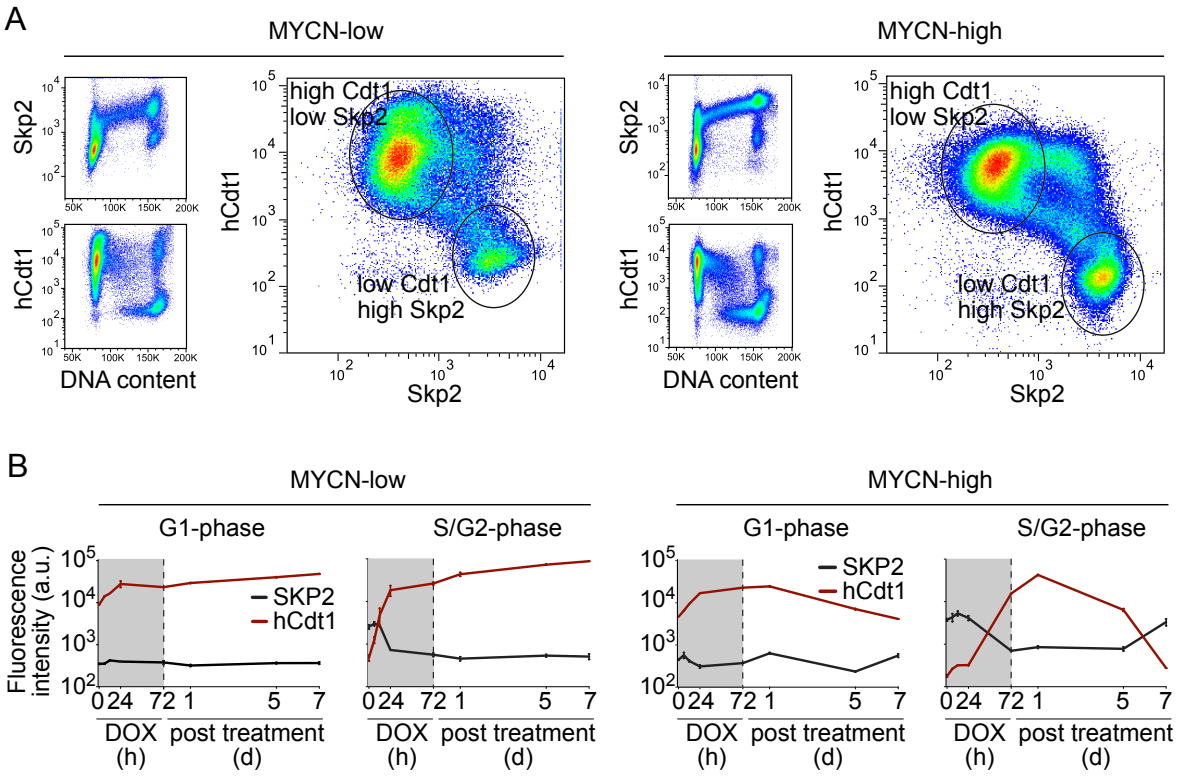

Figure 24. High Cdt1 expression after DOX treatment in all cell cycle phases due to the loss of Skp2 expression. A Untreated TET21N_Cdt1 cells were stained with Skp2 antibody and analyzed by FACS. Plotted Skp2 and Cdt1 intensities versus DNA content visualize changes in the expression level of both proteins in different cell cycle phases. Skp2 versus Cdt1 plots visualize mutually regulation of both. n=3; representative experiments are shown. **B** Skp2 and Cdt1 expression in different cell cycle phases. Cells were harvested during and after DOX treatment fixed and stained with Skp2 antibody for FACS analysis. For DNA content cells were stained with Vio-Blue. Median intensities of Skp2 and Cdt1 in G1 and S/G2 cells cycle phases were analyzed by FlowJo. Mean ±SEM, n=2.

3.4.2. Single cell classification based on treatment-dependent cell cycle dynamics

Despite the deregulation of FUCCI markers during DOX treatment it was possible to analyze the phases of cell cycle arrest in single cells. It was found that the deregulation of Cdt1 and Geminin occurs mostly 20-24 hour after DOX adding. To this time G1/S and G2/M checkpoints were activated and both MYCN-high and therefore MYCN-low cells already established cell cycle arrest, Figure 8B,C. Hence, knowing the cell cycle phase of cells in the time period between 12 and 20 hours after DOX adding is sufficient to identify in which phase they were arrested.

Thus, all single cells in the population could be classified according their cell-cycle phase immediately prior to treatment and their phase of cell-cycle arrest during treatment. According to these criteria four groups were identified: M/G1->G1 arrest, G1->S->G2 arrest, S/G2->G2 arrest and G2->M-G1arrest, Figure 25.

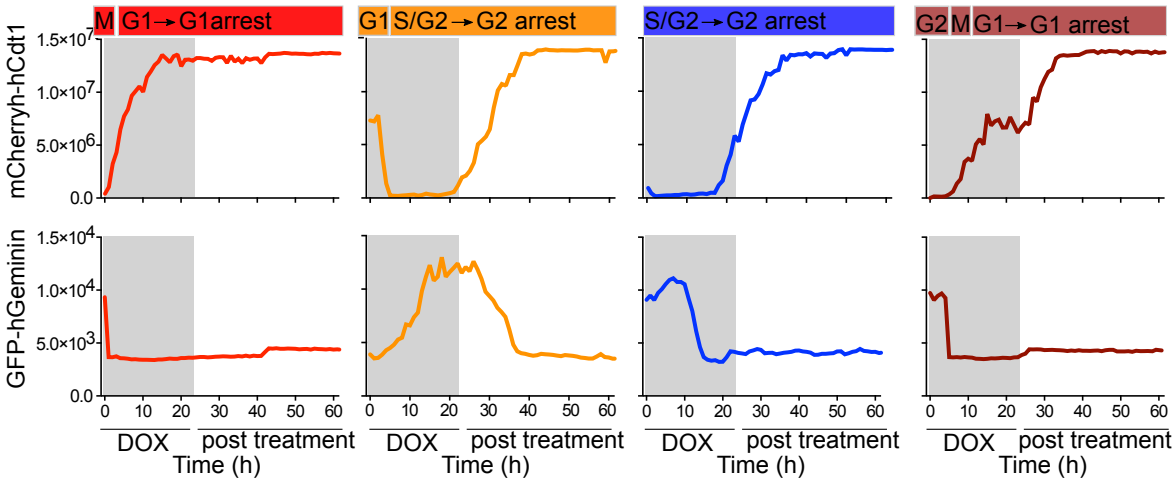

Figure 25. Live-cell imaging using Cdt1 and Geminin cell cycle markers uncovers four groups with different kinds of treatment-dependent cell-cycle arrests. Different dynamics of Cdt1 and Geminin changes upon DOX treatment in single cells. Single cells were classified into four groups according to their cell-cycle phase immediately prior to treatment and their phase of cell-cycle arrest during treatment. Cell-cycle phases were detected by either Cdt1 (high in G1) or Geminin (high in S/G2/M) fluorescence intensity. During cell cycle arrest the expression of these markers becomes decoupled from the underlying cell-cycle stage, with Cdt1 increasing substantially and Geminin decreasing. The more detailed descriptions to the each group see in text.

The M/earlyG1->G1 arrested group includes cells which were in M or early G1 phase at the beginning of treatment (low Cdt1, high Geminin). During treatment they stayed in G1 (Cdt1 increases, Geminin decreases). After treatment they remained G1 phase arrested.

The G1->S/G2->G2 arrested group contains cells which were in G1 phase at the beginning of treatment (high Cdt1, low Geminin). Within a few hours of treatment, these cells entered S phase and then entered G2 phase (Cdt1 decreases, Geminin increases). Cells arrested in G2, but fluorescence expression switched to that of the arrested phenotype (high Cdt1, low Geminin).

The S/G2->G2 arrested group, contains cells which were in S or early G2 phase at the moment of treatment (Cdt1 decreases, Geminin increases). Cells arrested in G2 during and after treatment, but fluorescence expression switched to that of the arrested phenotype (high Cdt1, low Geminin).

The G2->M->G1 arrested group, includes cells which were in G2 phase at the beginning of treatment (Cdt1 low, Geminin high), but entered mitosis and divided within a few hours of DOX treatment (Cdt1 increases, Geminin decreases). Cells stay arrested in G1.

3.4.3. Only G1 arrested cells have exclusive potential to regrow

To better understand features that allow resister cells to regrow, the phenotypes and cell fates of cells imaged by live-cell imaging were analyzed. The time of DOX treatment was reduced to 20 hours, which helped to enrich the proportion of regrowing cells, Figure 26A. Since MYCN-low cells stayed mostly arrested and did not regrow after DOX washout, the further analysis was focused only on MYCN-high cells.

To investigate the importance of cell cycle phases on treatment-induced cell fate, the individual FUCCI cells were followed continuously before, during and after treatment. Single cells were classified into four groups according their cell cycle phase immediately prior to treatment and the phase in which they arrested, Figure 25, 26B. The behavior of cells in each individual group after drug removal was monitored. For each group the percentage of cells that underwent death, mitosis or arrest was measured. Cells, which were in M/G1 before treatment and arrested in G1, had the lowest probability to die after drug removal and highest probability of entering mitosis and dividing successfully, Figure 26C. Cells in the other three

groups died frequently after treatment. The cells, which entered mitosis, could not successfully divide and died shortly after mitosis.

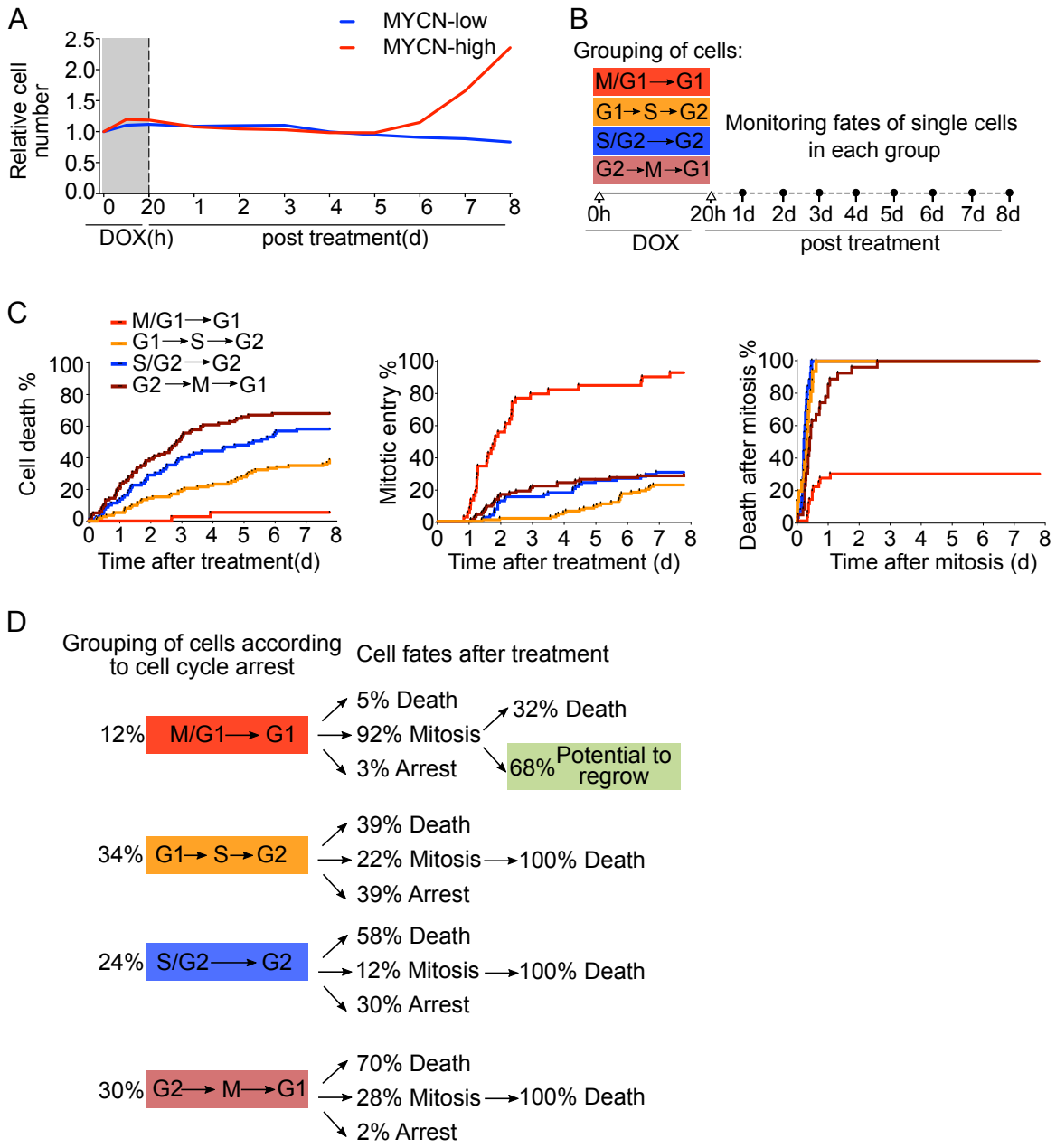

Figure 26. Resister cells are exclusively arrested in G1. A Relative cell numbers of population dynamics in TET21N_Cdt1 cells captured by live-cell imaging. Cells were treated with DOX for 20h and subsequently incubated in drug-free medium. Images were taken every 15 min for 9 days. Grey area indicates time of DOX treatment. **B** Experimental approach: MYCN-high cells that survived 20h of DOX treatment were grouped into four groups according their cell cycle progression and arrest during the fist 20h of DOX treatment. The grouping was based on the changes in Cdt1 expression level before and during treatment (described in Figure 25). The fates of single cells after treatment were tracked in FIJI using MTrackJ plugin. **C** Cell death, mitotic entry and death following mitosis for each group. **D** Summary of (C). Percentage of cells in each group and their fates 8 days after treatment. Only G1 arrested cells had the potential to regrow.

In general, G1-arrested cells had a higher potential to escape treatment-induced cell cycle arrest compared to G2-arrested cells and entered mitosis earlier after drug removal. The cumulative percentage of cell fate decisions of each group 8 days after drug removal is summarized in figure 26C. Strikingly, resister cells exclusively arose from cells, which were in M/G1 before treatment and arrested in G2 (M/G1->G1 group).

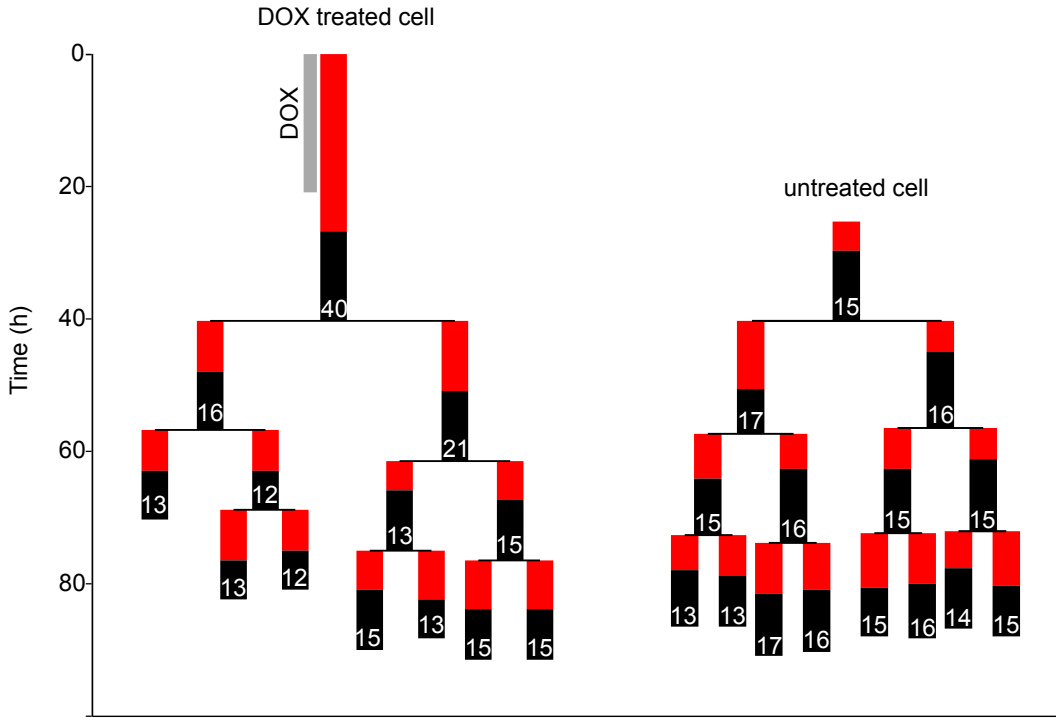

Figure 27. Visualization of single cell tracks of resister and untreated cells. Grey box indicates time of DOX treatment. Red boxes indicate G1, and black boxes S/G2 phases of the cell cycle. White numbers in the black boxes mean the time of whole cell cycle length in hours. Time of cell cycle phases can be determined from Y-axis. **Tree left:** Resister cell arrested in G1 during treatment, however post treatment it escaped G1 arrest and after some time properly divided into two cells and gave birth to the clonal population. **Tree right:** example of cell cycle lengths and divisions for one untreated cell.

Visualizing of the track from one resister cell shows how this cell gives birth to a population of cells, Figure 27. Thus, the resister cell was in early G1 at the beginning of treatment and arrested in G1. 8 hours after DOX washout the cell could escape G1 arrest, transited further in the cell cycle and divided correctly into two cells. Its daughter cells divided again and the colony of resister cells arose. Interestingly, the lengths of cell cycle phases in progeny of resister and in untreated cells were similar. This suggests that only the mother cell, arrested by DOX treatment, had extended cell cycle length but after its division, the normal cell cycle is reestablished in the daughter cells.

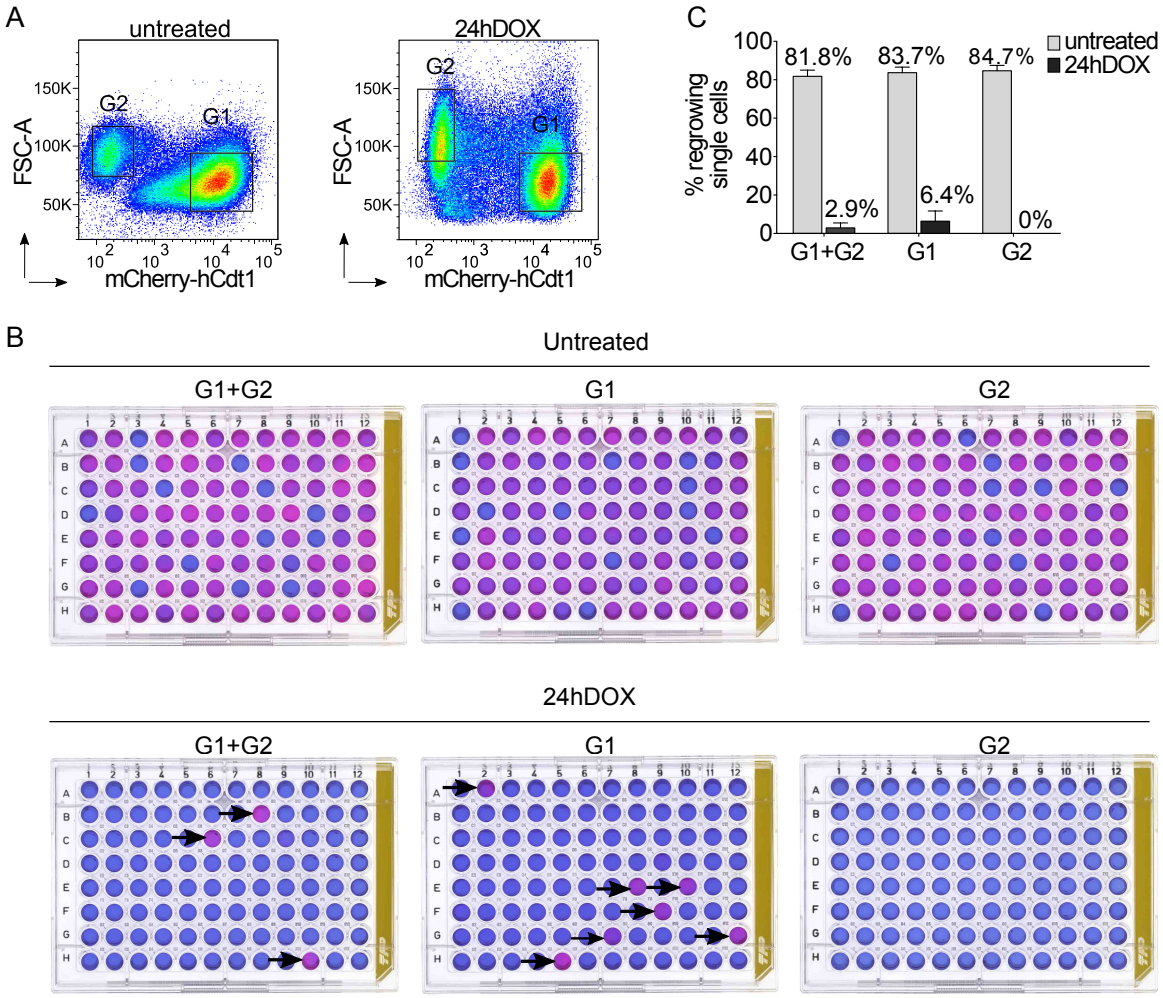

Figure 28. Probability of regrowth is cell cycle dependent. A Untreated or DOX treated G1-only, G2-only, or G1+G2 single TET21N_Cdt1 cells were sorted into 96-well plates using FACS-sorter. Sort gates are indicated as squares. **B** After sorting plates with single cells were incubated for 3 weeks and subsequently stained with cell titer blue assay. Wells with medium stained purple were counted as colony positive and wells with medium stained blue were considered as colony negative. Arrows highlight wells in the plates where single cells regrew after DOX treatment. **C** Quantification of regrown single cells after sorting. Mean ±SEM, n=3.

To confirm the microscopy results the colony forming potential of treatment-arrested single cells was analyzed. Single G1 and/or G2 phase cells were sorted into 96-well plates by FACS sorting, Figure 28A. While in untreated cells the regrown colonies were observed from G1 and G2 sorted cells, only G1-arrested cells were able to form colonies after DOX treatment, Figure 27B, C. When the G1 and G2 arrested single cells were sorted randomly into one plate, the number of colonies was reduced.

Taken together, regrowth is driven by a small number of resister cells that originate from the subpopulation arrested in G1 during treatment.

3.4.4. 53BP1 is differently activated in MYCN-low and MYCN-high cells

To better understand the features that allow MYCN-high G1-arrested cells to regrow, the DNA damage repair was investigated. DOX generates mainly double strand breaks (DSBs), which can be repaired by two pathways, non-homologous end-joining (NHEJ) and homologous recombination (HR). However, HR is specific to the G2 phase. Taking into account that resister cells arise from G1, the analysis was focused on DNA damage repair by NHEJ, a repair pathway employed throughout the cell cycle.

To study the activation of NHEJ in single cells, a fluorescence reporter system based on the protein 53BP1, which promotes NHEJ-mediated double-strand break repair, was used. 53BP1 localizes to chromatin regions adjacent to DSBs in a short time after damage and forms foci that can be visualized by light microscopy. These foci can serve as markers for activation of NHEJ repair. The TET21N cells were stably transfected with a construct containing a fragment of human 53BP1 protein fused to mCherry. The 53BP1 foci, detected by fluorescent construct were completely co-localized with foci detected by 53BP1 antibody staining, Figure 29.

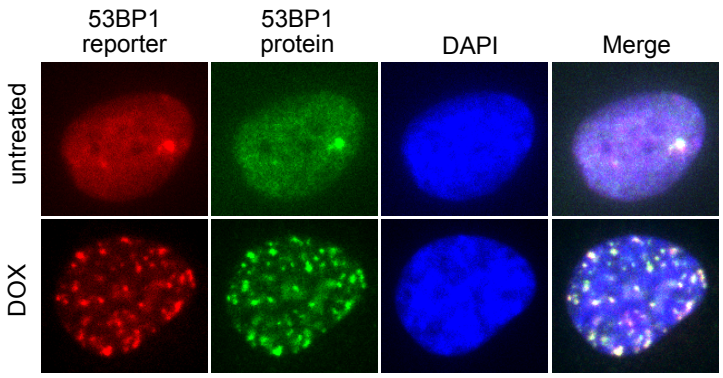

Figure 29. 53PB1 foci accumulation and localization. TET21N_53BP1 cells were either untreated or DOX treated for 24h and immunostained with the 53BP1 antibody following by staining with Alexa-488 conjugated antibody. The localization of 53BP1 foci visualized by mCherry_53BP1 reporter or by 53BP1 antibody staining was compared. DAPI used as a nuclear marker.

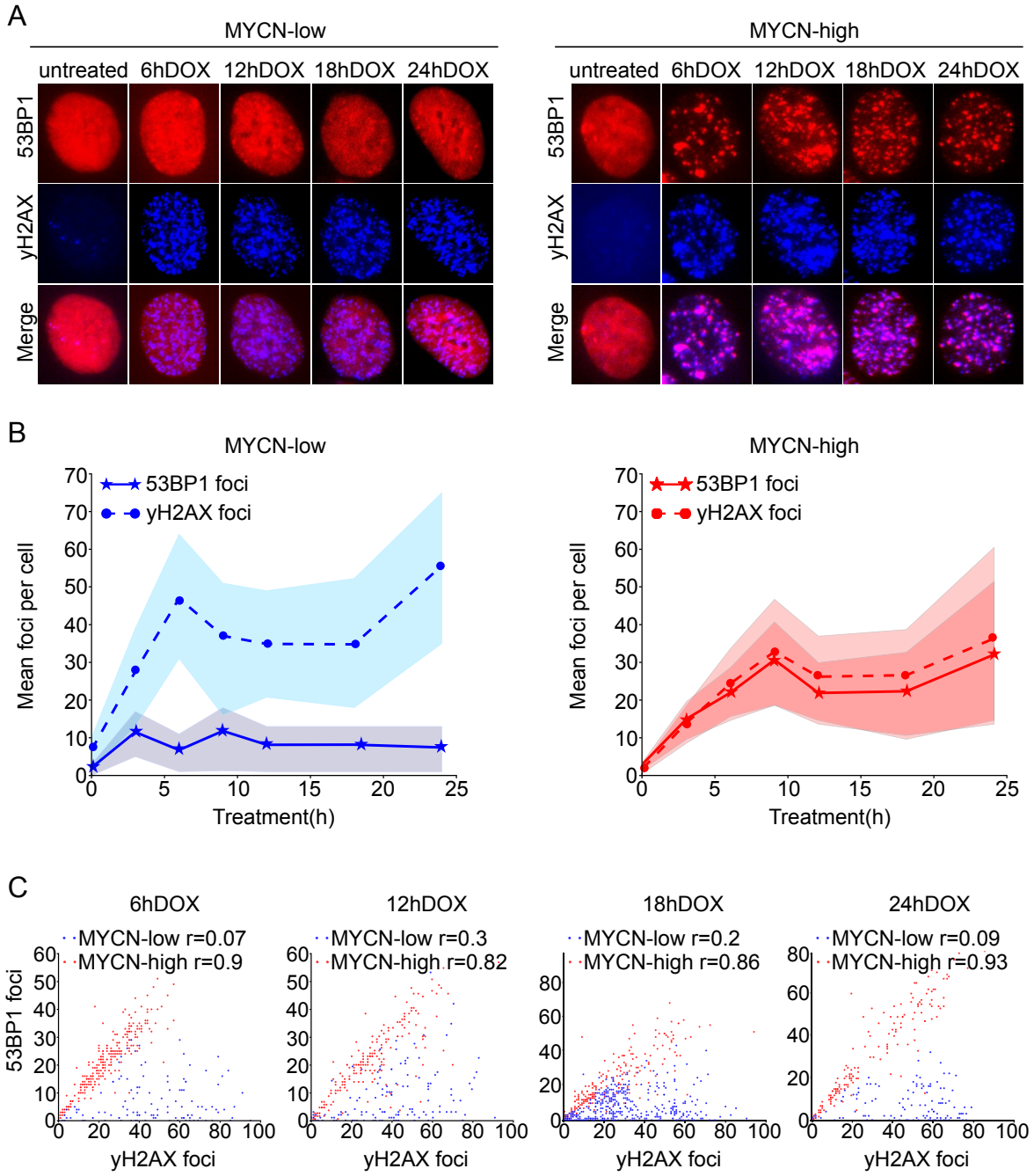

Figure 30. 53BP1 foci formation is differently activated in MYCN-high and MYCN-low cells. A TET21N cells expressing 53BP1 were fixed and stained with y-H2AX antibody following by staining with Alexa-405 conjugated antibody at indicated time points after DOX treatment. DAPI was used as a nuclear marker, n=3, representative cells are shown **B** Quantification of 53BP1 and yH2AX foci dynamics after DOX treatment in MYCN-low and MYCN-high cells. Shadowed areas indicate population's distributions. **C** Correlations between 53BP1 and yH2AX foci localization in MYCN-low and MYC-high cells at selected time points after DOX treatment.

To analyze whether the amount of DOX-induced DSBs correlates with activation of NHEJ, the 53BP1 expressing cells were stained with, y-H2AX, a phosphorylated version of H2AX, Figure 30A. yH2AX forms foci at sites of DNA damage and these foci provide an indirect measurement of DSBs in cells. 53BP1 can bind to yH2AX foci and initiate DNA repair by NHEJ (Kleiner et al., 2015). It was found that MYCN-low cells rapidly accumulate a high number of yH2AX foci, suggesting a high amount of DNA damage. However, these cells were not able to significantly activate 53BP1 foci formation over the complete treatment period, which may indicate reduced repair activation, Figure 30A, B. In contrast, in MYCN-high cells both 53BP1 and yH2AX foci accumulated at a high levels and showed similar dynamics after DNA damage. Additionally, the analysis of colocalization between 53BP1 and yH2AX foci revealed no correlation of these both markers in MYCN-low cells and a strong correlation in MYCN-high cells for all analyzed time points, Figure 30C.

Thus, both MYCN-low and MYCN-high cells accumulate high amounts of DNA damage after DOX treatment but only MYCN-high cells recruit 53BP1 to the damage sites and activate NHEJ repair.

3.4.5. G1-arrested cells have effective DNA-damage response during treatment

To follow the dynamics of 53BP1 foci in MYCN-high cells over time and to investigated whether the G1-resister cells vary in their repair from other cells the live-time imaging with TET21N cells expressing 53PB1 and Geminin was performed. It was observed that 53BP1 foci dynamics in individual cells showed a large heterogeneity in the foci numbers and the time of foci induction. Hence, imaged cells were grouped according to their cell cycle progression and average foci dynamics were analyzed for each group individually. Only cells from the M/G1->G1 group, which includes resister cells, showed a reduction in average foci numbers already during treatment, indicating early and efficient DNA-repair via the NHEJ pathway, Figure 31A. An example of a G1-arrested single cell indicates that after successful repair, the cell made G1/S transition and entered mitosis, Figure 31B. In other groups, cells transitioned through S-phase and maintained very high

foci numbers after drug removal indicating a continued occupancy of NHEJ pathway and incomplete repair. Cells with high numbers of 53BP1 foci were not able to escape cell cycle arrest and either stayed arrested or died, Figure 31C,D.

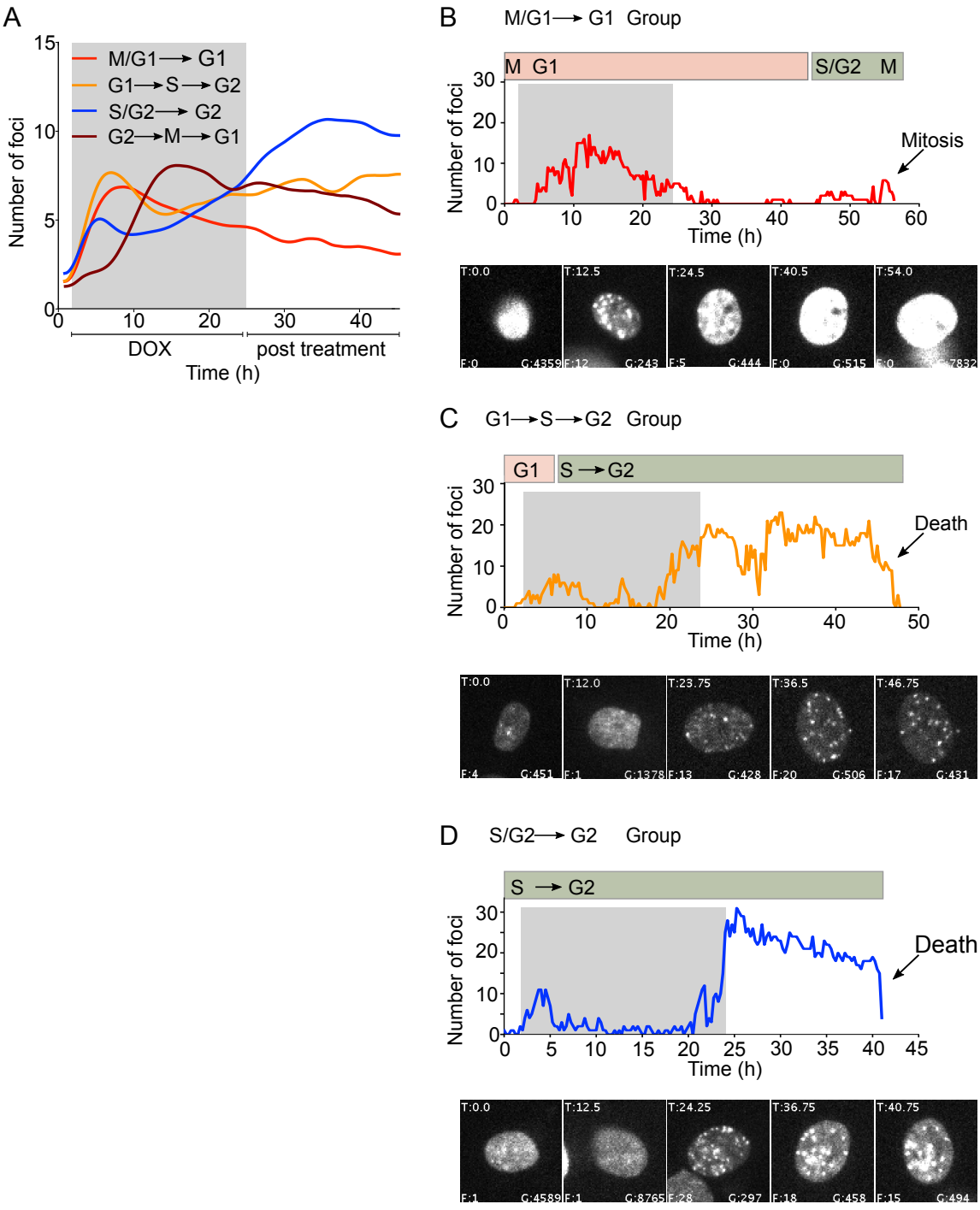

Figure 31. **G1-arrested cells have effective DNA-damage response during treatment. A** Average 53BP1 foci dynamics of cells grouped according to their cell cycle progression as indicated in the top left. Only the G1-arrested cells (in red) show a foci dynamic suggesting effective repair via the NHEJ pathway. **B, C, D** Three single cell 53BP1 foci tracks representing each of the groups shown in A. Cell cycle phases are indicated as bars above the tracks. Gray area indicates time of DOX treatment. The screenshots from analyzed cells are shown. Inside screenshots: T-the time after DOX adding, F-number of foci; G1-geminin level.

Taken together, the resister cells, which accumulate in a G1 arrested subpopulation, did not pass through S-phase during treatment, possibly sustaining less DOX-induced damage, and showed enhanced activity of the NHEJ repair. Thus, an important synergy between a genetic lesion, MYCN, and non-genetic heterogeneity which allows to escape chemotherapy was identified.

3.5. Tailored combination therapy that targets specific properties of resister cells successfully abolishes regrowth

3.5.1. Cell cycle synchronization reduces resisters

Applying the obtained knowledge on to resister cells may help to improve first-line therapy by specifically targeting the properties of these resister cells. Resister cells were characterized by MYCN expression, G1 arrest and efficient DNA-damage repair. It was therefore hypothesized that depletion of the G1-population prior to treatment should abolish resister cells.

To test this, cells were pre-treated for 20h with either DMSO or with inhibitor against CDK1, which reversibly arrests cells at the G2/M border of the cell cycle. Pre-treatment with CDK1 inhibitor resulted in decrease of the G1 phase from 70% to 49% in MYCN-low cells and from 40% to 16% in MYCN-high cells, Figure 32A. After the DMSO or CDK1 inhibitor were washed out cells were subsequently treated with either DOX only, or with DOX in combination with CDK1 inhibitor. MYCN-low cells underwent cell cycle arrest without regrowth under all treatment conditions, suggesting that cell cycle phase distribution in these cells does not influence treatment outcome, Figure 32B. Upon DOX treatment MYCN-high cells pre-treated with CDK1i had similar regrowth as cells pretreated with DMSO. Upon combined DOX plus CDK1 inhibitor treatment a higher rate of cell death was observed, which is in agreement with previous studies reporting that inhibition of CDK1 sensitizes MYCN-amplified cells to death (Chen et al., 2013). However, while delayed, regrowth was not completely abolished in these cells.

Live-cell imaging of cells pretreated with CDK1 inhibitor and subsequently treated with DOX plus CDK1 inhibitor revealed that resister cells originated from a small but persistent G1 subpopulation, Figure 32C.

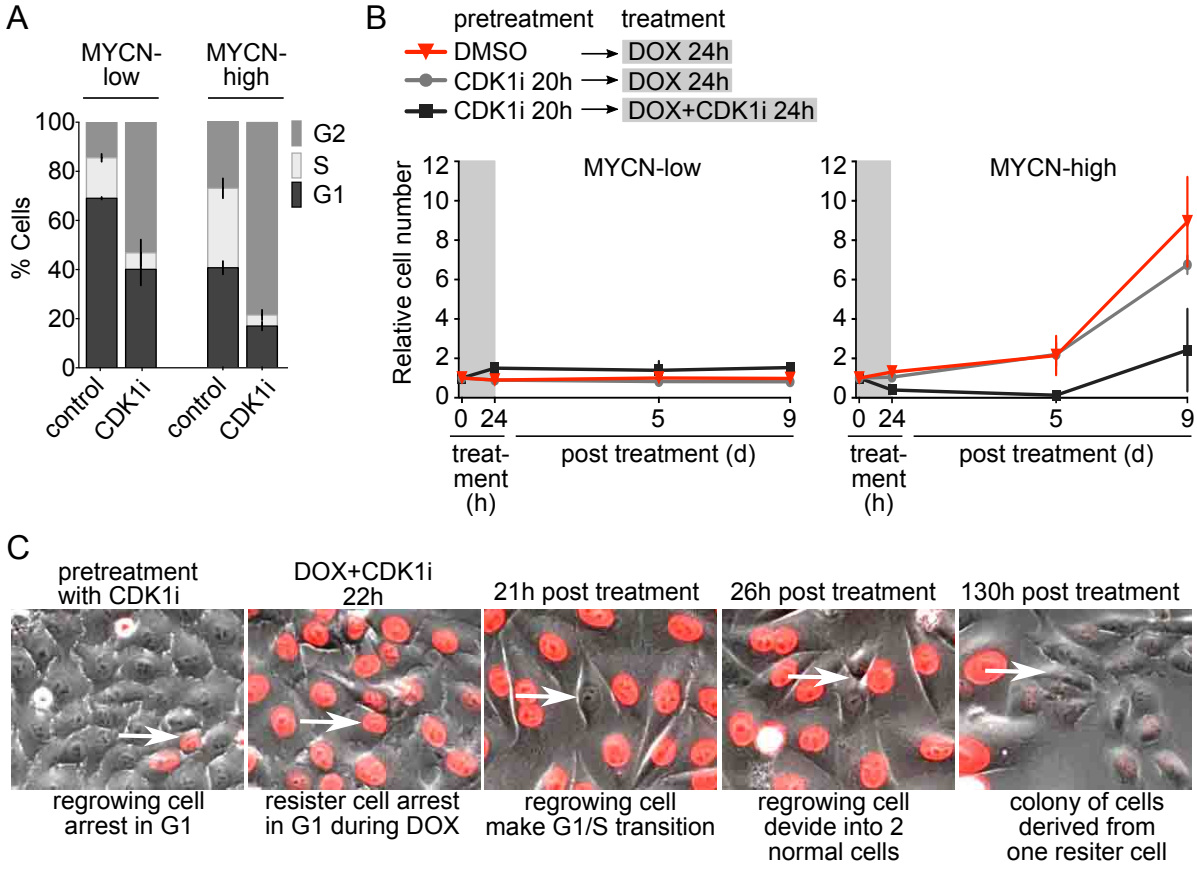

Figure 32. Combined treatment with CDK1 inhibitor reduces but not abolishes resisters. A Cell cycle distribution of untreated cells (control) or cells treated with 7μM CDK1 inhibitor RO-3306 for 24h. Cell cycle was measured by FACS and analyzed by FlowJo. Mean ±SEM, n=3. **B** Comparison of cellular regrowth. Cells were pretreated with either DMSO or with CDK1 inhibitor. 20h after pretreatment CDK1 inhibitor was washed out and cells were treated with either DOX alone or with DOX+CDK1i. Cell numbers were counted with FACS. Mean ±SEM, n=2. **C** Live cell imaging of TET21N_Cdt cells. During pretreatment with CDK1 inhibitor cells mostly arrested in G2 phase (cells without nuclear marker). But a small fraction of cells stayed in G1 phase (cells with red nuclear marker). One G1-arreted resister cell (indicated by white arrow) regrew and gave birth to a colony of cells.

Additionally, cellular regrowth in cells pretreated with CDK4 inhibitor was investigated. Inhibition of CDK4 activates G1 cell cycle arrest through decrease of Rb phosphorylation. Thus, after pretreatment with CDK4 inhibitor for 20h 98% of MYCN-low and 85% of MYCN-high cells were accumulated in G1 phase Figure 32A. It was hypothesized that accumulation of cells in G1 phase should enrich the number of regrowing cells after DOX treatment. The same treatment conditions as for CDK1 inhibitor were applied. As expected, MYCN-low cells arrested and maintained the same cell numbers irrespective of treatment conditions, Figure 33B. MYCN-high cells, despite high proportion of G1 cells, exhibited reduced regrowth. Low regrowth rate of cells enriched in G1 may indicate that inhibition of CDK4

suppresses important players responsible for G1/S transition and through this CDK4 inhibition can delay but not abolish regrowth.

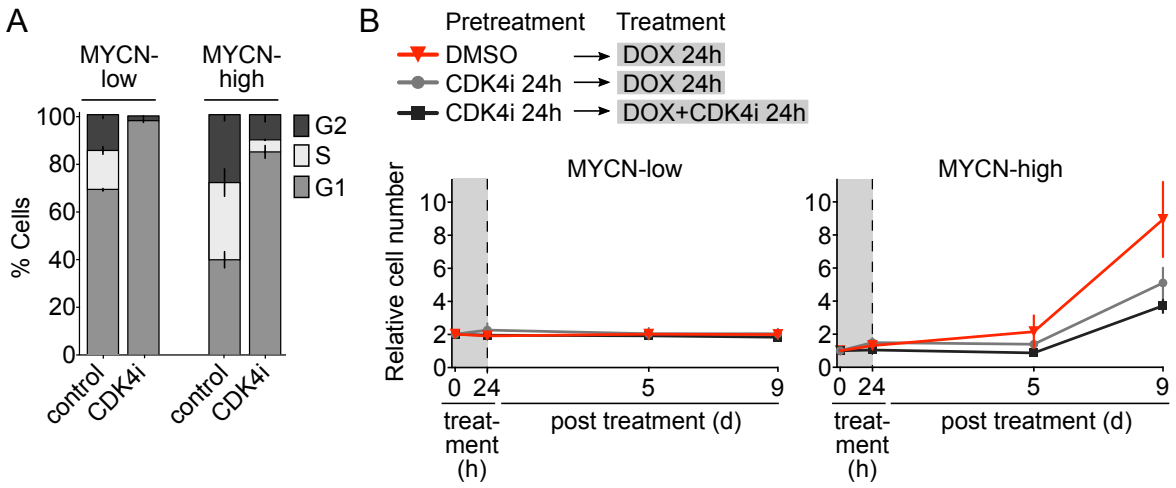

Figure 33. CDK4 inhibitor reduces regrowth. A Cell cycle distribution in untreated cells (control) or cells treated with 4µM CDK4 inhibitor LEE011 for 24h. Cell cycle was measured by FACS and analyzed by FlowJo. Mean ±SEM, n=3. **B** Comparison of cellular regrowth. Cells were pretreated with either DMSO or CDK4 inhibitor. 24h after pretreatment CDK4 inhibitor was washed out and cells were treated with either DOX alone or with DOX+CDK4 inhibitor. Cells were counted with FACS. Mean ±SEM, n=2.

To summarize, already a single resister cell is sufficient for relapse. Since even in vitro it is impossible to achieve a complete synchronization, this strategy, although good in theory is unlikely to be effective in the clinic.

3.5.2. AMT inhibition during DNA damage completely prevents regrowth of resister cells

Since the synchronization of the cell cycle cannot completely abolish regrowth after chemotherapy, the second property of resister cells, DNA-damage repair was targeted. The activation of DSBs leads primarily to activation of ATM-Chk2 kinases, but ATR-Chk1 kinases, which primarily respond to single strand breaks, can also be activated by DSBs. Inhibitors against these kinases in combination with DOX were tested, Figure 34. It was found that after combined treatment with DOX and ATM inhibitor for 24h the numbers of MYCN-high cells declined rapidly and regrowth was completely abolished, Figure 34B. Whereas MYCN-low cells were just slightly affected by ATMi, and s majority of the cells stayed arrested. The Chk1 inhibitor strongly reduced regrowth of MYCN-high cells, however few resister cells

survived and started to grow again, Figure 34E. The ART inhibitor and combined inhibitor against Chk1&Chk2 were less effective, the regrowth of MYCN-high cells was delayed compared to DOX only treatment but still a high fraction of cell regrew, Figure 34 C,D.

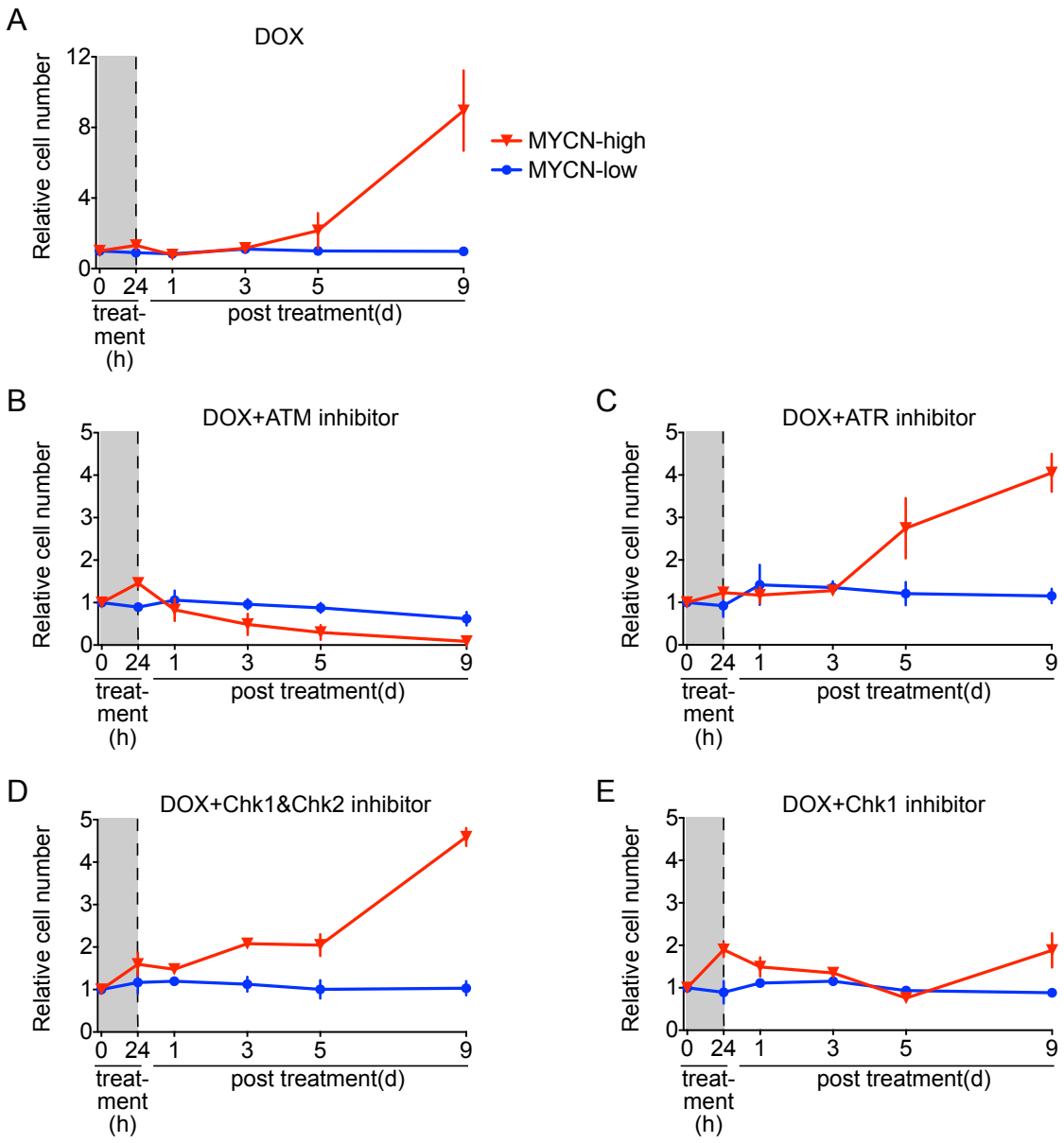

Figure 34. Comparison of regrowth after combined treatment of DOX together with DNA damage repair inhibitors. A Cells were treated with DOX for 24h and subsequently incubated in drugs-free medium. At indicated time points cells were collected and counted with FACS. Mean ±SEM, n=3. **B** Same as in A, except DOX was used in combination with 10 µM ATM inhibitor KU-60019, n=3. **C** DOX was used in combination with 5 µM ATR inhibitor VE821, n=3. **D** DOX was used in combination with 300 nM Chk1&Chk2 inhibitor AZD7762, n=2. **D** DOX was used in combination with 3 µM Chk1 inhibitor LY2603618, n=2.

Thus, from all inhibitors tested, only combined therapy with DOX and ATM inhibitor was sufficient to abrogate regrowth of resister cells. ATM is a key regulator of DNA

damage repair and promotes NHEJ by recruiting 53BP1 to the damaged sites. Therefore, it was tested whether treatment with ATM inhibitor impairs the activation of 53BP1 foci formation in MYCN-high cells during treatment. In line with the results from figure 33B, live-cell imaging confirmed that under combined treatment with DOX and ATM inhibitor cells were continuously dying and not regrowing, Figure 35. As expected, inhibition of ATM during DNA damage strongly decreased the number of 53BP foci, suggesting inhibition of NHEJ during DNA damage. Geminin levels decreased after both treatment conditions suggesting cell cycle arrest, and started to increase again only in regrowing resister cells which were treated with DOX only. Interestingly, Geminin decrease in cells treated with DOX plus ATMi was delayed compared to DOX only treated cells, hinting that ATMi impairs cell cycle arrest.

The strong regrowth abolishing effect of combined treatment with DOX and ATM inhibitor was confirmed on several MYCN-tunable cells lines, Figure 36. Thus, two MYCN-overexpressing and two MYCN-amplifying cells lines treated for 24h with DOX were not able to build colonies after combination therapy, whereas a large number of colonies arose after treatment with DOX only.

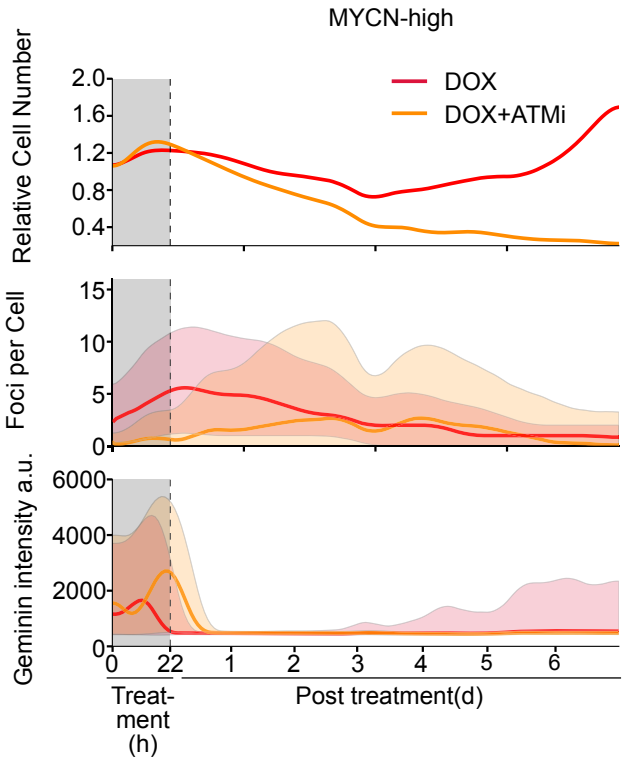

Figure 35. Inhibition of ATM abolishes regrowth and suppresses 53BP1 foci formation. Quantification of live-cell imaging of MYCN-high TET21N_Geminin_53BP1 cells treated either with DOX alone or with DOX plus ATM inhibitor. The quantified relative cell numbers, average foci numbers and Geminin intensities of populations are shown.

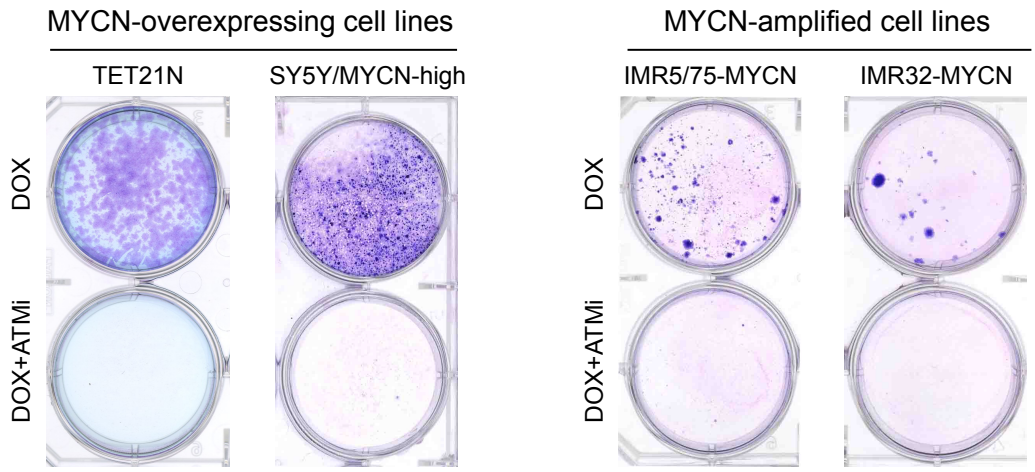

Figure 36. Combined treatment with DOX plus ATM inhibitor prevents regrowth in all tested cell lines. Two cell lines with transgenic inducible MYCN and two MYCN-amplified cells lines were treated for 24h either with DOX alone or with DOX and ATM inhibitor. 14 days after treatment cells were fixed, stained with methylene blue and colonies were imaged.

To summarize, the enhanced repair ability of G1 arrested cells allows some cells to successfully repair, recover and regrow. It was shown that suppression of DNA DSB repair combined with DNA damage induction completely abolishes resister cells.

3.5.3. Inhibition of ATM suppresses p53 signaling after DNA damage and impairs G1 checkpoint.

To better understand mechanisms by which inhibition of ATM upon DNA damage prevents regrowth, the activation of p53 signaling and cell cycle arrest during combined treatment were analyzed.

It was found that cells treated with DOX and ATMi failed to autophosphorylate ATM at Ser1981, Figure 37A. This autophosphorylation is essential for the activation of ATM. As a result, upon combined treatment p53 signaling stayed inactive, indicated by low p53 Ser15 phosphorylation and the absence of p21 activation, Figure 37B,C. Notably, 24 hours after treatment MYCN-high cells managed to increase p53 activity and p21 expression, suggesting that in absence of ATM other kinases, i.e. ATR or DNA-PK, could phosphorylate p53.

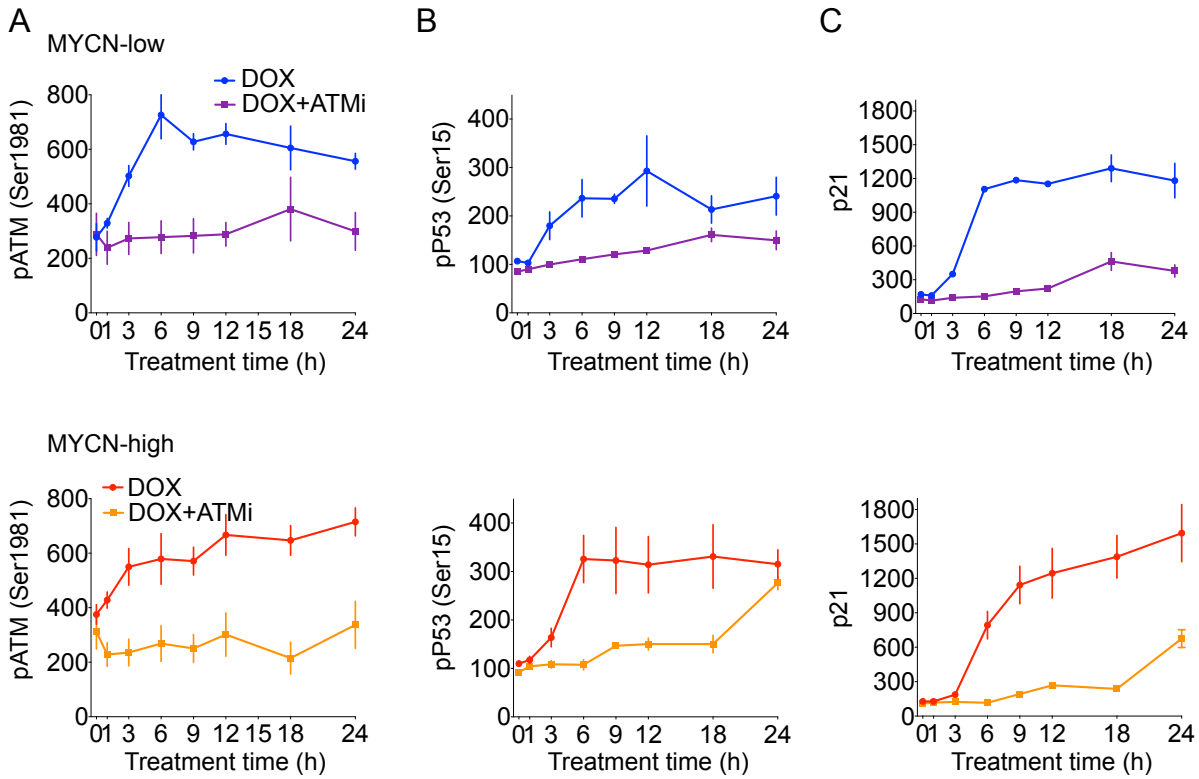

Figure 37. ATM inhibitor suppresses p53 signaling after DOX treatment. A Expression of ATM protein phosphorylated at Ser1981. Cells were treated either with DOX alone or with DOX plus ATM inhibitor for 24h. Cells were collected at indicated time points, fixed, and stained with fluorescein-conjugated antibodies and measured by FACS. Medium intensities of pATM (Ser1981) are plotted. Mean ±SEM, n=3. **B** Same as in A, except p53 protein phosphorylated at Ser15 was measured. **C** Same as in A, except p21 protein expression was measured.

Analysis of the cell cycle revealed that upon combined treatment cells had delayed cell cycle arrest, as shown by disappearing of S-phase only 24 hours after treatment, Figure 38A,B. Activation of cell cycle arrest was temporally in line with the increase of p53 phosphorylation and p21 expression in DOX and ATM inhibitor treated cells. Interestingly, MYCN-high cells were arrested predominantly in G2 phase, indicating that inhibition of ATM impairs G1/S cell cycle checkpoint and more cells transit through S phase before arrest. 7 days after treatment, only a small number of MYCN-high cell left, as they were continuously dying after treatment, whereas MYCN-low cells stayed arrested, Figure 38C.

Taken together, inhibition of ATM upon DNA damage leads to the suppression of p53 activation and delayed cell cycle arrest, which means that damaged cells move through S and M phases and accumulate even more damage. Together with the reduced activation of NHEJ repair this leads to the cell death and results in complete elimination of G1 resister cells.

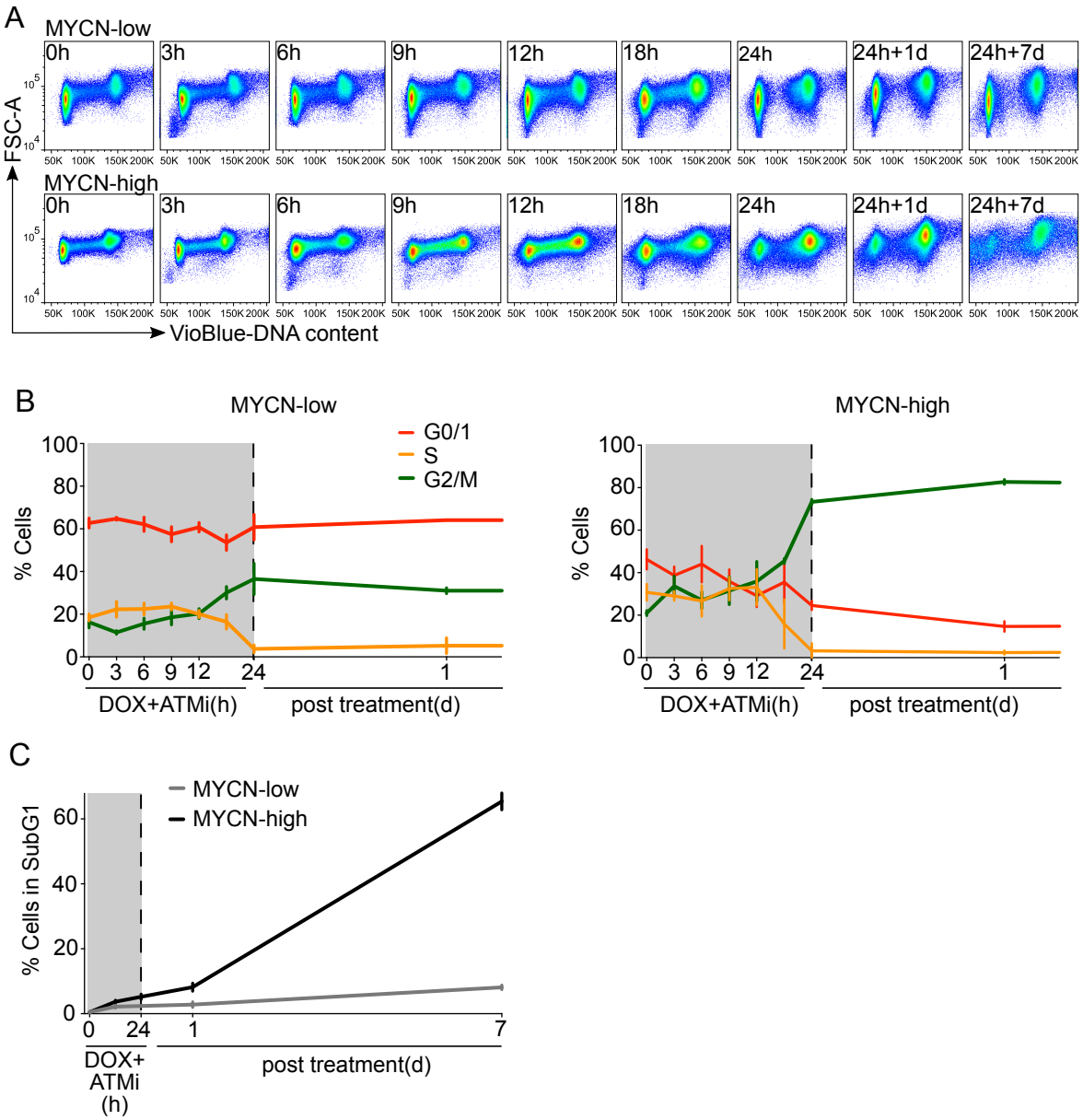

Figure 38. ATM inhibition during DNA damage impairs G1 cell cycle checkpoint. A Cell cycle progression of cells treated with DOX and ATM inhibitor for 24h and subsequently incubated in drug-free medium. DNA content was measured by FACS. n=3; a representative experiment is shown. **B** Time-course of cell cycle distributions of cells treated as in A. Cell cycle is analyzed by FlowJo. Mean ±SD; n=3. **C** Cell death measured by gating Sub-G1 fraction from DNA content using FACS. Mean ±SEM, n=3.

4. Discussion

4.1.1. MYCN accelerates cell cycle progression under normal conditions and impairs cell cycle arrest during DNA damage

The role of MYCN on the cell cycle and response to chemotherapy was investigated in well-established MYCN tunable, p53 wild type neuroblastoma cell lines. The conditional MYCN overexpression in TET21N cells was sufficient to reduce the duration of G1 phase and to accelerate cell proliferation, Figure 6C,E (Lutz et al., 1996; Muth et al., 2010). Conversely, reduction of *MYCN* expression in *MYCN*-amplified IMR5/75 cell line resulted in the increase of the proportion of cells in G1 and reduction of proliferating cells in S, Figure 6D.

Analysis of FUCCI fluorescence sensors, Cdt1 and Geminin, in cells imaged by time-lapse microscopy allows to calculate the total cell cycle lengths and the duration of cell cycle phases (Sakaue-Sawano et al., 2008). In TET21N cells MYCN overexpression leads to the reduced overall cell cycle time achieved mostly by shortening of G1, Figure 7. The results of live-cell imaging analysis are in agreement with the original study on TET21N cells, which found that MYCN expression shortens time to needed progress through the cell cycle, specifically shortening the G1 phase (Lutz et al., 1996).

In the present study one of the most widely used chemotherapeutic agents, Doxorubicin (DOX), was used to analyze the role of MYCN on cellular regrowth after treatment. Doxorubicin is a well-known topoisomerase II inhibitor, generating DSBs, but also inhibiting DNA and RNA synthesis and producing single stranded breaks (Dees et al., 2008; LoConte et al., 2008). DNA damage, induced by DOX, resulted in the arrest of both MYCN-low and MYCN-high cells at G1 and G2 phases of the cell cycle. However, the activation of cell cycle checkpoints was established only 2-10 hours after induction of DNA damage. These findings are in line with previous observations, which showed that G1/S and G2/M cell cycle checkpoints are not fully initiated until several hours post irradiation (Deckbar et al., 2010; Krempler et al., 2007; Linke et al., 1997; Lobrich and Jeggo, 2007; Syljuasen, 2007). This implies that many cells with unrepaired DBSs enter S and M phases, which leads to the accumulation of additional damage (Linke et al., 1997). DNA

damage is particularly harmful in S and M phases of the cell cycle. During S phase, DNA damage interferes with the replication fork progression and base damages lead to base mispairing resulting in point mutational changes (Deckbar et al., 2011; Tercero and Diffley, 2001). Moreover, unrepaired DSBs and single strand breaks can lead to replication fork stalling or collapse, which can aggravate the damage causing further DSBs and chromosome breaks (Deckbar et al., 2011; Tercero and Diffley, 2001). During M phase, DNA damage can result in loss of genetic material leading to genetic alterations or even to the death of the daughter cells (Deckbar et al., 2011; Lobrich and Jeggo, 2007). Therefore, it is very critical for cells to have active checkpoint signaling to control cell cycle progression in the presence of DNA damage.

Two major pathways, p53/p21 and Chk2/Cdc25, regulating checkpoint activation after DNA damage are known (Iliakis et al., 2003; Lukas et al., 2004). The former pathway mostly regulates the G1/S transition and involves the phosphorylation of p53 and its negative regulator MDM2 by ATM and Chk2 leading to p53 activation and stabilization (Kastan and Bartek, 2004; Kastan et al., 1992; Khosravi et al., 1999). Thereafter p53 transcriptionally upregulates the expression of its target genes, of which p21 is essential for inhibiting G1/S entry (Bartek and Lukas, 2001; Sherr and Roberts, 1999). This pathway requires transcriptional activation following posttranslational modifications and therefore the full activation of this mechanism takes several hours. Additionally, under DNA damage p21 can also contribute to the G2/M checkpoint by p21-mediated degradation of the G2-associated Cyclin B1 (Gillis et al., 2009). A second ATM dependent pathway, which regulates both G1/S and G2/M checkpoints is based on the ATM-dependent phosphorylation of Chk2. Activated Chk2 targets the phosphatase Cdc25A for rapid ubiquitylation and degradation. This prevents the removal of inhibitory phosphates from CDK1/CDK2 and leads to the cell cycle arrest (Mailand et al., 2000). This pathway is activated more rapidly because it involves only posttranslational modifications, such as phosphorylations and ubiquitylations.

In this study, MYCN was found to delay activation of both cell cycle checkpoints for 2 to 3 hours and to increase the proportion of transiting cells up to 25%, Figure 9. These findings raise two questions. First, why does it take several hours till complete cell cycle arrest and second, how can MYCN delay the cell cycle

checkpoint activation. One possible explanation of the first question is that p53 mediated p21 activation is slow since it requires posttranslational modifications and transcriptional activation (Riley et al., 2008). In TET21N cells the significant activation of p21 mRNA and protein expression was observed only 6 hours after DOX addition. However after 6 hours of treatment still a high number of cells, especially MYCN-high cells, were able to enter S phase. The understanding of the concept of the restriction point is important for the explanation of how the cell cycle transitions work. The restriction point is defined as the time in G1 progression when Rb phosphorylation passes a certain threshold level leading to initial E2F1 release, which subsequently activates the CyclinE/CDK2 complex (Yao et al., 2008). That results in further Rb phosphorylation and more E2F1 release (Yao et al., 2008). Both pathways, the activation of the p53/p21 and the Chk2/Cdc25A, act to inhibit CDK activity. Therefore cells, which passed through the restriction point may already have sufficient Rb phosphorylation and therefore are less dependent on CDK inhibition. MYCN-high cells have short G1 phase (~4 hours), meaning that these cells are quickly passing through the restriction point. This explains why a higher proportion of MYCN-high cells accomplishes the G1/S transition compared to MYCN-low cells. The observation that the G2/M checkpoint is activated earlier than the G1/S checkpoint can be explained by the fact that cells use the fast Chk2/Cdc25 pathway to establish G2 arrest, Figure 9.

An explanation for the second question, how MYCN delays cell cycle arrest, could be the upregulation of many critical cell cycle drivers such as *E2F1*, *SKP2*, *CCNA2*, *CCNE1*, *CDK4*, *CCNB1*, *Cdc25A* already under untreated conditions, Figure 15,18. Under DNA damage, it takes longer for MYCN-high cells to reduce the expression of these genes and as a consequence to establish the cell cycle arrest, Figure15. Additionally, MYCN can delay or suppress cell cycle arrest by the inhibition of p21 (Bell et al., 2007). Interestingly, although the p53 protein was more strongly activated in MYCN-high cells, the p21 protein and RNA levels were almost equally activated under MYCN-low and MYCN-high conditions. This confirms the results of previous studies, which showed that MYCN, the same as MYCC, activates p53 but suppresses p21 expression (Bell et al., 2006; Chen et al., 2010; Reisman et al., 1993; Roy et al., 1994; Seoane et al., 2002). It was suggested that MYCN represses p21 expression by increasing *SKP2* and decreasing *TP53INP1* expression, (Bell et al., 2007).

4.1.2. MYCN sensitizes cells to apoptosis, suppresses cellular senescence and drives clonal regrowth of resister cells

In consistence with observations made by other groups it was found that MYCN increases the proportion of cell death during treatment, Figure 9B,C (Bell et al., 2006; Fulda et al., 2000; Gogolin et al., 2013). It has been reported that MYCN and MYCC upregulate p53 expression and switch p53 downstream effects from G1 arrest to apoptosis, by increasing the transcription of the pro-apoptotic genes *PUMA*, *BAX* and *PIG3* instead of *CDKN1A* (Chen et al., 2010; Seoane et al., 2002). Additionally, delayed cell cycle arrest activation and a high proportion of damaged cells passing through S and M phases early during treatment also contribute to the increased rate of cell death under MYCN-high conditions.

Nevertheless, observations of cells after treatment showed that MYCN neither induces complete cell death in the whole population nor it allows cells to stay in the senescence stage, Figure 9,10,15. Here it was shown that a proportion of surviving cells was able to resume the cell cycle after treatment and a small fraction of these cells could divide properly and re-establish proliferation, Figure 9,15. The regrowth of MYCN-high cells was clonal, suggesting that only a very small number of cells could overcome chemotherapy. These data are in line with clinical observations for high-risk MYCN-amplified neuroblastomas, which are generally sensitive to the first-line therapy. However, the initial regression is frequently followed by the fast relapses and unfavorable disease progression (Canete et al., 2009; Kushner et al., 2014).

Of particular importance is the finding that ta second DOX treatment of resister cells resulted again in clonal regrowth with a comparable number of colonies as after the first treatment. This indicates that the therapy did not select for genetically distinct subpopulations that are resistant to DOX. Induction therapy for high-risk neuroblastoma usually consists of four to six cycles of chemotherapy (Kushner et al., 1994; Pradhan et al., 2006). The data of this study propose that after the first several rounds of chemotherapy the non-genetic heterogeneity rather than accumulated genetic mutations during treatment could be a reason for relapses.

4.1.3. Molecular expression profiles of resister cells are equal to untreated cells

MYCN-low cells undergo drug-induced senescence and have active p53 and high p21 expression even two weeks after DOX treatment, Figure16. The p21 is a multifunctional protein that not only activates transient cell cycle checkpoints, but also inhibits apoptosis, regulates transcription, induces senescence-associated genes and suppresses mitosis-associated genes (Chang et al., 2000; Han et al., 2002; Suzuki et al., 1999). The sustained upregulation of p21 is universally accepted to be primarily responsible inducing the senescence program (Chen et al., 2006; Mirzayans et al., 2010; Roninson, 2003). Moreover, p21 is responsible for the apoptotic resistance of different cancer cell lines undergoing senescence after treatment with DOX (Crescenzi et al., 2008).

Early after treatment MYCN-high cells had active p53 signaling and exhibited senescent morphology. Nevertheless, after regrowth the resister cells looked phenotypically similar to untreated cells and had low expression of p53 and p21 proteins, Figure 16. The negative correlation between MYCN status and senescence was observed previously (Xue et al., 2007). It was described that at high doses of irradiation *MYCN*-amplified cell lines undergo apoptosis rather than cell cycle arrest, whereas *MYCN* single copy cells undergo senescence (Xue et al., 2007). Thus, observations of this and previous studies suggest that MYCN suppresses cellular senescence.

Global analysis of the transcriptome by RNA-Seq and the epigenome by Chip-Seq revealed that MYCN-high resister cells completely re-established the pre-treatment expression profiles, Figure 17,18,19. Analysis of molecular profiles together with observations made by live-cell imaging suggest that reduced activation of p53-p21 signaling, the same as recovery of genome and epigenome in MYCN-high resister cells are a consequence of changes in the composition of the population over time. Early after treatment the culture was dominated by senescent cells, which later become diluted by the regrown resister cells that took over the population.

In contrast, MYCN-low senescent cells maintained molecular profiles similar to that of cells during treatment: activated p53-signaling, suppression of cell cycle genes and, Figure 15,16,18. Senescence involves a tight interplay between the p53 and RB pathways (Chicas et al., 2012). The p53 acts as an inducer of various cell-cycle

inhibitory proteins, while RB acts as a repressor of E2F1 transcription (Courtois-Cox et al., 2008). The analyzed histone modifications showed that senescent cells lose trimethylations of H3K4, H3K27 and H3K9, which correlated with the expression of histone-specific methyltransferases and demethylases. H3K4 methylation is associated with actively transcribed genes; therefore the loss of this modification in senescent cells suggests that active histone demethylation might contribute to gene repression during senescence (Chicas et al., 2012). Decreased levels of histone H3K27me3 and its methyltransferase *EZH2* are known markers for cellular senescence (Bracken et al., 2007; Fan et al., 2011). *EZH2* depletion in melanoma cells inhibits cell proliferation, activates p21 and induces cellular senescence (Fan et al., 2011). The role of H3K9me3 on cellular senescence is controversial. Several studies reported the increase of H3K9me3 and its methyltransferase *SUV39H1* in senescent cells (Di Micco et al., 2011; Dorr et al., 2013). Whereas other studies showed that the decrease in global H3K9 trimethylation together with downregulation of *SUV39H1* leads to heterochromatin relaxation in pericentric satellite regions and thereby contributes to genomic instability and senescence (Czvitkovich et al., 2001; Peters et al., 2001; Sidler et al., 2014).

4.1.4. Cellular regrowth is MYCN- and p21-dependent

This work indicated that p21 is a critical factor for maintaining cellular senescence and preventing regrowth after treatment. Experiments on cells stably expressing shRNA against p21 revealed that activation of p53 without induction of p21 expression leads to the suppression of senescence and induction of regrowth even in MYCN-low cells, Figure 20,21,22. It was found that absence of p21 during treatment significantly reduced the proportion of G1 arrested cells and increased percentage of cell death. As described previously, inhibition of p21 under DNA damage impedes activation of the G1/S checkpoint and leads to the induction of cell death (Crescenzi et al., 2008; Rousseau et al., 1999). The behavior of DOX treated MYCN-low cells with shRNA against p21 was very similar to those of MYCN-high cells with active p21. MYCN-low p21 knockdown cells were sensitized to death during and early after treatment, however this cell death was not complete

and a fraction of cells could form colonies and regrow. These results indicate that regrowth after chemotherapy can be explained by MYCN mediated suppression of p21.

Switching the *MYCN* conditional expression after DOX treatment suggests that regulation of p21 is mediated by MYCN. During treatment both MYCN-low and MYCN-high cells arrest and have potential to undergo senescence. Lowering of the MYCN level after treatment is sufficient to maintain elevated p21 expression, push cells into senescence and reduce regrowth. Whereas inducing MYCN expression only after treatment leads to the reduction of p21 expression, escape from senescence, and the induction of proliferation. Interestingly, a small proportion of cells, which were MYCN-high during treatment and MYCN-low after treatment still could escape senescence and proliferate. This may indicate that either the switching of the MYCN status by doxycycline was not complete, or that these cells exhibit properties enabling cellular regrowth, which were influenced by MYCN already during treatment.

In summary, experiments with p21 knockdown and with conditional regulation of MYCN expression after treatment provide a strong evidence that MYCN highly enhances the regrowth probability by repressing p21 expression after DOX treatment.

4.1.5. Altered expression of FUCCI markers after DNA damage

Under normal cycling conditions expression of FUCCI Cdt1 was found only during the G1 cell cycle phase, whereas FUCCI Geminin was expressed in G2 phase. Remarkably, altered expression of Cdt1 and Geminin was found in cells, which underwent cell cycle arrest after DNA damage. 20-24 hours after DOX addition cells showed deregulated expression of Cdt1 and Geminin fluorescence markers. Arrested cells exhibited high Cdt1 expression in G1 and G2 phases, while Geminin expression was completely lost in these cells, Figure 24, 25. Cells expressing high Cdt1 in G2 failed to process through mitosis. Similar loss of the Geminin FUCCI marker in G2 phase was observed after irradiation and establishment of the cell cycle in retinal epithelial cells (Krenning et al., 2014).

The expression of Cdt1 and Geminin is regulated by the sequential regulation of the E3 ubiquitin ligases APC^{Cdh1} and SCF^{Skp2}. Under normal cycling conditions the APC^{Cdh1} ubiquitin ligase is active in the late M and G1 phases and targets Geminin for degradation, while the SCF^{Skp2} ubiquitin ligase is active only during S and G2 phases and target Cdt1 for degradation (McGarry and Kirschner, 1998; Nishitani et al., 2004). Both Geminin and Ctd1 are highly expressed in G2, where Geminin binds and inhibits Cdt1 to prevent DNA re-replication (Klotz-Noack et al., 2012; Tada et al., 2001).

In this study, accumulation of Cdt1 and loss of Geminin were correlated with low Skp2 expression in G2. Skp2 is a component of the E3 ubiquitin ligase SCF^{Skp2} complex (Bornstein et al., 2003; Yu et al., 1998). In cycling cells, the levels of Skp2 are low at late M and during G1, increase during G1/S transition and reach a maximum in G2 phase (Bashir et al., 2004; Wei et al., 2004). Skp1's stability is also regulated by degradation in G1 phase through the APC^{Cdh1} complex (Bashir et al., 2004; Wei et al., 2004). Thus, high Cdt1 expression in G2 phase after DNA damage can be in part explained by the loss of its inhibitor Skp2, Figure 24B.

A study on human fibroblasts and the colon cancer cell line showed that the APC^{cdh1} ligase activity can be prematurely activated in G2 as a part of a p53-p21-dependent long-term response to DNA damage (Wiebusch and Hagemeier, 2010). Based on these data, loss of the Skp2 and Geminin in G2 phase after DNA damage can be explained by their degradation via APC^{cdh1} complex.

The deregulation of FUCCI markers occurs 20-24 hours after DOX add whereas checkpoints are activated in the first 4 to 10 hours, therefore it was still possible to determine the phase of cell cycle arrest in single cells after DNA damage, Figure 25.

4.1.6. Resister cells arise from G1-arrested subpopulation

Using extensive live-cell imaging, it was found that MYCN-high cells displayed great phenotypic variability after treatment washout. A fraction of cells died after treatment without entering mitosis, another fraction stayed arrested until the end of the observations, whereas a fraction of cells resumed the cell cycle within a few

days after treatment washout and entered mitosis. Most of the cells failed to correctly carry out the cytokinesis during mitosis, which resulted in undivided cells with fragmented nuclei and subsequent death of such cells, Figure 11. A minority of cells divided successfully into two phenotypical normal sister cells. These formed the basis for the new clonal population of resister cells.

The fact that checkpoints are activated only several hours after DOX addition means that cells move from one cell cycle phase into the next before arrest. It was found that the progression of single cells through the cell cycle during treatment and the phase of their arrest are powerful predictors for the cell fates after treatment.

Classification of the single cells into four groups according their phase of cell cycle immediately prior to treatment and at the end of the treatment indicated a specific subpopulation from where the resister cells arise. These were cells, which were at the M or early G1 phase at the time of DOX addition and stayed G1 arrested to the end of the treatment. In general, cells which transited through S or though M phases before arrest were more likely to die after treatment, had very low probability to re-enter the cell cycle and completely lacked the potential to regrow.

The ability of more than 90% of MYCN-high cells arrested in G1 to resume the cell cycle suggests that the G1/S checkpoint is inefficiently maintained after treatment. These results can in part be explained by the twofold effect of MYCN the on cells cycle: activation of cell cycle genes and suppression of cell cycle inhibitor p21 (Bell et al., 2006; Tweddle et al., 2001). The observation that more than half of the cells which re-entered cell cycle after G1-arrest divided correctly and had potential to regrow points to the sufficient repair of DSBs in these cells.

One possible explanation for the finding that G2-arrested cells lack the potential to regrow is the higher amount of DNA damage due to the limitation of the G1/S checkpoint during treatment (Deckbar et al., 2010). Since the G1/S checkpoint fails to prevent cells with DBSs from entering S phase within the first hours after treatment, such cells accumulate significantly elevated levels of unrepaired DSBs and chromosome breaks (Deckbar et al., 2010). Thus, high cell death and low cell cycle re-entry of G2-arrested cells could mean that these cells obtain irreparable damage and are eliminated from the population by p53-mediated apoptotic mechanisms (Petersen et al., 2010; Wahl et al., 1997). The limitations of the G2/S

checkpoint could be responsible for the strong death after treatment of cells transiting through M phase before arresting in G1 because cells which undergo mitosis with unrepaired DSBs very frequently lose their genetic material (Lobrich and Jeggo, 2007).

One study on retinal epithelial cells also showed that after irradiation G1 arrested cells showed high cell cycle re-entry, while G2 cells mostly failed to enter mitosis and underwent senescence from their G2 arrested state (Krenning et al., 2014). It was shown that cell fate decisions after DNA damage in G2 are largely determined by activation the of p53 and APC^{Cdh1} (Krenning et al., 2014). The irreversible withdrawal from cell cycle in G2 and establishment of senescence was explained by p21 and APC^{Cdh1} mediated nuclear retention and degradation of Cyclin B1 (Krenning et al., 2014). Other studies reported that p53-dependent downregulation of G2 cyclins, Cyclin B and Cyclin A, leads to permanent cell cycle arrest and that this is the first step in establishing senescence (d'Adda di Fagagna, 2008; Toettcher et al., 2009). This mechanism could explain the constant cell cycle arrest of MYCN-low senescent cells, which had continuous low levels of Cyclins and an elevated level of p21 after treatment.

4.1.7. G1-arrested resister cells have efficient DNA damage repair during treatment

The earliest event of the DNA damage response is the phosphorylation of H2AX to yH2AX by the ATM, ATR and/or DNA/PK kinases (Harper and Elledge, 2007; Jackson and Bartek, 2009). yH2AX forms foci at DNA damage sites and these foci provide an indirect measure for DSBs in single cells. The ubiquitylation of yH2AX allows the accumulation of key repair factors like 53BP1 and BRCA1, which respectively determine the choice between NHEJ and HR repair pathways (Bergink and Jentsch, 2009; Callen et al., 2013; Lukas and Bartek, 2009; Mattiroli et al., 2012; Zhu et al., 2015). NHEJ is active throughout the cell cycle, whereas HR is active only in S-G2 phases (Heyer et al., 2010; Lieber, 2010; Shrivastav et al., 2008). Due to the finding that resister cells arise exclusively from G1-arrested subpopulation, this study was focusing on the analysis of DSBs repaired by NHEJ.

It was found that both MYCN-low and MYCN-high cells accumulate high amounts of DNA damage after DOX treatment but only MYCN-high cells recruit significantly more 53BP1 to the damage sites and activate NHEJ repair, Figure 30. Interestingly, the mean number of yH2AX foci at all analyzed time points was lower in MYCN-high cells, and higher in MYCN-low cells, although all cells obtained the same amount of DNA damage. This may indicate that MYCN-high cells have higher repair efficiency. While MYCN-low cells had impaired NHEJ during treatment, therefore they were unable to repair their damage sites and through this accumulated a higher amount of yH2AX.

53BP1 binding to DSBs is very complex and requires many determinants, including H4K20 methylation, RNF8-dependent degradation of competing H4K20me reads, H4K16 deacetylation, RNF168-mediated H2AK15 ubiquitylation and Ring1B/Bmil1-reguated H2AX K118/119 ubiquitylation (Acs et al., 2011; Botuyan et al., 2006; Fradet-Turcotte et al., 2013; Hsiao and Mizzen, 2013; Tang et al., 2013; Zhu et al., 2015). One possible explanation for the low 53BP1 foci formation in MYCN-low cells could be the low expression level of deubiquitinase USP7, which regulates the stability of RNF68 and Ring1B/Bmil1 (Ismail et al., 2010; Zhu et al., 2015). RNF68 and Ring1B/Bmil1 are both ubiquitin ligases, which regulate 53BP1 recruitment to damaged sites (Bohgaki et al., 2013; Ismail et al., 2010). TET21N MYCN-low cells expressed lower basal level of USP7 (RNA-Seq data not shown) compared to MYCN-high cells. Thus, low USP7 expression could reduce 53BP1 recruitment and activation in MYCN-low cells.

Analysis of 53BP1 foci dynamics in single cells by live-cell microscopy showed that G1 resister cells exhibit the most efficient DNA repair already during treatment, Figure 31. Only cells, which were in M/G1 at the beginning of treatment and arrested in G1 showed reduction in average foci numbers during treatment, indicating an early and efficient DNA repair via the NHEJ. Cells, which proceeded through S-phase during treatment and arrested in G2, had delayed repair induction, which resulted in subsequent cell death.

Thus, the resister cells which accumulate in the G1 arrested subpopulation did not pass through S or M phase during treatment, possibly sustaining less DNA damage and showed enhanced activity of the NHEJ. Efficient DNA repair of G1-arrested

cells explains the high proportion of G1 cells re-entering cell cycle after DNA damage and as a consequence derivation of resister cells from this subpopulation.

The efficiency of HR pathway was not investigated in this work; however, it is likely that this repair pathway plays a minor role in the DSBs repair after DOX. A study on colon cancer cells showed that NHEJ is the major contributor to the repair of DOX-induced DNA damage (Schonn et al., 2011). Inhibition of HR did not affect the amount of DOX-induced damage and was not required for the repair of DSBs (Schonn et al., 2011). Interesting results were obtained by analysis of NHEJ and HR repair in live single cells using florescence reporters (Karanam et al., 2012). It was shown that NHEJ is a dominant repair pathway in G1 and in G2 even if both repair pathways are functional, while in S phase the activity of the NHEJ pathway was found to be low (Karanam et al., 2012). The HR is inactivated in G1, increases gradually in S and achieves maximum in the middle of S phase where the amount of DNA replication is highest and declines toward late S and G2 (Karanam et al., 2012; Karanam et al., 2013). Furthermore, the it was shown that HR is slow in its activation reaches the maximum only 11h post DNA damage induction (Karanam et al., 2012). It is possible that cells transiting from G1 into S during the first several hours after treatment accumulate the highest amount of damage, which stays unrepaired because of the delayed activation of HR and downregulated NHEJ. A study in human fibroblasts demonstrated a double amount of yH2AX foci numbers in G2 compared to parallel cells in G1, which suggests that additional unrepaired DSBs arise during processing through S phase (Deckbar et al., 2010).

DNA repair is usually suppressed during mitosis therefore mitotic cells continue to divide without repairing broken chromosomes (Zirkle and Bloom, 1953). 53BP1 does not localize to sites of DNA damage during mitosis preventing sustaining NHEJ (Giunta et al., 2010; Nelson et al., 2009). Data from this work also indicate that cells transited from G2 into M never regrew and had delayed activation of NHEJ, probably only when they achieved G1 phase. Remarkably, it was found that if cells were already in M phases at the moment when treatment was applied then they usually arrested in G1, exhibited successful early repair and could regrow. Thus, these observations suggest that early activation of the NHEJ pathway is essential for efficient repair.

Collectively, these data indicate that delayed activation of cell cycle checkpoints during treatment results in the cellular accumulation of additional unrepaired DBSs, which probably can't be completely repaired. While, early and efficient repair via the NHEJ of G1-arrested cells contributes to cell cycle re-entry and regrowth after chemotherapy.

4.1.8. Tailored combined therapy that targets specific properties of resister cells successfully abolishes resisters.

This work identified that resister cells are characterized by MYCN expression, G1 arrest and efficient DNA repair. The specific features of resister cells were targeted to optimize the first-line therapy and to prevent regrowth after treatment.

Synchronization of cells in G2 by CDK1 inhibitor prior to treatment resulted in the increased proportion of death during treatment and in the delayed regrowth of MYCN-high cells, Figure 32. It was not possible to completely abolish G1 subpopulation and approximately 8 to 12 percent of the cells were always arrested in G1 during treatment. Live cells imaging revealed that exactly these G1 arrested cells could re-enter the cell cycle and generate colonies. The inhibition of CDK1 in cells overexpressing MYCC and MYCN is known to increase apoptosis through suppression of the apoptotic protein survivin (Chen et al., 2013; Goga et al., 2007). This work demonstrated that upon combined treatment with DOX plus CDK1 inhibitor the cell death occurs mostly in G2 cells, whereas cells arrested in G1 phase still have potential to regrow. Hence, already a single resister cell is sufficient to generate a colony and initiate tumor relapse. Since even in vitro it is impossible to achieve a complete synchronization, this strategy is unlikely to be effective in clinical applications.

Interesting results were achieved by synchronizing of cells in G1 using CDK4 inhibitor. One could expect that accumulation of the population in G1 should enrich number of regrowing cells, however, after combined treatment with DOX plus CDK4 inhibitor only a reduced regrowth of MYCN-high cells was observed, Figure 33. CDK4 is usually unregulated by MYCN, which leads to the activation of Rb signaling and represents the mechanism by which MYCN cells evade G1 arrest (Westermann et al., 2008). Therefore the inhibition of CDK4 restores the G1/S

arrest in *MYCN*-amplified neuroblastoma cell lines (Gogolin et al., 2013; Rihani et al., 2015). The reduced regrowth rate of cells enriched in G1 may indicate that inhibition of CDK4 suppresses important players responsible for G1/S transition after treatment and that CDK4 inhibition can delay but not abolish resistance. Thus, DNA repair alone is not sufficient to initiate regrowth, and the synergy between activation of cell cycle proteins and efficient DNA repair is responsible for chemoresistance.

Targeting another property of resister cells, the efficient DNA damage repair resulted in the eradication of resister cells. Several inhibitors against proteins involved in DNA damage response in combination with DOX treatment were tested. In general all of the tested inhibitors delayed regrowth but only combined treatment of DOX plus ATMi completely abolished resistance in all analyzed cell lines, Figure 34, 36.

In response to DSBs, ATM initiates a cascade of phosphorylation events, which activate cell cycle arrest by p53 signaling and promote DNA repair by both HR and NHEJ (Cortez et al., 1999; Riballo et al., 2004; Shiloh, 2006). Previous studies with ATM inhibitors showed significant chemo- and radiosensitization, in *in vivo* and *in virto* models of colon cancer and glioma, with the absence of toxicity (Batey et al., 2013; Vecchio et al., 2014; Vecchio et al., 2015). It was shown that ATM inhibition sensitizes some glioma cell lines to ionizing irradiation by pushing cells into proliferation (Raso et al., 2012). This study showed similar effects, combined treatment with DOX plus ATM inhibitor prevented ATM phosphorylation and activation of p53 signaling, Figure 37. This resulted in the failure of G1/S checkpoint with accumulation of MYCN-high cells in G2, failed NHEJ repair activation, and subsequent cell death with eradication of resister cells, Figure 38. Interestingly, the MYCN-low cells just very slightly increased the number of cell death and permanently stayed arrested after combined therapy. Thus the almost complete death of MYCN-high cells compared with the low death rate of MYCN-low cells suggests that in context with combined therapy the MYCN-promoted apoptosis is an important feature that helps to abolish resistance.

The success of combined treatment with DOX and ATM can be explained by targeting the specific features of resister cells. This include the reduction of G1 arrested cells and the increase of the number of cells transiting into S phase during

treatment, inhibition of DSB repair, and activation of MYCN-mediated apoptosis in unrepaired cells.

4.1.9. Conclusions

The present study provides the basis for the understanding of the mechanisms through which oncoprotein MYCN sensitizes cells to death during chemotherapy and promotes cellular regrowth thereafter, Figure 39.

MYCN shortens cell cycle phases and accelerates proliferation by enhancing the expression of cell cycle genes under standard *in vitro* growth conditions. This results in delayed activation of cell cycle arrest and increases the proportion of cells transiting through G1/S and G2/M upon chemotherapy. High proportion of cells entering S and M phases during DNA damage is one of the mechanisms how MYCN sensitizes cells to death. Another mechanism is that MYCN switches the p53 function in favor of apoptosis rather than cell cycle arrest and senescence by activation of 53-induced cell death and suppression of cell cycle inhibitor p21.

However, MYCN-induced cell death is not complete and MYCN also drives the clonal regrowth of a small fraction of surviving resister cells after therapy. The closer characterization revealed that resister cells arise exclusively from the G1-arrested subpopulation. MYCN-dependent regrowth can be explained by efficient DNA repair in G1 and activation of cell cycle genes after treatment, both promoted by MYCN.

Suppression of DNA DSBs repair by inhibition of ATM during DNA damage reduces the proportion of G1-arrested cells and prevents DNA repair, leading to complete eradication of resister cells. This work shows that targeting specific features of resister cells may help to improve first-line therapy and to avoid resistance.

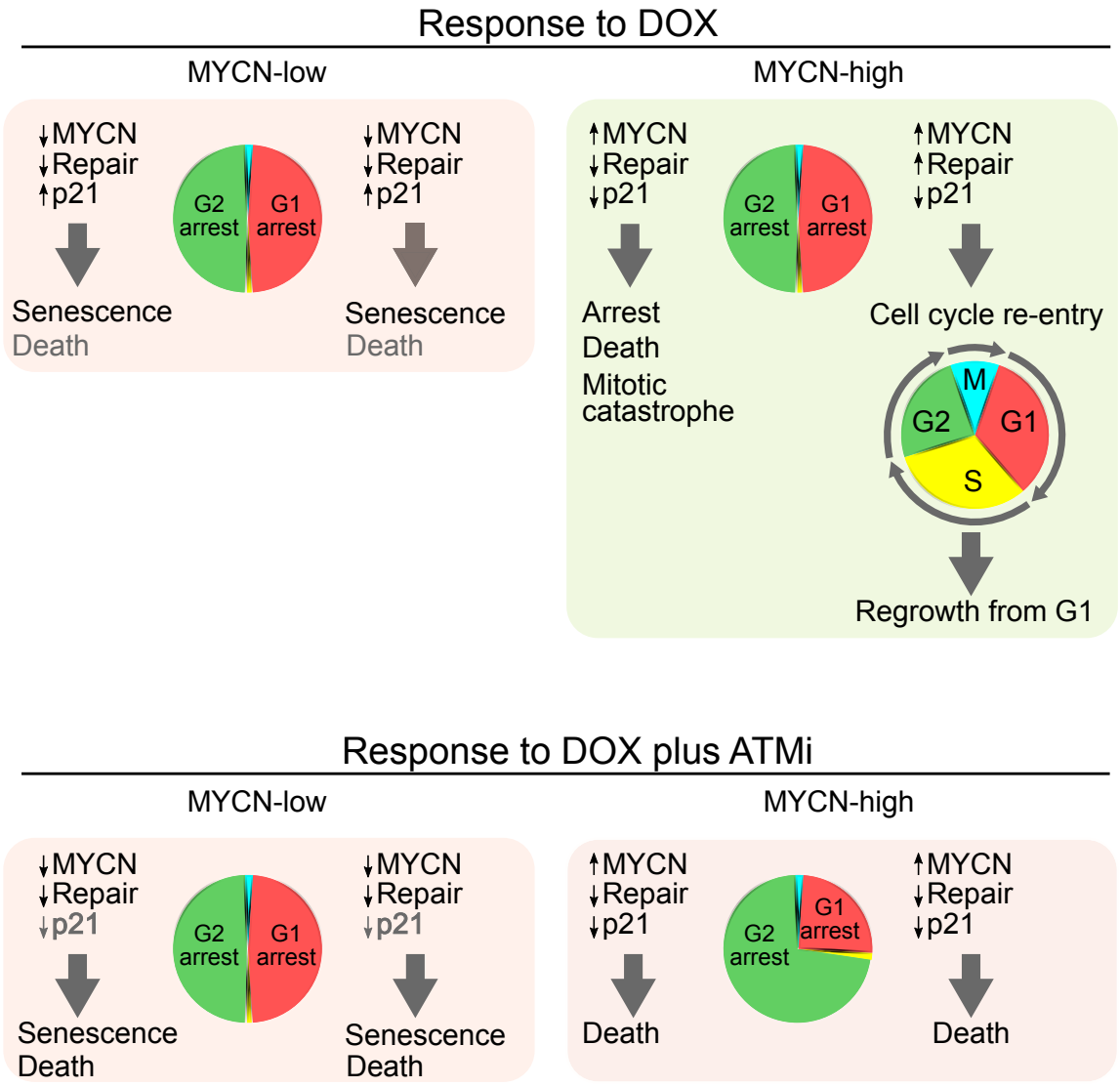

Figure 39. Summary of cellular outcomes after chemotherapy.

5. References

Acs, K., Luijsterburg, M.S., Ackermann, L., Salomons, F.A., Hoppe, T., and Dantuma, N.P. (2011). The AAA-ATPase VCP/p97 promotes 53BP1 recruitment by removing L3MBTL1 from DNA double-strand breaks. Nat Struct Mol Biol *18*, 1345-1350.

Adhikary, S., and Eilers, M. (2005). Transcriptional regulation and transformation by Myc proteins. Nat Rev Mol Cell Biol *6*, 635-645.

Aldosari, N., Bigner, S.H., Burger, P.C., Becker, L., Kepner, J.L., Friedman, H.S., and McLendon, R.E. (2002). MYCC and MYCN oncogene amplification in medulloblastoma. A fluorescence in situ hybridization study on paraffin sections from the Children's Oncology Group. Arch Pathol Lab Med *126*, 540-544.

Altungoz, O., Aygun, N., Tumer, S., Ozer, E., Olgun, N., and Sakizli, M. (2007). Correlation of modified Shimada classification with MYCN and 1p36 status detected by fluorescence in situ hybridization in neuroblastoma. Cancer Genet Cytogenet *172*, 113-119.

Amiel, J., Laudier, B., Attie-Bitach, T., Trang, H., de Pontual, L., Gener, B., Trochet, D., Etchevers, H., Ray, P., Simonneau, M.*, et al.* (2003). Polyalanine expansion and frameshift mutations of the paired-like homeobox gene PHOX2B in congenital central hypoventilation syndrome. Nat Genet *33*, 459-461.

Aparicio, T., Baer, R., and Gautier, J. (2014). DNA double-strand break repair pathway choice and cancer. DNA Repair (Amst) *19*, 169-175.

Arias, E.E., and Walter, J.C. (2007). Strength in numbers: preventing rereplication via multiple mechanisms in eukaryotic cells. Genes Dev *21*, 497-518.

Atadja, P., Wong, H., Veillette, C., and Riabowol, K. (1995). Overexpression of cyclin D1 blocks proliferation of normal diploid fibroblasts. Exp Cell Res *217*, 205-216.

Attiyeh, E.F., London, W.B., Mosse, Y.P., Wang, Q., Winter, C., Khazi, D., McGrady, P.W., Seeger, R.C., Look, A.T., Shimada, H.*, et al.* (2005). Chromosome 1p and 11q deletions and outcome in neuroblastoma. N Engl J Med *353*, 2243-2253.

Baker, D.L., Schmidt, M.L., Cohn, S.L., Maris, J.M., London, W.B., Buxton, A., Stram, D., Castleberry, R.P., Shimada, H., Sandler, A.*, et al.* (2010). Outcome after reduced chemotherapy for intermediate-risk neuroblastoma. N Engl J Med *363*, 1313-1323.

Baldwin, E.L., and Osheroff, N. (2005). Etoposide, topoisomerase II and cancer. Curr Med Chem Anticancer Agents *5*, 363-372.

Banin, S., Moyal, L., Shieh, S., Taya, Y., Anderson, C.W., Chessa, L., Smorodinsky, N.I., Prives, C., Reiss, Y., Shiloh, Y.*, et al.* (1998). Enhanced phosphorylation of p53 by ATM in response to DNA damage. Science *281*, 1674-1677.

Bartek, J., Lukas, C., and Lukas, J. (2004). Checking on DNA damage in S phase. Nat Rev Mol Cell Biol *5*, 792-804.

Bartek, J., and Lukas, J. (2001). Pathways governing G1/S transition and their response to DNA damage. FEBS Lett *490*, 117-122.

Bashir, T., Dorrello, N.V., Amador, V., Guardavaccaro, D., and Pagano, M. (2004). Control of the SCF(Skp2-Cks1) ubiquitin ligase by the APC/C(Cdh1) ubiquitin ligase. Nature *428*, 190-193.

Batey, M.A., Zhao, Y., Kyle, S., Richardson, C., Slade, A., Martin, N.M., Lau, A., Newell, D.R., and Curtin, N.J. (2013). Preclinical evaluation of a novel ATM inhibitor, KU59403, in vitro and in vivo in p53 functional and dysfunctional models of human cancer. Mol Cancer Ther *12*, 959-967.

Bell, E., Chen, L., Liu, T., Marshall, G.M., Lunec, J., and Tweddle, D.A. (2010). MYCN oncoprotein targets and their therapeutic potential. Cancer Lett *293*, 144-157.

Bell, E., Lunec, J., and Tweddle, D.A. (2007). Cell cycle regulation targets of MYCN identified by gene expression microarrays. Cell Cycle *6*, 1249-1256.

Bell, E., Premkumar, R., Carr, J., Lu, X., Lovat, P.E., Kees, U.R., Lunec, J., and Tweddle, D.A. (2006). The role of MYCN in the failure of MYCN amplified neuroblastoma cell lines to G1 arrest after DNA damage. Cell Cycle *5*, 2639-2647.

Beltran, H. (2014). The N-myc Oncogene: Maximizing its Targets, Regulation, and Therapeutic Potential. Mol Cancer Res *12*, 815-822.

Beltran, H., Rickman, D.S., Park, K., Chae, S.S., Sboner, A., MacDonald, T.Y., Wang, Y., Sheikh, K.L., Terry, S., Tagawa, S.T.*, et al.* (2011). Molecular characterization of neuroendocrine prostate cancer and identification of new drug targets. Cancer Discov *1*, 487-495.

Bergink, S., and Jentsch, S. (2009). Principles of ubiquitin and SUMO modifications in DNA repair. Nature *458*, 461-467.

Betters, E., Liu, Y., Kjaeldgaard, A., Sundstrom, E., and Garcia-Castro, M.I. (2010). Analysis of early human neural crest development. Dev Biol *344*, 578-592.

Bjerke, L., Mackay, A., Nandhabalan, M., Burford, A., Jury, A., Popov, S., Bax, D.A., Carvalho, D., Taylor, K.R., Vinci, M.*, et al.* (2013). Histone H3.3. mutations drive pediatric glioblastoma through upregulation of MYCN. Cancer Discov *3*, 512-519.

Bohgaki, M., Bohgaki, T., El Ghamrasni, S., Srikumar, T., Maire, G., Panier, S., Fradet-Turcotte, A., Stewart, G.S., Raught, B., Hakem, A.*, et al.* (2013). RNF168 ubiquitylates 53BP1 and controls its response to DNA double-strand breaks. Proc Natl Acad Sci U S A *110*, 20982-20987.

Bornstein, G., Bloom, J., Sitry-Shevah, D., Nakayama, K., Pagano, M., and Hershko, A. (2003). Role of the SCFSkp2 ubiquitin ligase in the degradation of p21Cip1 in S phase. J Biol Chem *278*, 25752-25757.

Bosse, K.R., and Maris, J.M. (2015). Advances in the translational genomics of neuroblastoma: From improving risk stratification and revealing novel biology to identifying actionable genomic alterations. Cancer.

Botuyan, M.V., Lee, J., Ward, I.M., Kim, J.E., Thompson, J.R., Chen, J., and Mer, G. (2006). Structural basis for the methylation state-specific recognition of histone H4-K20 by 53BP1 and Crb2 in DNA repair. Cell *127*, 1361-1373.

Bracken, A.P., Kleine-Kohlbrecher, D., Dietrich, N., Pasini, D., Gargiulo, G., Beekman, C., Theilgaard-Monch, K., Minucci, S., Porse, B.T., Marine, J.C.*, et al.* (2007). The Polycomb group proteins bind throughout the INK4A-ARF locus and are disassociated in senescent cells. Genes Dev *21*, 525-530.

Bresler, S.C., Weiser, D.A., Huwe, P.J., Park, J.H., Krytska, K., Ryles, H., Laudenslager, M., Rappaport, E.F., Wood, A.C., McGrady, P.W.*, et al.* (2014). ALK mutations confer differential oncogenic activation and sensitivity to ALK inhibition therapy in neuroblastoma. Cancer Cell *26*, 682-694.

Brodeur, G.M., Seeger, R.C., Schwab, M., Varmus, H.E., and Bishop, J.M. (1984). Amplification of N-myc in untreated human neuroblastomas correlates with advanced disease stage. Science *224*, 1121-1124.

Callen, E., Di Virgilio, M., Kruhlak, M.J., Nieto-Soler, M., Wong, N., Chen, H.T., Faryabi, R.B., Polato, F., Santos, M., Starnes, L.M.*, et al.* (2013). 53BP1 mediates productive and mutagenic DNA repair through distinct phosphoprotein interactions. Cell *153*, 1266-1280.

Canete, A., Gerrard, M., Rubie, H., Castel, V., Di Cataldo, A., Munzer, C., Ladenstein, R., Brichard, B., Bermudez, J.D., Couturier, J.*, et al.* (2009). Poor survival for infants with MYCN-amplified metastatic neuroblastoma despite intensified treatment: the International Society of Paediatric Oncology European Neuroblastoma Experience. J Clin Oncol *27*, 1014-1019.

Caren, H., Erichsen, J., Olsson, L., Enerback, C., Sjoberg, R.M., Abrahamsson, J., Kogner, P., and Martinsson, T. (2008). High-resolution array copy number analyses for detection of deletion, gain, amplification and copy-neutral LOH in primary neuroblastoma tumors: four cases of homozygous deletions of the CDKN2A gene. BMC Genomics *9*, 353.

Caron, H., van Sluis, P., van Hoeve, M., de Kraker, J., Bras, J., Slater, R., Mannens, M., Voute, P.A., Westerveld, A., and Versteeg, R. (1993). Allelic loss of chromosome 1p36 in neuroblastoma is of preferential maternal origin and correlates with N-myc amplification. Nat Genet *4*, 187-190.

Carpenter, E.L., and Mosse, Y.P. (2012). Targeting ALK in neuroblastoma--preclinical and clinical advancements. Nat Rev Clin Oncol *9*, 391-399.

Carr-Wilkinson, J., O'Toole, K., Wood, K.M., Challen, C.C., Baker, A.G., Board, J.R., Evans, L., Cole, M., Cheung, N.K., Boos, J.*, et al.* (2010). High Frequency of p53/MDM2/p14ARF Pathway Abnormalities in Relapsed Neuroblastoma. Clin Cancer Res *16*, 1108-1118.

Chang, B.D., Watanabe, K., Broude, E.V., Fang, J., Poole, J.C., Kalinichenko, T.V., and Roninson, I.B. (2000). Effects of p21Waf1/Cip1/Sdi1 on cellular gene expression: implications for carcinogenesis, senescence, and age-related diseases. Proc Natl Acad Sci U S A *97*, 4291-4296.

Charron, J., Malynn, B.A., Fisher, P., Stewart, V., Jeannotte, L., Goff, S.P., Robertson, E.J., and Alt, F.W. (1992). Embryonic lethality in mice homozygous for a targeted disruption of the N-myc gene. Genes Dev *6*, 2248-2257.

Chen, J., Huang, X., Halicka, D., Brodsky, S., Avram, A., Eskander, J., Bloomgarden, N.A., Darzynkiewicz, Z., and Goligorsky, M.S. (2006). Contribution of p16INK4a and p21CIP1 pathways to induction of premature senescence of human endothelial cells: permissive role of p53. Am J Physiol Heart Circ Physiol *290*, H1575-1586.

Chen, L., Iraci, N., Gherardi, S., Gamble, L.D., Wood, K.M., Perini, G., Lunec, J., and Tweddle, D.A. (2010). p53 is a direct transcriptional target of MYCN in neuroblastoma. Cancer Res *70*, 1377-1388.

Chen, Y., Tsai, Y.H., and Tseng, S.H. (2013). Inhibition of cyclin-dependent kinase 1-induced cell death in neuroblastoma cells through the microRNA-34a-MYCN-survivin pathway. Surgery *153*, 4-16.

Chesler, L., Goldenberg, D.D., Collins, R., Grimmer, M., Kim, G.E., Tihan, T., Nguyen, K., Yakovenko, S., Matthay, K.K., and Weiss, W.A. (2008). Chemotherapy-induced apoptosis in a transgenic model of neuroblastoma proceeds through p53 induction. Neoplasia *10*, 1268-1274.

Cheung, N.K., Zhang, J., Lu, C., Parker, M., Bahrami, A., Tickoo, S.K., Heguy, A., Pappo, A.S., Federico, S., Dalton, J.*, et al.* (2012). Association of age at diagnosis and genetic mutations in patients with neuroblastoma. JAMA *307*, 1062-1071.

Chicas, A., Kapoor, A., Wang, X., Aksoy, O., Evertts, A.G., Zhang, M.Q., Garcia, B.A., Bernstein, E., and Lowe, S.W. (2012). H3K4 demethylation by Jarid1a and Jarid1b contributes to retinoblastoma-mediated gene silencing during cellular senescence. Proc Natl Acad Sci U S A *109*, 8971-8976.

Cohn, S.L., Pearson, A.D., London, W.B., Monclair, T., Ambros, P.F., Brodeur, G.M., Faldum, A., Hero, B., Iehara, T., Machin, D.*, et al.* (2009). The International Neuroblastoma Risk Group (INRG) classification system: an INRG Task Force report. J Clin Oncol *27*, 289-297.

Cortez, D., Wang, Y., Qin, J., and Elledge, S.J. (1999). Requirement of ATM-dependent phosphorylation of brca1 in the DNA damage response to double-strand breaks. Science *286*, 1162-1166.

Courtois-Cox, S., Jones, S.L., and Cichowski, K. (2008). Many roads lead to oncogene-induced senescence. Oncogene *27*, 2801-2809.

Crescenzi, E., Palumbo, G., de Boer, J., and Brady, H.J. (2008). Ataxia telangiectasia mutated and p21CIP1 modulate cell survival of drug-induced senescent tumor cells: implications for chemotherapy. Clin Cancer Res *14*, 1877-1887.

Cui, H., Li, T., and Ding, H.F. (2005). Linking of N-Myc to death receptor machinery in neuroblastoma cells. J Biol Chem *280*, 9474-9481.

Czvitkovich, S., Sauer, S., Peters, A.H., Deiner, E., Wolf, A., Laible, G., Opravil, S., Beug, H., and Jenuwein, T. (2001). Over-expression of the SUV39H1 histone methyltransferase induces altered proliferation and differentiation in transgenic mice. Mech Dev *107*, 141-153.

d'Adda di Fagagna, F. (2008). Living on a break: cellular senescence as a DNA-damage response. Nat Rev Cancer *8*, 512-522.

Dang, C.V., O'Donnell, K.A., Zeller, K.I., Nguyen, T., Osthus, R.C., and Li, F. (2006). The c-Myc target gene network. Semin Cancer Biol *16*, 253-264.

Davis, A.J., Chen, B.P., and Chen, D.J. (2014). DNA-PK: a dynamic enzyme in a versatile DSB repair pathway. DNA Repair (Amst) *17*, 21-29.

De Bernardi, B., Gerrard, M., Boni, L., Rubie, H., Canete, A., Di Cataldo, A., Castel, V., Forjaz de Lacerda, A., Ladenstein, R., Ruud, E.*, et al.* (2009). Excellent outcome with reduced treatment for

infants with disseminated neuroblastoma without MYCN gene amplification. J Clin Oncol *27*, 1034-1040.

De Bernardi, B., Mosseri, V., Rubie, H., Castel, V., Foot, A., Ladenstein, R., Laureys, G., Beck-Popovic, M., de Lacerda, A.F., Pearson, A.D.*, et al.* (2008). Treatment of localised resectable neuroblastoma. Results of the LNESG1 study by the SIOP Europe Neuroblastoma Group. Br J Cancer *99*, 1027-1033.

Deckbar, D., Jeggo, P.A., and Lobrich, M. (2011). Understanding the limitations of radiation-induced cell cycle checkpoints. Crit Rev Biochem Mol Biol *46*, 271-283.

Deckbar, D., Stiff, T., Koch, B., Reis, C., Lobrich, M., and Jeggo, P.A. (2010). The limitations of the G1-S checkpoint. Cancer Res *70*, 4412-4421.

Dees, E.C., O'Neil, B.H., Lindley, C.M., Collichio, F., Carey, L.A., Collins, J., Riordan, W.J., Ivanova, A., Esseltine, D., and Orlowski, R.Z. (2008). A phase I and pharmacologic study of the combination of bortezomib and pegylated liposomal doxorubicin in patients with refractory solid tumors. Cancer Chemother Pharmacol *63*, 99-107.

Di Micco, R., Sulli, G., Dobreva, M., Liontos, M., Botrugno, O.A., Gargiulo, G., dal Zuffo, R., Matti, V., d'Ario, G., Montani, E.*, et al.* (2011). Interplay between oncogene-induced DNA damage response and heterochromatin in senescence and cancer. Nat Cell Biol *13*, 292-302.

Dorr, J.R., Yu, Y., Milanovic, M., Beuster, G., Zasada, C., Dabritz, J.H., Lisec, J., Lenze, D., Gerhardt, A., Schleicher, K.*, et al.* (2013). Synthetic lethal metabolic targeting of cellular senescence in cancer therapy. Nature *501*, 421-425.

Downes, C.S., Clarke, D.J., Mullinger, A.M., Gimenez-Abian, J.F., Creighton, A.M., and Johnson, R.T. (1994). A topoisomerase II-dependent G2 cycle checkpoint in mammalian cells. Nature *372*, 467-470.

Dynan, W.S., and Yoo, S. (1998). Interaction of Ku protein and DNA-dependent protein kinase catalytic subunit with nucleic acids. Nucleic Acids Res *26*, 1551-1559.

Dyson, N. (1998). The regulation of E2F by pRB-family proteins. Genes Dev *12*, 2245-2262.

Eleveld, T.F., Oldridge, D.A., Bernard, V., Koster, J., Daage, L.C., Diskin, S.J., Schild, L., Bentahar, N.B., Bellini, A., Chicard, M.*, et al.* (2015). Relapsed neuroblastomas show frequent RAS-MAPK pathway mutations. Nat Genet *47*, 864-871.

Escribano-Diaz, C., Orthwein, A., Fradet-Turcotte, A., Xing, M., Young, J.T., Tkac, J., Cook, M.A., Rosebrock, A.P., Munro, M., Canny, M.D.*, et al.* (2013). A cell cycle-dependent regulatory circuit composed of 53BP1-RIF1 and BRCA1-CtIP controls DNA repair pathway choice. Mol Cell *49*, 872-883.

Fan, T., Jiang, S., Chung, N., Alikhan, A., Ni, C., Lee, C.C., and Hornyak, T.J. (2011). EZH2-dependent suppression of a cellular senescence phenotype in melanoma cells by inhibition of p21/CDKN1A expression. Mol Cancer Res *9*, 418-429.

Feng, L., Fong, K.W., Wang, J., Wang, W., and Chen, J. (2013). RIF1 counteracts BRCA1-mediated end resection during DNA repair. J Biol Chem *288*, 11135-11143.

Fradet-Turcotte, A., Canny, M.D., Escribano-Diaz, C., Orthwein, A., Leung, C.C., Huang, H., Landry, M.C., Kitevski-LeBlanc, J., Noordermeer, S.M., Sicheri, F.*, et al.* (2013). 53BP1 is a reader of the DNA-damage-induced H2A Lys 15 ubiquitin mark. Nature *499*, 50-54.

Franks, L.M., Bollen, A., Seeger, R.C., Stram, D.O., and Matthay, K.K. (1997). Neuroblastoma in adults and adolescents: an indolent course with poor survival. Cancer *79*, 2028-2035.

Friend, S.H., Bernards, R., Rogelj, S., Weinberg, R.A., Rapaport, J.M., Albert, D.M., and Dryja, T.P. (1986). A human DNA segment with properties of the gene that predisposes to retinoblastoma and osteosarcoma. Nature *323*, 643-646.

Fukami, J., Anno, K., Ueda, K., Takahashi, T., and Ide, T. (1995). Enhanced expression of cyclin D1 in senescent human fibroblasts. Mech Ageing Dev *81*, 139-157.

Fulda, S., Lutz, W., Schwab, M., and Debatin, K.M. (2000). MycN sensitizes neuroblastoma cells for drug-triggered apoptosis. Med Pediatr Oncol *35*, 582-584.

Funa, K., Steinholtz, L., Nou, E., and Bergh, J. (1987). Increased expression of N-myc in human small cell lung cancer biopsies predicts lack of response to chemotherapy and poor prognosis. Am J Clin Pathol *88*, 216-220.

Gatta, G., Botta, L., Rossi, S., Aareleid, T., Bielska-Lasota, M., Clavel, J., Dimitrova, N., Jakab, Z., Kaatsch, P., Lacour, B.*, et al.* (2014). Childhood cancer survival in Europe 1999-2007: results of EUROCARE-5--a population-based study. Lancet Oncol *15*, 35-47.

George, R.E., London, W.B., Cohn, S.L., Maris, J.M., Kretschmar, C., Diller, L., Brodeur, G.M., Castleberry, R.P., and Look, A.T. (2005). Hyperdiploidy plus nonamplified MYCN confers a favorable prognosis in children 12 to 18 months old with disseminated neuroblastoma: a Pediatric Oncology Group study. J Clin Oncol *23*, 6466-6473.

George, R.E., Sanda, T., Hanna, M., Frohling, S., Luther, W., 2nd, Zhang, J., Ahn, Y., Zhou, W., London, W.B., McGrady, P.*, et al.* (2008). Activating mutations in ALK provide a therapeutic target in neuroblastoma. Nature *455*, 975-978.

Gillis, L.D., Leidal, A.M., Hill, R., and Lee, P.W. (2009). p21Cip1/WAF1 mediates cyclin B1 degradation in response to DNA damage. Cell Cycle *8*, 253-256.

Giunta, S., Belotserkovskaya, R., and Jackson, S.P. (2010). DNA damage signaling in response to double-strand breaks during mitosis. J Cell Biol *190*, 197-207.

Goga, A., Yang, D., Tward, A.D., Morgan, D.O., and Bishop, J.M. (2007). Inhibition of CDK1 as a potential therapy for tumors over-expressing MYC. Nat Med *13*, 820-827.

Gogolin, S., Ehemann, V., Becker, G., Brueckner, L.M., Dreidax, D., Bannert, S., Nolte, I., Savelyeva, L., Bell, E., and Westermann, F. (2013). CDK4 inhibition restores G(1)-S arrest in MYCN-amplified neuroblastoma cells in the context of doxorubicin-induced DNA damage. Cell Cycle *12*, 1091-1104.

Goodarzi, A.A., and Jeggo, P.A. (2013). The repair and signaling responses to DNA double-strand breaks. Adv Genet *82*, 1-45.

Goto, S., Umehara, S., Gerbing, R.B., Stram, D.O., Brodeur, G.M., Seeger, R.C., Lukens, J.N., Matthay, K.K., and Shimada, H. (2001). Histopathology (International Neuroblastoma Pathology Classification) and MYCN status in patients with peripheral neuroblastic tumors: a report from the Children's Cancer Group. Cancer *92*, 2699-2708.

Grandori, C., Cowley, S.M., James, L.P., and Eisenman, R.N. (2000). The Myc/Max/Mad network and the transcriptional control of cell behavior. Annu Rev Cell Dev Biol *16*, 653-699.

Hall, P.A., and Watt, F.M. (1989). Stem cells: the generation and maintenance of cellular diversity. Development *106*, 619-633.

Han, Z., Wei, W., Dunaway, S., Darnowski, J.W., Calabresi, P., Sedivy, J., Hendrickson, E.A., Balan, K.V., Pantazis, P., and Wyche, J.H. (2002). Role of p21 in apoptosis and senescence of human colon cancer cells treated with camptothecin. J Biol Chem *277*, 17154-17160.

Hanahan, D., and Weinberg, R.A. (2011). Hallmarks of cancer: the next generation. Cell *144*, 646-674.

Harper, J.W., and Elledge, S.J. (2007). The DNA damage response: ten years after. Mol Cell *28*, 739-745.

Hartwell, L.H., and Weinert, T.A. (1989). Checkpoints: controls that ensure the order of cell cycle events. Science *246*, 629-634.

Heaphy, C.M., de Wilde, R.F., Jiao, Y., Klein, A.P., Edil, B.H., Shi, C., Bettegowda, C., Rodriguez, F.J., Eberhart, C.G., Hebbar, S.*, et al.* (2011). Altered telomeres in tumors with ATRX and DAXX mutations. Science *333*, 425.

Henriksson, M., and Luscher, B. (1996). Proteins of the Myc network: essential regulators of cell growth and differentiation. Adv Cancer Res *68*, 109-182.

Hero, B., Simon, T., Spitz, R., Ernestus, K., Gnekow, A.K., Scheel-Walter, H.G., Schwabe, D., Schilling, F.H., Benz-Bohm, G., and Berthold, F. (2008). Localized infant neuroblastomas often show spontaneous regression: results of the prospective trials NB95-S and NB97. J Clin Oncol *26*, 1504-1510.

Heyer, W.D., Ehmsen, K.T., and Liu, J. (2010). Regulation of homologous recombination in eukaryotes. Annu Rev Genet *44*, 113-139.

Hodgson, J.G., Yeh, R.F., Ray, A., Wang, N.J., Smirnov, I., Yu, M., Hariono, S., Silber, J., Feiler, H.S., Gray, J.W.*, et al.* (2009). Comparative analyses of gene copy number and mRNA expression in glioblastoma multiforme tumors and xenografts. Neuro Oncol *11*, 477-487.

Holm, C., Covey, J.M., Kerrigan, D., and Pommier, Y. (1989). Differential requirement of DNA replication for the cytotoxicity of DNA topoisomerase I and II inhibitors in Chinese hamster DC3F cells. Cancer Res *49*, 6365-6368.

Honda, R., Tanaka, H., and Yasuda, H. (1997). Oncoprotein MDM2 is a ubiquitin ligase E3 for tumor suppressor p53. FEBS Lett *420*, 25-27.

Howard, M.T., Neece, S.H., Matson, S.W., and Kreuzer, K.N. (1994). Disruption of a topoisomerase-DNA cleavage complex by a DNA helicase. Proc Natl Acad Sci U S A *91*, 12031-12035.

Hsiao, K.Y., and Mizzen, C.A. (2013). Histone H4 deacetylation facilitates 53BP1 DNA damage signaling and double-strand break repair. J Mol Cell Biol *5*, 157-165.

Huang, M., and Weiss, W.A. (2013). Neuroblastoma and MYCN. Cold Spring Harb Perspect Med *3*, a014415.

Huang, X., Traganos, F., and Darzynkiewicz, Z. (2003). DNA damage induced by DNA topoisomerase I- and topoisomerase II-inhibitors detected by histone H2AX phosphorylation in relation to the cell cycle phase and apoptosis. Cell Cycle *2*, 614-619.

Iliakis, G. (2009). Backup pathways of NHEJ in cells of higher eukaryotes: cell cycle dependence. Radiother Oncol *92*, 310-315.

Iliakis, G., Wang, Y., Guan, J., and Wang, H. (2003). DNA damage checkpoint control in cells exposed to ionizing radiation. Oncogene *22*, 5834-5847.

Ismail, I.H., Andrin, C., McDonald, D., and Hendzel, M.J. (2010). BMI1-mediated histone ubiquitylation promotes DNA double-strand break repair. J Cell Biol *191*, 45-60.

Jackson, S.P., and Bartek, J. (2009). The DNA-damage response in human biology and disease. Nature *461*, 1071-1078.

Janoueix-Lerosey, I., Lequin, D., Brugieres, L., Ribeiro, A., de Pontual, L., Combaret, V., Raynal, V., Puisieux, A., Schleiermacher, G., Pierron, G.*, et al.* (2008). Somatic and germline activating mutations of the ALK kinase receptor in neuroblastoma. Nature *455*, 967-970.

Janoueix-Lerosey, I., Schleiermacher, G., Michels, E., Mosseri, V., Ribeiro, A., Lequin, D., Vermeulen, J., Couturier, J., Peuchmaur, M., Valent, A.*, et al.* (2009). Overall genomic pattern is a predictor of outcome in neuroblastoma. J Clin Oncol *27*, 1026-1033.

Jasin, M., and Rothstein, R. (2013). Repair of strand breaks by homologous recombination. Cold Spring Harb Perspect Biol *5*, a012740.

Jeggo, P.A., and Lobrich, M. (2015). How cancer cells hijack DNA double-strand break repair pathways to gain genomic instability. Biochem J *471*, 1-11.

Karanam, K., Kafri, R., Loewer, A., and Lahav, G. (2012). Quantitative live cell imaging reveals a gradual shift between DNA repair mechanisms and a maximal use of HR in mid S phase. Mol Cell *47*, 320-329.

Karanam, K., Loewer, A., and Lahav, G. (2013). Dynamics of the DNA damage response: insights from live-cell imaging. Brief Funct Genomics *12*, 109-117.

Kastan, M.B., and Bartek, J. (2004). Cell-cycle checkpoints and cancer. Nature *432*, 316-323.

Kastan, M.B., Zhan, Q., el-Deiry, W.S., Carrier, F., Jacks, T., Walsh, W.V., Plunkett, B.S., Vogelstein, B., and Fornace, A.J., Jr. (1992). A mammalian cell cycle checkpoint pathway utilizing p53 and GADD45 is defective in ataxia-telangiectasia. Cell *71*, 587-597.

Khosravi, R., Maya, R., Gottlieb, T., Oren, M., Shiloh, Y., and Shkedy, D. (1999). Rapid ATM-dependent phosphorylation of MDM2 precedes p53 accumulation in response to DNA damage. Proc Natl Acad Sci U S A *96*, 14973-14977.

Kleiner, R.E., Verma, P., Molloy, K.R., Chait, B.T., and Kapoor, T.M. (2015). Chemical proteomics reveals a gammaH2AX-53BP1 interaction in the DNA damage response. Nat Chem Biol *11*, 807-814.

Klotz-Noack, K., McIntosh, D., Schurch, N., Pratt, N., and Blow, J.J. (2012). Re-replication induced by geminin depletion occurs from G2 and is enhanced by checkpoint activation. J Cell Sci *125*, 2436-2445.

Knoepfler, P.S., Cheng, P.F., and Eisenman, R.N. (2002). N-myc is essential during neurogenesis for the rapid expansion of progenitor cell populations and the inhibition of neuronal differentiation. Genes Dev *16*, 2699-2712.

Kohl, N.E., Kanda, N., Schreck, R.R., Bruns, G., Latt, S.A., Gilbert, F., and Alt, F.W. (1983). Transposition and amplification of oncogene-related sequences in human neuroblastomas. Cell *35*, 359-367.

Kohler, J.A., Rubie, H., Castel, V., Beiske, K., Holmes, K., Gambini, C., Casale, F., Munzer, C., Erminio, G., Parodi, S.*, et al.* (2013). Treatment of children over the age of one year with unresectable localised neuroblastoma without MYCN amplification: results of the SIOPEN study. Eur J Cancer *49*, 3671-3679.

Krasnoselsky, A.L., Whiteford, C.C., Wei, J.S., Bilke, S., Westermann, F., Chen, Q.R., and Khan, J. (2005). Altered expression of cell cycle genes distinguishes aggressive neuroblastoma. Oncogene *24*, 1533-1541.

Kreissman, S.G., Seeger, R.C., Matthay, K.K., London, W.B., Sposto, R., Grupp, S.A., Haas-Kogan, D.A., Laquaglia, M.P., Yu, A.L., Diller, L.*, et al.* (2013). Purged versus non-purged peripheral blood stem-cell transplantation for high-risk neuroblastoma (COG A3973): a randomised phase 3 trial. Lancet Oncol *14*, 999-1008.

Krempler, A., Deckbar, D., Jeggo, P.A., and Lobrich, M. (2007). An imperfect G2M checkpoint contributes to chromosome instability following irradiation of S and G2 phase cells. Cell Cycle *6*, 1682-1686.

Krenning, L., Feringa, F.M., Shaltiel, I.A., van den Berg, J., and Medema, R.H. (2014). Transient activation of p53 in G2 phase is sufficient to induce senescence. Mol Cell *55*, 59-72.

Kurihara, S., Hiyama, E., Onitake, Y., Yamaoka, E., and Hiyama, K. (2014). Clinical features of ATRX or DAXX mutated neuroblastoma. J Pediatr Surg *49*, 1835-1838.

Kushner, B.H., Kramer, K., LaQuaglia, M.P., Modak, S., Yataghene, K., and Cheung, N.K. (2004). Reduction from seven to five cycles of intensive induction chemotherapy in children with high-risk neuroblastoma. J Clin Oncol *22*, 4888-4892.

Kushner, B.H., LaQuaglia, M.P., Bonilla, M.A., Lindsley, K., Rosenfield, N., Yeh, S., Eddy, J., Gerald, W.L., Heller, G., and Cheung, N.K. (1994). Highly effective induction therapy for stage 4 neuroblastoma in children over 1 year of age. J Clin Oncol *12*, 2607-2613.

Kushner, B.H., Modak, S., Kramer, K., LaQuaglia, M.P., Yataghene, K., Basu, E.M., Roberts, S.S., and Cheung, N.K. (2014). Striking dichotomy in outcome of MYCN-amplified neuroblastoma in the contemporary era. Cancer *120*, 2050-2059.

Laemmli, U.K. (1970). Cleavage of structural proteins during the assembly of the head of bacteriophage T4. Nature *227*, 680-685.

Lane, D.P. (1992). Cancer. p53, guardian of the genome. Nature *358*, 15-16.

Lee, W.H., Murphree, A.L., and Benedict, W.F. (1984). Expression and amplification of the N-myc gene in primary retinoblastoma. Nature *309*, 458-460.

Li, X., Zhao, Q., Liao, R., Sun, P., and Wu, X. (2003). The SCF(Skp2) ubiquitin ligase complex interacts with the human replication licensing factor Cdt1 and regulates Cdt1 degradation. J Biol Chem *278*, 30854-30858.

Lieber, M.R. (2010). The mechanism of double-strand DNA break repair by the nonhomologous DNA end-joining pathway. Annu Rev Biochem *79*, 181-211.

Lieu, C., Chow, L., Pierson, A.S., Eckhardt, S.G., O'Bryant, C.L., Morrow, M., Tran, Z.V., Wright, J.J., and Gore, L. (2009). A phase I study of bortezomib, etoposide and carboplatin in patients with advanced solid tumors refractory to standard therapy. Invest New Drugs *27*, 53-62.

Linke, S.P., Harris, M.P., Neugebauer, S.E., Clarkin, K.C., Shepard, H.M., Maneval, D.C., and Wahl, G.M. (1997). p53-mediated accumulation of hypophosphorylated pRb after the G1 restriction point fails to halt cell cycle progression. Oncogene *15*, 337-345.

Livak, K.J., and Schmittgen, T.D. (2001). Analysis of relative gene expression data using real-time quantitative PCR and the 2(-Delta Delta C(T)) Method. Methods *25*, 402-408.

Lobrich, M., and Jeggo, P.A. (2007). The impact of a negligent G2/M checkpoint on genomic instability and cancer induction. Nat Rev Cancer *7*, 861-869.

LoConte, N.K., Thomas, J.P., Alberti, D., Heideman, J., Binger, K., Marnocha, R., Utecht, K., Geiger, P., Eickhoff, J., Wilding, G.*, et al.* (2008). A phase I pharmacodynamic trial of bortezomib in combination with doxorubicin in patients with advanced cancer. Cancer Chemother Pharmacol *63*, 109-115.

London, W.B., Castleberry, R.P., Matthay, K.K., Look, A.T., Seeger, R.C., Shimada, H., Thorner, P., Brodeur, G., Maris, J.M., Reynolds, C.P.*, et al.* (2005). Evidence for an age cutoff greater than 365 days for neuroblastoma risk group stratification in the Children's Oncology Group. J Clin Oncol *23*, 6459-6465.

Look, A.T., Hayes, F.A., Shuster, J.J., Douglass, E.C., Castleberry, R.P., Bowman, L.C., Smith, E.I., and Brodeur, G.M. (1991). Clinical relevance of tumor cell ploidy and N-myc gene amplification in childhood neuroblastoma: a Pediatric Oncology Group study. J Clin Oncol *9*, 581-591.

Louis, C.U., and Shohet, J.M. (2015). Neuroblastoma: molecular pathogenesis and therapy. Annu Rev Med *66*, 49-63.

Lucibello, F.C., Sewing, A., Brusselbach, S., Burger, C., and Muller, R. (1993). Deregulation of cyclins D1 and E and suppression of cdk2 and cdk4 in senescent human fibroblasts. J Cell Sci *105 (Pt 1)*, 123-133.

Lukas, J., and Bartek, J. (2009). DNA repair: New tales of an old tail. Nature *458*, 581-583.

Lukas, J., Lukas, C., and Bartek, J. (2004). Mammalian cell cycle checkpoints: signalling pathways and their organization in space and time. DNA Repair (Amst) *3*, 997-1007.

Lutz, W., Stohr, M., Schurmann, J., Wenzel, A., Lohr, A., and Schwab, M. (1996). Conditional expression of N-myc in human neuroblastoma cells increases expression of alpha-prothymosin and ornithine decarboxylase and accelerates progression into S-phase early after mitogenic stimulation of quiescent cells. Oncogene *13*, 803-812.

Ma, Y., Pannicke, U., Schwarz, K., and Lieber, M.R. (2002). Hairpin opening and overhang processing by an Artemis/DNA-dependent protein kinase complex in nonhomologous end joining and V(D)J recombination. Cell *108*, 781-794.

Mailand, N., Falck, J., Lukas, C., Syljuasen, R.G., Welcker, M., Bartek, J., and Lukas, J. (2000). Rapid destruction of human Cdc25A in response to DNA damage. Science *288*, 1425-1429.

Malumbres, M., and Barbacid, M. (2005). Mammalian cyclin-dependent kinases. Trends Biochem Sci *30*, 630-641.

Malumbres, M., and Barbacid, M. (2006). Is Cyclin D1-CDK4 kinase a bona fide cancer target? Cancer Cell *9*, 2-4.

Malumbres, M., Harlow, E., Hunt, T., Hunter, T., Lahti, J.M., Manning, G., Morgan, D.O., Tsai, L.H., and Wolgemuth, D.J. (2009). Cyclin-dependent kinases: a family portrait. Nat Cell Biol *11*, 1275-1276.

Marine, J.C., Francoz, S., Maetens, M., Wahl, G., Toledo, F., and Lozano, G. (2006). Keeping p53 in check: essential and synergistic functions of Mdm2 and Mdm4. Cell Death Differ *13*, 927-934.

Maris, J.M. (2005). The biologic basis for neuroblastoma heterogeneity and risk stratification. Curr Opin Pediatr *17*, 7-13.

Maris, J.M. (2010). Recent advances in neuroblastoma. N Engl J Med *362*, 2202-2211.

Maris, J.M., Hogarty, M.D., Bagatell, R., and Cohn, S.L. (2007). Neuroblastoma. Lancet *369*, 2106-2120.

Maris, J.M., Weiss, M.J., Guo, C., Gerbing, R.B., Stram, D.O., White, P.S., Hogarty, M.D., Sulman, E.P., Thompson, P.M., Lukens, J.N*., et al.* (2000). Loss of heterozygosity at 1p36 independently predicts for disease progression but not decreased overall survival probability in neuroblastoma patients: a Children's Cancer Group study. J Clin Oncol *18*, 1888-1899.

Markovits, J., Pommier, Y., Kerrigan, D., Covey, J.M., Tilchen, E.J., and Kohn, K.W. (1987). Topoisomerase II-mediated DNA breaks and cytotoxicity in relation to cell proliferation and the cell cycle in NIH 3T3 fibroblasts and L1210 leukemia cells. Cancer Res *47*, 2050-2055.

Mattiroli, F., Vissers, J.H., van Dijk, W.J., Ikpa, P., Citterio, E., Vermeulen, W., Marteijn, J.A., and Sixma, T.K. (2012). RNF168 ubiquitinates K13-15 on H2A/H2AX to drive DNA damage signaling. Cell *150*, 1182-1195.

McGarry, T.J., and Kirschner, M.W. (1998). Geminin, an inhibitor of DNA replication, is degraded during mitosis. Cell *93*, 1043-1053.

Meijering, E., Dzyubachyk, O., and Smal, I. (2012). Methods for cell and particle tracking. Methods Enzymol *504*, 183-200.

Meyer, N., and Penn, L.Z. (2008). Reflecting on 25 years with MYC. Nat Rev Cancer *8*, 976-990.

Michel, B., Grompone, G., Flores, M.J., and Bidnenko, V. (2004). Multiple pathways process stalled replication forks. Proc Natl Acad Sci U S A *101*, 12783-12788.

Mirzayans, R., Andrais, B., Scott, A., and Murray, D. (2012). New insights into p53 signaling and cancer cell response to DNA damage: implications for cancer therapy. J Biomed Biotechnol *2012*, 170325.

Mirzayans, R., Andrais, B., Scott, A., Paterson, M.C., and Murray, D. (2010). Single-cell analysis of p16(INK4a) and p21(WAF1) expression suggests distinct mechanisms of senescence in normal human and Li-Fraumeni Syndrome fibroblasts. J Cell Physiol *223*, 57-67.

Mizukami, Y., Nonomura, A., Takizawa, T., Noguchi, M., Michigishi, T., Nakamura, S., and Ishizaki, T. (1995). N-myc protein expression in human breast carcinoma: prognostic implications. Anticancer Res *15*, 2899-2905.

Mohapatra, S., Yannone, S.M., Lee, S.H., Hromas, R.A., Akopiants, K., Menon, V., Ramsden, D.A., and Povirk, L.F. (2013). Trimming of damaged 3' overhangs of DNA double-strand breaks by the Metnase and Artemis endonucleases. DNA Repair (Amst) *12*, 422-432.

Molenaar, J.J., Koster, J., Ebus, M.E., van Sluis, P., Westerhout, E.M., de Preter, K., Gisselsson, D., Ora, I., Speleman, F., Caron, H.N*., et al.* (2012a). Copy number defects of G1-cell cycle genes in neuroblastoma are frequent and correlate with high expression of E2F target genes and a poor prognosis. Genes Chromosomes Cancer *51*, 10-19.

Molenaar, J.J., Koster, J., Zwijnenburg, D.A., van Sluis, P., Valentijn, L.J., van der Ploeg, I., Hamdi, M., van Nes, J., Westerman, B.A., van Arkel, J*., et al.* (2012b). Sequencing of neuroblastoma identifies chromothripsis and defects in neuritogenesis genes. Nature *483*, 589-593.

Molenaar, J.J., van Sluis, P., Boon, K., Versteeg, R., and Caron, H.N. (2003). Rearrangements and increased expression of cyclin D1 (CCND1) in neuroblastoma. Genes Chromosomes Cancer *36*, 242-249.

Monclair, T., Brodeur, G.M., Ambros, P.F., Brisse, H.J., Cecchetto, G., Holmes, K., Kaneko, M., London, W.B., Matthay, K.K., Nuchtern, J.G*., et al.* (2009). The International Neuroblastoma Risk Group (INRG) staging system: an INRG Task Force report. J Clin Oncol *27*, 298-303.

Moore, H.C., Wood, K.M., Jackson, M.S., Lastowska, M.A., Hall, D., Imrie, H., Redfern, C.P., Lovat, P.E., Ponthan, F., O'Toole, K*., et al.* (2008). Histological profile of tumours from MYCN transgenic mice. J Clin Pathol *61*, 1098-1103.

Mosquera, J.M., Beltran, H., Park, K., MacDonald, T.Y., Robinson, B.D., Tagawa, S.T., Perner, S., Bismar, T.A., Erbersdobler, A., Dhir, R*., et al.* (2013). Concurrent AURKA and MYCN gene amplifications are harbingers of lethal treatment-related neuroendocrine prostate cancer. Neoplasia *15*, 1-10.

Mosse, Y.P., Laudenslager, M., Longo, L., Cole, K.A., Wood, A., Attiyeh, E.F., Laquaglia, M.J., Sennett, R., Lynch, J.E., Perri, P.*, et al.* (2008). Identification of ALK as a major familial neuroblastoma predisposition gene. Nature *455*, 930-935.

Mosse, Y.P., Lim, M.S., Voss, S.D., Wilner, K., Ruffner, K., Laliberte, J., Rolland, D., Balis, F.M., Maris, J.M., Weigel, B.J.*, et al.* (2013). Safety and activity of crizotinib for paediatric patients with refractory solid tumours or anaplastic large-cell lymphoma: a Children's Oncology Group phase 1 consortium study. Lancet Oncol *14*, 472-480.

Murray, A.W. (1993). Cell-cycle control: turning on mitosis. Curr Biol *3*, 291-293.

Musacchio, A., and Salmon, E.D. (2007). The spindle-assembly checkpoint in space and time. Nat Rev Mol Cell Biol *8*, 379-393.

Muth, D., Ghazaryan, S., Eckerle, I., Beckett, E., Pohler, C., Batzler, J., Beisel, C., Gogolin, S., Fischer, M., Henrich, K.O.*, et al.* (2010). Transcriptional repression of SKP2 is impaired in MYCN-amplified neuroblastoma. Cancer Res *70*, 3791-3802.

Nau, M.M., Brooks, B.J., Jr., Carney, D.N., Gazdar, A.F., Battey, J.F., Sausville, E.A., and Minna, J.D. (1986). Human small-cell lung cancers show amplification and expression of the N-myc gene. Proc Natl Acad Sci U S A *83*, 1092-1096.

Nelson, G., Buhmann, M., and von Zglinicki, T. (2009). DNA damage foci in mitosis are devoid of 53BP1. Cell Cycle *8*, 3379-3383.

Nevins, J.R. (2001). The Rb/E2F pathway and cancer. Hum Mol Genet *10*, 699-703.

Nishitani, H., Lygerou, Z., and Nishimoto, T. (2004). Proteolysis of DNA replication licensing factor Cdt1 in S-phase is performed independently of geminin through its N-terminal region. J Biol Chem *279*, 30807-30816.

Nishitani, H., Lygerou, Z., Nishimoto, T., and Nurse, P. (2000). The Cdt1 protein is required to license DNA for replication in fission yeast. Nature *404*, 625-628.

Nishitani, H., Sugimoto, N., Roukos, V., Nakanishi, Y., Saijo, M., Obuse, C., Tsurimoto, T., Nakayama, K.I., Nakayama, K., Fujita, M.*, et al.* (2006). Two E3 ubiquitin ligases, SCF-Skp2 and DDB1-Cul4, target human Cdt1 for proteolysis. EMBO J *25*, 1126-1136.

Nitiss, J.L., and Beck, W.T. (1996). Antitopoisomerase drug action and resistance. Eur J Cancer *32A*, 958-966.

Nitiss, J.L., Liu, Y.X., Harbury, P., Jannatipour, M., Wasserman, R., and Wang, J.C. (1992). Amsacrine and etoposide hypersensitivity of yeast cells overexpressing DNA topoisomerase II. Cancer Res *52*, 4467-4472.

Nitiss, J.L., Liu, Y.X., and Hsiung, Y. (1993). A temperature sensitive topoisomerase II allele confers temperature dependent drug resistance on amsacrine and etoposide: a genetic system for determining the targets of topoisomerase II inhibitors. Cancer Res *53*, 89-93.

Nitiss, J.L., Soans, E., Rogojina, A., Seth, A., and Mishina, M. (2012). Topoisomerase assays. Curr Protoc Pharmacol *Chapter 3*, Unit 3 3.

Noda, A., Ning, Y., Venable, S.F., Pereira-Smith, O.M., and Smith, J.R. (1994). Cloning of senescent cell-derived inhibitors of DNA synthesis using an expression screen. Exp Cell Res *211*, 90-98.

Nuchtern, J.G., London, W.B., Barnewolt, C.E., Naranjo, A., McGrady, P.W., Geiger, J.D., Diller, L., Schmidt, M.L., Maris, J.M., Cohn, S.L.*, et al.* (2012). A prospective study of expectant observation as primary therapy for neuroblastoma in young infants: a Children's Oncology Group study. Ann Surg *256*, 573-580.

Oberthuer, A., Theissen, J., Westermann, F., Hero, B., and Fischer, M. (2009). Molecular characterization and classification of neuroblastoma. Future Oncol *5*, 625-639.

Oliner, J.D., Pietenpol, J.A., Thiagalingam, S., Gyuris, J., Kinzler, K.W., and Vogelstein, B. (1993). Oncoprotein MDM2 conceals the activation domain of tumour suppressor p53. Nature *362*, 857-860.

Omura-Minamisawa, M., Diccianni, M.B., Chang, R.C., Batova, A., Bridgeman, L.J., Schiff, J., Cohn, S.L., London, W.B., and Yu, A.L. (2001). p16/p14(ARF) cell cycle regulatory pathways in primary neuroblastoma: p16 expression is associated with advanced stage disease. Clin Cancer Res *7*, 3481-3490.

Paffhausen, T., Schwab, M., and Westermann, F. (2007). Targeted MYCN expression affects cytotoxic potential of chemotherapeutic drugs in neuroblastoma cells. Cancer Lett *250*, 17-24.

Panier, S., and Boulton, S.J. (2014). Double-strand break repair: 53BP1 comes into focus. Nat Rev Mol Cell Biol *15*, 7-18.

Park, J.R., Bagatell, R., London, W.B., Maris, J.M., Cohn, S.L., Mattay, K.K., Hogarty, M., and Committee, C.O.G.N. (2013). Children's Oncology Group's 2013 blueprint for research: neuroblastoma. Pediatr Blood Cancer *60*, 985-993.

Pavletich, N.P. (1999). Mechanisms of cyclin-dependent kinase regulation: structures of Cdks, their cyclin activators, and Cip and INK4 inhibitors. J Mol Biol *287*, 821-828.

Paz, A., Brownstein, Z., Ber, Y., Bialik, S., David, E., Sagir, D., Ulitsky, I., Elkon, R., Kimchi, A., Avraham, K.B.*, et al.* (2011). SPIKE: a database of highly curated human signaling pathways. Nucleic Acids Res *39*, D793-799.

Peifer, M., Hertwig, F., Roels, F., Dreidax, D., Gartlgruber, M., Menon, R., Kramer, A., Roncaioli, J.L., Sand, F., Heuckmann, J.M.*, et al.* (2015). Telomerase activation by genomic rearrangements in high-risk neuroblastoma. Nature *526*, 700-704.

Peters, A.H., O'Carroll, D., Scherthan, H., Mechtler, K., Sauer, S., Schofer, C., Weipoltshammer, K., Pagani, M., Lachner, M., Kohlmaier, A.*, et al.* (2001). Loss of the Suv39h histone methyltransferases impairs mammalian heterochromatin and genome stability. Cell *107*, 323-337.

Petersen, L., Hasvold, G., Lukas, J., Bartek, J., and Syljuasen, R.G. (2010). p53-dependent G(1) arrest in 1st or 2nd cell cycle may protect human cancer cells from cell death after treatment with ionizing radiation and Chk1 inhibitors. Cell Prolif *43*, 365-371.

Pinto, N.R., Applebaum, M.A., Volchenboum, S.L., Matthay, K.K., London, W.B., Ambros, P.F., Nakagawara, A., Berthold, F., Schleiermacher, G., Park, J.R.*, et al.* (2015). Advances in Risk Classification and Treatment Strategies for Neuroblastoma. J Clin Oncol *33*, 3008-3017.

Pradhan, K.R., Johnson, C.S., Vik, T.A., Sender, L.S., and Kreissman, S.G. (2006). A novel intensive induction therapy for high-risk neuroblastoma utilizing sequential peripheral blood stem cell collection and infusion as hematopoietic support. Pediatr Blood Cancer *46*, 793-802.

Pritchard, J., and Hickman, J.A. (1994). Why does stage 4s neuroblastoma regress spontaneously? Lancet *344*, 869-870.

Pugh, T.J., Morozova, O., Attiyeh, E.F., Asgharzadeh, S., Wei, J.S., Auclair, D., Carter, S.L., Cibulskis, K., Hanna, M., Kiezun, A.*, et al.* (2013). The genetic landscape of high-risk neuroblastoma. Nat Genet *45*, 279-284.

Rader, J., Russell, M.R., Hart, L.S., Nakazawa, M.S., Belcastro, L.T., Martinez, D., Li, Y., Carpenter, E.L., Attiyeh, E.F., Diskin, S.J.*, et al.* (2013). Dual CDK4/CDK6 inhibition induces cell-cycle arrest and senescence in neuroblastoma. Clin Cancer Res *19*, 6173-6182.

Raso, A., Vecchio, D., Cappelli, E., Ropolo, M., Poggi, A., Nozza, P., Biassoni, R., Mascelli, S., Capra, V., Kalfas, F.*, et al.* (2012). Characterization of glioma stem cells through multiple stem cell markers and their specific sensitization to double-strand break-inducing agents by pharmacological inhibition of ataxia telangiectasia mutated protein. Brain Pathol *22*, 677-688.

Reisman, D., Elkind, N.B., Roy, B., Beamon, J., and Rotter, V. (1993). c-Myc trans-activates the p53 promoter through a required downstream CACGTG motif. Cell Growth Differ *4*, 57-65.

Riballo, E., Kuhne, M., Rief, N., Doherty, A., Smith, G.C., Recio, M.J., Reis, C., Dahm, K., Fricke, A., Krempler, A.*, et al.* (2004). A pathway of double-strand break rejoining dependent upon ATM, Artemis, and proteins locating to gamma-H2AX foci. Mol Cell *16*, 715-724.

Rihani, A., Vandesompele, J., Speleman, F., and Van Maerken, T. (2015). Inhibition of CDK4/6 as a novel therapeutic option for neuroblastoma. Cancer Cell Int *15*, 76.

Riley, T., Sontag, E., Chen, P., and Levine, A. (2008). Transcriptional control of human p53-regulated genes. Nat Rev Mol Cell Biol *9*, 402-412.

Robinson, M.J., and Osheroff, N. (1990). Stabilization of the topoisomerase II-DNA cleavage complex by antineoplastic drugs: inhibition of enzyme-mediated DNA religation by 4'-(9-acridinylamino)methanesulfon-m-anisidide. Biochemistry *29*, 2511-2515.

Roninson, I.B. (2003). Tumor cell senescence in cancer treatment. Cancer Res *63*, 2705-2715.

Ross, R.A., Spengler, B.A., and Biedler, J.L. (1983). Coordinate morphological and biochemical interconversion of human neuroblastoma cells. J Natl Cancer Inst *71*, 741-747.

Rothkamm, K., Barnard, S., Moquet, J., Ellender, M., Rana, Z., and Burdak-Rothkamm, S. (2015). DNA damage foci: Meaning and significance. Environ Mol Mutagen *56*, 491-504.

Rousseau, D., Cannella, D., Boulaire, J., Fitzgerald, P., Fotedar, A., and Fotedar, R. (1999). Growth inhibition by CDK-cyclin and PCNA binding domains of p21 occurs by distinct mechanisms and is regulated by ubiquitin-proteasome pathway. Oncogene *18*, 4313-4325.

Roy, B., Beamon, J., Balint, E., and Reisman, D. (1994). Transactivation of the human p53 tumor suppressor gene by c-Myc/Max contributes to elevated mutant p53 expression in some tumors. Mol Cell Biol *14*, 7805-7815.

Rubie, H., De Bernardi, B., Gerrard, M., Canete, A., Ladenstein, R., Couturier, J., Ambros, P., Munzer, C., Pearson, A.D., Garaventa, A.*, et al.* (2011). Excellent outcome with reduced treatment in infants with nonmetastatic and unresectable neuroblastoma without MYCN amplification: results of the prospective INES 99.1. J Clin Oncol *29*, 449-455.

Rushlow, D.E., Mol, B.M., Kennett, J.Y., Yee, S., Pajovic, S., Theriault, B.L., Prigoda-Lee, N.L., Spencer, C., Dimaras, H., Corson, T.W.*, et al.* (2013). Characterisation of retinoblastomas without RB1 mutations: genomic, gene expression, and clinical studies. Lancet Oncol *14*, 327-334.

Sabo, A., Kress, T.R., Pelizzola, M., de Pretis, S., Gorski, M.M., Tesi, A., Morelli, M.J., Bora, P., Doni, M., Verrecchia, A.*, et al.* (2014). Selective transcriptional regulation by Myc in cellular growth control and lymphomagenesis. Nature *511*, 488-492.

Sakaue-Sawano, A., Hoshida, T., Yo, M., Takahashi, R., Ohtawa, K., Arai, T., Takahashi, E., Noda, S., Miyoshi, H., and Miyawaki, A. (2013). Visualizing developmentally programmed endoreplication in mammals using ubiquitin oscillators. Development *140*, 4624-4632.

Sakaue-Sawano, A., Kobayashi, T., Ohtawa, K., and Miyawaki, A. (2011). Drug-induced cell cycle modulation leading to cell-cycle arrest, nuclear mis-segregation, or endoreplication. BMC Cell Biol *12*, 2.

Sakaue-Sawano, A., Kurokawa, H., Morimura, T., Hanyu, A., Hama, H., Osawa, H., Kashiwagi, S., Fukami, K., Miyata, T., Miyoshi, H.*, et al.* (2008). Visualizing spatiotemporal dynamics of multicellular cell-cycle progression. Cell *132*, 487-498.

Sarbajna, S., and West, S.C. (2014). Holliday junction processing enzymes as guardians of genome stability. Trends Biochem Sci *39*, 409-419.

Sausen, M., Leary, R.J., Jones, S., Wu, J., Reynolds, C.P., Liu, X., Blackford, A., Parmigiani, G., Diaz, L.A., Jr., Papadopoulos, N.*, et al.* (2013). Integrated genomic analyses identify ARID1A and ARID1B alterations in the childhood cancer neuroblastoma. Nat Genet *45*, 12-17.

Schleiermacher, G., Javanmardi, N., Bernard, V., Leroy, Q., Cappo, J., Rio Frio, T., Pierron, G., Lapouble, E., Combaret, V., Speleman, F.*, et al.* (2014). Emergence of new ALK mutations at relapse of neuroblastoma. J Clin Oncol *32*, 2727-2734.

Schleiermacher, G., Mosseri, V., London, W.B., Maris, J.M., Brodeur, G.M., Attiyeh, E., Haber, M., Khan, J., Nakagawara, A., Speleman, F.*, et al.* (2012). Segmental chromosomal alterations have prognostic impact in neuroblastoma: a report from the INRG project. Br J Cancer *107*, 1418-1422.

Schmidt, M.L., Lal, A., Seeger, R.C., Maris, J.M., Shimada, H., O'Leary, M., Gerbing, R.B., and Matthay, K.K. (2005). Favorable prognosis for patients 12 to 18 months of age with stage 4 nonamplified MYCN neuroblastoma: a Children's Cancer Group Study. J Clin Oncol *23*, 6474-6480.

Schneiderman, J., London, W.B., Brodeur, G.M., Castleberry, R.P., Look, A.T., and Cohn, S.L. (2008). Clinical significance of MYCN amplification and ploidy in favorable-stage neuroblastoma: a report from the Children's Oncology Group. J Clin Oncol *26*, 913-918.

Schoeffler, A.J., and Berger, J.M. (2008). DNA topoisomerases: harnessing and constraining energy to govern chromosome topology. Q Rev Biophys *41*, 41-101.

Schonn, I., Hennesen, J., and Dartsch, D.C. (2011). Ku70 and Rad51 vary in their importance for the repair of doxorubicin- versus etoposide-induced DNA damage. Apoptosis *16*, 359-369.

Schwab, M., Alitalo, K., Klempnauer, K.H., Varmus, H.E., Bishop, J.M., Gilbert, F., Brodeur, G., Goldstein, M., and Trent, J. (1983). Amplified DNA with limited homology to myc cellular oncogene is shared by human neuroblastoma cell lines and a neuroblastoma tumour. Nature *305*, 245-248.

Seeger, R.C., Brodeur, G.M., Sather, H., Dalton, A., Siegel, S.E., Wong, K.Y., and Hammond, D. (1985). Association of multiple copies of the N-myc oncogene with rapid progression of neuroblastomas. N Engl J Med *313*, 1111-1116.

Seoane, J., Le, H.V., and Massague, J. (2002). Myc suppression of the p21(Cip1) Cdk inhibitor influences the outcome of the p53 response to DNA damage. Nature *419*, 729-734.

Shay, J.W. (1999). At the end of the millennium, a view of the end. Nat Genet *23*, 382-383.

Sheen, J.H., and Dickson, R.B. (2002). Overexpression of c-Myc alters G(1)/S arrest following ionizing radiation. Mol Cell Biol *22*, 1819-1833.

Sherr, C.J. (1998). Tumor surveillance via the ARF-p53 pathway. Genes Dev *12*, 2984-2991.

Sherr, C.J., and Roberts, J.M. (1999). CDK inhibitors: positive and negative regulators of G1-phase progression. Genes Dev *13*, 1501-1512.

Shibata, A., Conrad, S., Birraux, J., Geuting, V., Barton, O., Ismail, A., Kakarougkas, A., Meek, K., Taucher-Scholz, G., Lobrich, M*., et al.* (2011). Factors determining DNA double-strand break repair pathway choice in G2 phase. EMBO J *30*, 1079-1092.

Shieh, S.Y., Ahn, J., Tamai, K., Taya, Y., and Prives, C. (2000). The human homologs of checkpoint kinases Chk1 and Cds1 (Chk2) phosphorylate p53 at multiple DNA damage-inducible sites. Genes Dev *14*, 289-300.

Shiloh, Y. (2006). The ATM-mediated DNA-damage response: taking shape. Trends Biochem Sci *31*, 402-410.

Shimada, H., Ambros, I.M., Dehner, L.P., Hata, J., Joshi, V.V., and Roald, B. (1999). Terminology and morphologic criteria of neuroblastic tumors: recommendations by the International Neuroblastoma Pathology Committee. Cancer *86*, 349-363.

Shimada, H., Stram, D.O., Chatten, J., Joshi, V.V., Hachitanda, Y., Brodeur, G.M., Lukens, J.N., Matthay, K.K., and Seeger, R.C. (1995). Identification of subsets of neuroblastomas by combined histopathologic and N-myc analysis. J Natl Cancer Inst *87*, 1470-1476.

Shojaei-Brosseau, T., Chompret, A., Abel, A., de Vathaire, F., Raquin, M.A., Brugieres, L., Feunteun, J., Hartmann, O., and Bonaiti-Pellie, C. (2004). Genetic epidemiology of neuroblastoma: a study of 426 cases at the Institut Gustave-Roussy in France. Pediatr Blood Cancer *42*, 99-105.

Shrivastav, M., De Haro, L.P., and Nickoloff, J.A. (2008). Regulation of DNA double-strand break repair pathway choice. Cell Res *18*, 134-147.

Shukla, N., Ameur, N., Yilmaz, I., Nafa, K., Lau, C.Y., Marchetti, A., Borsu, L., Barr, F.G., and Ladanyi, M. (2012). Oncogene mutation profiling of pediatric solid tumors reveals significant subsets of embryonal rhabdomyosarcoma and neuroblastoma with mutated genes in growth signaling pathways. Clin Cancer Res *18*, 748-757.

Sidler, C., Li, D., Wang, B., Kovalchuk, I., and Kovalchuk, O. (2014). SUV39H1 downregulation induces deheterochromatinization of satellite regions and senescence after exposure to ionizing radiation. Front Genet *5*, 411.

Slack, A., Chen, Z., Tonelli, R., Pule, M., Hunt, L., Pession, A., and Shohet, J.M. (2005). The p53 regulatory gene MDM2 is a direct transcriptional target of MYCN in neuroblastoma. Proc Natl Acad Sci U S A *102*, 731-736.

Smith, M.A., Seibel, N.L., Altekruse, S.F., Ries, L.A., Melbert, D.L., O'Leary, M., Smith, F.O., and Reaman, G.H. (2010). Outcomes for children and adolescents with cancer: challenges for the twenty-first century. J Clin Oncol *28*, 2625-2634.

Sorkin, L.S., Otto, M., Baldwin, W.M., 3rd, Vail, E., Gillies, S.D., Handgretinger, R., Barfield, R.C., Ming Yu, H., and Yu, A.L. (2010). Anti-GD(2) with an FC point mutation reduces complement fixation and decreases antibody-induced allodynia. Pain *149*, 135-142.

Stanton, B.R., Perkins, A.S., Tessarollo, L., Sassoon, D.A., and Parada, L.F. (1992). Loss of N-myc function results in embryonic lethality and failure of the epithelial component of the embryo to develop. Genes Dev *6*, 2235-2247.

Stiff, T., O'Driscoll, M., Rief, N., Iwabuchi, K., Lobrich, M., and Jeggo, P.A. (2004). ATM and DNA-PK function redundantly to phosphorylate H2AX after exposure to ionizing radiation. Cancer Res *64*, 2390-2396.

Strother, D.R., London, W.B., Schmidt, M.L., Brodeur, G.M., Shimada, H., Thorner, P., Collins, M.H., Tagge, E., Adkins, S., Reynolds, C.P.*, et al.* (2012). Outcome after surgery alone or with restricted use of chemotherapy for patients with low-risk neuroblastoma: results of Children's Oncology Group study P9641. J Clin Oncol *30*, 1842-1848.

Suzuki, A., Tsutomi, Y., Yamamoto, N., Shibutani, T., and Akahane, K. (1999). Mitochondrial regulation of cell death: mitochondria are essential for procaspase 3-p21 complex formation to resist Fas-mediated cell death. Mol Cell Biol *19*, 3842-3847.

Swartling, F.J., Grimmer, M.R., Hackett, C.S., Northcott, P.A., Fan, Q.W., Goldenberg, D.D., Lau, J., Masic, S., Nguyen, K., Yakovenko, S.*, et al.* (2010). Pleiotropic role for MYCN in medulloblastoma. Genes Dev *24*, 1059-1072.

Swartling, F.J., Savov, V., Persson, A.I., Chen, J., Hackett, C.S., Northcott, P.A., Grimmer, M.R., Lau, J., Chesler, L., Perry, A.*, et al.* (2012). Distinct neural stem cell populations give rise to disparate brain tumors in response to N-MYC. Cancer Cell *21*, 601-613.

Syljuasen, R.G. (2007). Checkpoint adaptation in human cells. Oncogene *26*, 5833-5839.

Symington, L.S. (2014). End resection at double-strand breaks: mechanism and regulation. Cold Spring Harb Perspect Biol *6*.

Tada, S., Li, A., Maiorano, D., Mechali, M., and Blow, J.J. (2001). Repression of origin assembly in metaphase depends on inhibition of RLF-B/Cdt1 by geminin. Nat Cell Biol *3*, 107-113.

Tang, J., Cho, N.W., Cui, G., Manion, E.M., Shanbhag, N.M., Botuyan, M.V., Mer, G., and Greenberg, R.A. (2013). Acetylation limits 53BP1 association with damaged chromatin to promote homologous recombination. Nat Struct Mol Biol *20*, 317-325.

Tercero, J.A., and Diffley, J.F. (2001). Regulation of DNA replication fork progression through damaged DNA by the Mec1/Rad53 checkpoint. Nature *412*, 553-557.

Thut, C.J., Goodrich, J.A., and Tjian, R. (1997). Repression of p53-mediated transcription by MDM2: a dual mechanism. Genes Dev *11*, 1974-1986.

Toettcher, J.E., Loewer, A., Ostheimer, G.J., Yaffe, M.B., Tidor, B., and Lahav, G. (2009). Distinct mechanisms act in concert to mediate cell cycle arrest. Proc Natl Acad Sci U S A *106*, 785-790.

Tonelli, R., McIntyre, A., Camerin, C., Walters, Z.S., Di Leo, K., Selfe, J., Purgato, S., Missiaglia, E., Tortori, A., Renshaw, J.*, et al.* (2012). Antitumor activity of sustained N-myc reduction in rhabdomyosarcomas and transcriptional block by antigene therapy. Clin Cancer Res *18*, 796-807.

Tweddle, D.A., Malcolm, A.J., Cole, M., Pearson, A.D., and Lunec, J. (2001). p53 cellular localization and function in neuroblastoma: evidence for defective G(1) arrest despite WAF1 induction in MYCN-amplified cells. Am J Pathol *158*, 2067-2077.

Tweddle, D.A., Pearson, A.D., Haber, M., Norris, M.D., Xue, C., Flemming, C., and Lunec, J. (2003). The p53 pathway and its inactivation in neuroblastoma. Cancer Lett *197*, 93-98.

Vecchio, D., Daga, A., Carra, E., Marubbi, D., Baio, G., Neumaier, C.E., Vagge, S., Corvo, R., Pia Brisigotti, M., Louis Ravetti, J.*, et al.* (2014). Predictability, efficacy and safety of radiosensitization of glioblastoma-initiating cells by the ATM inhibitor KU-60019. Int J Cancer *135*, 479-491.

Vecchio, D., Daga, A., Carra, E., Marubbi, D., Raso, A., Mascelli, S., Nozza, P., Garre, M.L., Pitto, F., Ravetti, J.L.*, et al.* (2015). Pharmacokinetics, pharmacodynamics and efficacy on pediatric tumors of the glioma radiosensitizer KU60019. Int J Cancer *136*, 1445-1457.

Vogelstein, B., Papadopoulos, N., Velculescu, V.E., Zhou, S., Diaz, L.A., Jr., and Kinzler, K.W. (2013). Cancer genome landscapes. Science *339*, 1546-1558.

Wahl, G.M., Linke, S.P., Paulson, T.G., and Huang, L.C. (1997). Maintaining genetic stability through TP53 mediated checkpoint control. Cancer Surv *29*, 183-219.

Walker, J.V., and Nitiss, J.L. (2002). DNA topoisomerase II as a target for cancer chemotherapy. Cancer Invest *20*, 570-589.

Wang, J.C. (1998). Moving one DNA double helix through another by a type II DNA topoisomerase: the story of a simple molecular machine. Q Rev Biophys *31*, 107-144.

Wang, W., Nacusi, L., Sheaff, R.J., and Liu, X. (2005). Ubiquitination of p21Cip1/WAF1 by SCFSkp2: substrate requirement and ubiquitination site selection. Biochemistry *44*, 14553-14564.

Wei, W., Ayad, N.G., Wan, Y., Zhang, G.J., Kirschner, M.W., and Kaelin, W.G., Jr. (2004). Degradation of the SCF component Skp2 in cell-cycle phase G1 by the anaphase-promoting complex. Nature *428*, 194-198.

Westermann, F., Henrich, K.O., Wei, J.S., Lutz, W., Fischer, M., Konig, R., Wiedemeyer, R., Ehemann, V., Brors, B., Ernestus, K.*, et al.* (2007). High Skp2 expression characterizes high-risk neuroblastomas independent of MYCN status. Clin Cancer Res *13*, 4695-4703.

Westermann, F., Muth, D., Benner, A., Bauer, T., Henrich, K.O., Oberthuer, A., Brors, B., Beissbarth, T., Vandesompele, J., Pattyn, F.*, et al.* (2008). Distinct transcriptional MYCN/c-MYC activities are associated with spontaneous regression or malignant progression in neuroblastomas. Genome Biol *9*, R150.

Westermann, F., and Schwab, M. (2002). Genetic parameters of neuroblastomas. Cancer Lett *184*, 127-147.

White, P.S., Thompson, P.M., Seifried, B.A., Sulman, E.P., Jensen, S.J., Guo, C., Maris, J.M., Hogarty, M.D., Allen, C., Biegel, J.A.*, et al.* (2001). Detailed molecular analysis of 1p36 in neuroblastoma. Med Pediatr Oncol *36*, 37-41.

Wiebusch, L., and Hagemeier, C. (2010). p53- and p21-dependent premature APC/C-Cdh1 activation in G2 is part of the long-term response to genotoxic stress. Oncogene *29*, 3477-3489.

Williams, G.H., and Stoeber, K. (2012). The cell cycle and cancer. J Pathol *226*, 352-364.

Xue, C., Haber, M., Flemming, C., Marshall, G.M., Lock, R.B., MacKenzie, K.L., Gurova, K.V., Norris, M.D., and Gudkov, A.V. (2007). p53 determines multidrug sensitivity of childhood neuroblastoma. Cancer Res *67*, 10351-10360.

Yao, G., Lee, T.J., Mori, S., Nevins, J.R., and You, L. (2008). A bistable Rb-E2F switch underlies the restriction point. Nat Cell Biol *10*, 476-482.

Yu, Z.K., Gervais, J.L., and Zhang, H. (1998). Human CUL-1 associates with the SKP1/SKP2 complex and regulates p21(CIP1/WAF1) and cyclin D proteins. Proc Natl Acad Sci U S A *95*, 11324-11329.

Zelensky, A., Kanaar, R., and Wyman, C. (2014). Mediators of homologous DNA pairing. Cold Spring Harb Perspect Biol *6*, a016451.

Zeller, K.I., Jegga, A.G., Aronow, B.J., O'Donnell, K.A., and Dang, C.V. (2003). An integrated database of genes responsive to the Myc oncogenic transcription factor: identification of direct genomic targets. Genome Biol *4*, R69.

Zhang, A., Lyu, Y.L., Lin, C.P., Zhou, N., Azarova, A.M., Wood, L.M., and Liu, L.F. (2006). A protease pathway for the repair of topoisomerase II-DNA covalent complexes. J Biol Chem *281*, 35997-36003.

Zhu, Q., Sharma, N., He, J., Wani, G., and Wani, A.A. (2015). USP7 deubiquitinase promotes ubiquitin-dependent DNA damage signaling by stabilizing RNF168. Cell Cycle *14*, 1413-1425.

Zielke, N., and Edgar, B.A. (2015). FUCCI sensors: powerful new tools for analysis of cell proliferation. Wiley Interdiscip Rev Dev Biol *4*, 469-487.

Zimmerman, K.A., Yancopoulos, G.D., Collum, R.G., Smith, R.K., Kohl, N.E., Denis, K.A., Nau, M.M., Witte, O.N., Toran-Allerand, D., Gee, C.E.*, et al.* (1986). Differential expression of myc family genes during murine development. Nature *319*, 780-783.

Zirkle, R.E., and Bloom, W. (1953). Irradiation of parts of individual cells. Science *117*, 487-493.

6. List of abbreviations

aa	amino acids
b	base
bp	base pair
BSA	bovine serum albumin
cDNA	complementary DNA
ChIP	chromatin immunoprecipitation
ChIP	chip chromatin immunoprecipitation on chip
cm	centimeter
Cp	crossing point
d	day(s)
DAPI	4,6-Diamino-2-phenylindol
DNA	desoxyribonucleic acid
DNase	desoxyribonuclease
dNTP	2'-deoxyribonucleoside 5’-triphosphate
DSBs	double strand breaks
DMSO	dimethylsulfoxid
DOX	doxorubicin
EDTA	ethylendiamintetraacetic acid, Na-salt
EdU	5-ethynyl-2’-deoxyuridine
et al.	et alii (and other)
EtOH	ethanol
FACS	fluorescence activated cell sorting
FBS	fetal Bovine serum
FUCCI	Fluorescent Ubiquitination-based Cell Cycle Indicator
g	gram
xG	force of gravity, relative centrifugal force (RCF)
GFP	green fluorescence protein
H3K4me3	trimethylation of histone 3 at lysine residue 4
H3K27me3	trimethylation of histone 3 at lysine residue 27
H3K36me3	trimethylation of histone 3 at lysine residue 36
h	hour(s)
I	inhihbitor
i.e.	is est (that is)
IgG	immunoglobulin G

M	molar
m	milli
mA	millampere
mAbmin	minute(s)
mRNA	messenger RNA
µ	micro
n	nano
PAGE	polyacrylamide gel electrophoreses
PBS	phosphate buffered saline
PCR	polymerase chain reaction
PFA	paraformaldehyde
PVDF	polyvinylidenfluorid
qRT-PCR	quantitative Real-time RT-PCR
RNA	ribonucleic acid
RNase	ribonuclease
RPMI1640	Rosvell Park Memorial Institute, medium formulation 1640
RT	room temperature
RT-PCR	reverse Transcription reaction followed by PCR
SA-β-Gal	Senescence-associated β-Galactosidase
sec	second(s)
SEM	standard error of the mean
SD	standard deviation
SDS	sodiumdodecylsulfat
Tet	tetracycline
WB	western blotting